COMPARISON OF THE β-α ANGULAR CORRELATIONS IN THE BETA DECAYS OF Li^8 AND B^8

Thesis by

Martin Emery Nordberg, Jr.

In Partial Fulfillment of the Requirements
For the Degree of
Doctor of Philosophy

California Institute of Technology
Pasadena, California
1961

ACKNOWLEDGMENTS

It is a pleasure for the author to acknowledge the assistance offered him by all of the personnel of the Kellogg Radiation Laboratory. The author is especially indebted to Professors C. A. Barnes, H. A. Weidenmuller, and W. A. Fowler for discussions aiding the performance of this experiment. The collaboration of B. Povh and F. B. Morinigo in the execution of the experiment is gratefully acknowledged.

The author also wishes to express his appreciation for a fellowship offered by the General Electric Company and for the financial support of this research by the joint program of the Office of Naval Research and the U. S. Atomic Energy Commission.

ABSTRACT

This thesis describes a comparison of the β-α angular correlations of the beta decays of Li^8 and B^8 to the 2.90-Mev α-unstable state of Be^8. The data are fitted to the angular correlation function in the laboratory system, $W(\theta_{\beta\alpha}) = 1 + A \cos \theta_{\beta\alpha} + B \cos^2\theta_{\beta\alpha}$, where A and B are independently determined for each decay from measurements at $\theta_{\beta\alpha} = 0^\circ$, 90°, and 180°. The coefficient, A, is due to the recoil of Be^{8*} and has the same sign for both beta decays. The coefficient, B, arises from the interference of forbidden vector matrix elements with the allowed axial vector matrix element and changes sign in the two decays. The correlation for the Li^8 decay is measured with average total β-energies of $W_\beta \simeq 5$, 8, and 11 Mev. Both A and B are approximately linear in the energy. The correlation for the B^8 decay is measured only with average total β- energy of $W_\beta \simeq 11$ Mev. From the data with $W_\beta \simeq 11$ Mev, the difference of the coefficients, $B(Li^8) - B(B^8)$, is equal to $(0.0069 \pm 0.0011) W_\beta$. This result is compared with theoretical predictions based on the older Fermi and the newer Conserved Vector Current theories of beta decay. The experiment agrees with the prediction of the latter theory.

TABLE OF CONTENTS

I. INTRODUCTION

Although many of the features of beta decay have been satisfactorily understood since the 1930's, much effort in the past few years has been devoted to extending and refining the theoretical and experimental understanding of the weak interactions (1-5). The theoretical prediction of Lee and Yang that the weak interactions do not conserve parity (6) has especially stimulated much of the activity in the field. Experimentally it was promptly verified that indeed parity is not conserved in nuclear beta decay (7) nor in muon decay (8, 9). At a time when experiments posed some doubt as to the actual form of the coupling, Feynman and Gell-Mann (10), Sudarshan and Marshak (11), and Sakurai (12) proposed a universal vector-axial vector theory of the weak interactions. Many aspects of the theory have since been experimentally verified, including the vector and axial vector forms, the degree of parity violation, the helicity of electrons and neutrinos, and effects in muon decay (1, 2, 5, 13, 14). Feynman and Gell-Mann (10) also proposed as a feature of the theory, the idea of a conserved vector current (C. V. C.). This experiment tests a prediction of the C. V. C. theory about the β-α angular correlation in the beta decays of Li^8 and B^8.

Fermi Theory of Beta Decay

In the conventional Fermi theory of beta decay (1-4) the most general relativistically invariant forms of a four fermion point interaction are the five types described as scalar (S), vector (V), axial vector (A), tensor (T), and pseudoscalar (P). The allowed S and V interactions obey the Fermi selection rules ($\Delta I = 0$ but no $0 \rightarrow 0$, $\Delta J = 0$, no parity change) while the allowed A and T interactions obey the Gamow-Teller selection rules ($\Delta I = 0, \pm 1$ but no $0 \rightarrow 0$, $\Delta J = 0, \pm 1$ but no $0 \rightarrow 0$, no parity change), where I is the isotopic spin and J is the total angular momentum. Both types of allowed beta decays are observed. The P interaction does not contribute to allowed transitions. "A priori" all five interactions could occur in nature with various amplitudes, but the experimental absence of the "Fierz" interference terms was assumed to indicate on the basis of the parity conserving Fermi theory that either S or V is present and either T or A is present. On the basis of a general, parity non-conserving theory this conclusion is not justified. For some time it was believed the interactions were S and T, but more recent data definitely indicate that the interactions are V and A (5, 13, 60). Furthermore, the experimental amplitudes of the coupling constants are in the ratio, $(-G_A)/G_V \simeq 1.2$. A parity conserving Hamiltonian for nuclear beta decay would be written:

$$H = G_V(\bar{p}\gamma_\mu n)(\bar{e}\gamma_\mu \nu) - G_A(\bar{p}\gamma_\mu \gamma_5 n)(\bar{e}\gamma_\mu \gamma_5 \nu) + \text{h. c.}$$

where $\bar{p} = p^* \gamma_4$, $\bar{e} = e^* \gamma_4$ and p, n, e, ν represent wave functions. The coupling constants, G_S, G_T, and G_P, are zero in the Fermi theory only on the basis of experimental evidence.

The five interactions can be written in the Fermi theory either in parity conserving or parity non-conserving form. The violation of parity can be expressed by replacing the lepton operator, γ_μ, by $\gamma_\mu(1 + c\gamma_5)$. Lee and Yang (15), Landau (16), and Salam (17) predicted that c is real and equal to +1, in which case the product of Parity times Charge Conjugation is conserved and the neutrino is 100% polarized. In experiments on the asymmetric distribution of electrons from oriented nuclei, the longitudinal polarization of electrons from unoriented nuclei, and the asymmetric distribution and polarization of γ-rays following beta decay, the maximum effect is found indicating $c = +1$ (2, 14). The Hamiltonian for nuclear beta decay is thus:

$$H = (\bar{p}\gamma_\mu(G_V - G_A\gamma_5)n)(\bar{e}\gamma_\mu(1+\gamma_5)\nu) + \text{h. c.}$$

The idea that nuclear beta decay is but one facet of a universal weak interaction has been considered for many years. The Hamiltonian may easily be extended to the following:

$$\begin{aligned} H = & (\bar{p}\gamma_\mu(G_V - G_A\gamma_5)n)(\bar{e}\gamma_\mu(1+\gamma_5)\nu) + \text{h. c.} && \text{beta decay} \\ & + G_\mu(\bar{\mu}\gamma_\mu(1+\gamma_5)\nu)(\bar{e}\gamma_\mu(1+\gamma_5)\nu) + \text{h. c.} && \text{muon decay} \\ & + (\bar{p}\gamma_\mu(G_V - G_A\gamma_5)n)(\bar{\mu}\gamma_\mu(1+\gamma_5)\nu) + \text{h. c.} && \text{muon capture} \\ & + \ldots\ldots\ldots\ldots\ldots && \text{strange particle decays} \end{aligned}$$

Recently universality has been given a quantitative basis in the measurement of the muon decay rate and in the measurement of the ratio of $\pi^+ \rightarrow \mu^+ + \bar{\nu}$ to $\pi^+ \rightarrow e^+ + \bar{\nu}$ decays. In fact, it happens that the amplitude, G_μ, associated with muon decays is, within a few per cent, equal to the vector amplitude, G_V, of beta decay (18, 19). Although this result is not impossible in the Fermi theory it is rather surprising. Large renormalization effects arising from strong interactions would be expected to be present in nuclear beta decay which are not present in muon decay. In the older theory it would be a coincidence that the coupling constants, G_μ and G_V, are almost identically equal and that G_V and $-G_A$ are approximately equal.

Universal V-A Theory

The theory of a universal vector-axial vector interaction (10, 11, 12, 20) explains all the features of beta decay discussed above and also the equality of G_μ and G_V. The approximate equality of $-G_A$ and G_V is still not understood. Historically, the theory was proposed at a time when experiments were not yet clear on the form of the weak interactions.

There are two separate ideas advanced in this theory, the idea of a current-current interaction and the idea that the vector part of this current contains terms arising from pions and is thus conserved in strong interactions (10). In the universal V-A theory it is assumed that "bare" nucleons couple exactly as do leptons, that is, with the $1 + \gamma_5$ term. This has the effect that the S, T, and P interactions vanish and the V and A couplings are necessarily equal. The current-current hypothesis proposes that the various matrix elements of $\gamma_\mu(1 + \gamma_5)$ are summed to form a vector plus axial vector quantity which interacts with itself to form the weak interactions. If the symbols $(\overline{n}p)$, $(\overline{e}\nu)$, etc. are used to abbreviate the matrix elements, $(\overline{n}\gamma_\mu(1 + \gamma_5)p)$, $(\overline{e}\gamma_\mu(1 + \gamma_5)\nu)$, etc., the weak current is the sum:

$$J_\mu = (\overline{n}p) + (\overline{e}\nu) + (\overline{\mu}\nu) + \dots$$

The Hamiltonian for the weak interactions of universal strength, G, is:

$$H_{weak} = GJ_\mu J_\mu^+$$

The cross terms are those leading to beta decay, muon decay, muon capture, and strange particle decays. The product also contains squared terms of order $G \simeq 10^{-7}$, such as $(\overline{\nu}e)(\overline{e}\nu)$ which can lead to neutrino-electron scattering, and $(\overline{p}n)(\overline{n}p)$ which can lead to weak, parity non-conserving forces in the neutron-proton interaction. Experimental techniques are not yet sensitive enough to observe these effects but may be in the future. The older theory also leads to such effects but of the order $G^2 \simeq 10^{-14}$.

Feynman and Gell-Mann (10) also advanced the hypothesis that the vector part of the current, J_μ, contains a contribution from pions analagous to the pion contribution in the electromagnetic current, j_μ. The difference is that the electromagnetic interaction contains the z-component of the isotopic spin current whereas the weak interactions contain the (x ± iy)-components.

The addition of the pion term results in a conserved quantity in the weak interactions analogous to the conserved current in the electromagnetic interaction. The strong interactions are thus arranged not to renormalize the vector beta decay coupling constant; that is, $G = G_V$ within the accuracy of electromagnetic corrections. The axial vector coupling is apparently renormalized by the strong interactions, resulting in the ratio $(-G_A)/G_V = 1.2$.

Tests of the Conserved Vector Current Theory

In searching for other predictions of the conserved vector current theory, Gell-Mann (21) suggested an effect in beta decay which he called "weak magnetism." In the electromagnetic interaction the pion terms result in the anomalous magnetic moments of the proton and neutron which enhance the nuclear matrix elements for magnetic dipole emission of a γ-ray. Therefore the pion terms of the weak interaction would be expected to enhance the analogous matrix elements for β-emission. In other words, the Dirac magnetic moment operator is replaced by the total magnetic moment operator, Dirac plus anomalous. Gell-Mann suggested that the best situation to look for such an effect is in the interference of a second forbidden vector matrix element with an allowed axial vector beta decay. In mirror beta decays the interference effect changes sign in the positron and electron emissions and the magnitude of the effect can be predicted from the matrix element of the analogous γ-ray transition. He considered the effect on the spectra of the B^{12} and N^{12} decays. For an allowed axial vector β-transition with matrix element, X, Gell-Mann defines the quantity,

$$a \equiv \frac{\mu}{\sqrt{2}\,M} \frac{1}{\lambda X}$$

where M is the nucleon mass and $\lambda = 1.2$ is the ratio of $-G_A$ to G_V. The effect on the spectrum is a correction factor, $1 + \frac{8}{3}\,a W_\beta$. The matrix element of the magnetic dipole operator, μ, is obtained from the analogous γ-ray transition:

$$\Gamma_\gamma(M1) = \frac{\mu^2 \omega^3}{3(137)M^2}$$

where ω is the energy of the γ-ray. The allowed Gamow-Teller matrix element, X, is obtained from a comparison of the ft-value with that of O^{14}, which is a pure Fermi transition with a matrix element equal to $\sqrt{2}$. Then:

$$|a| = \left[\frac{3(137)\Gamma_\gamma}{4\omega^3} \frac{ft}{(ft)_{O^{14}}} \right]^{1/2}$$

Bernstein and Lewis have considered the effect of "weak magnetism" in other mass systems (22). In particular, they calculated the angular correlation of the electron from the beta decay of Li^8 or B^8 and the α-particles from the breakup of the 2.90 Mev daughter state in Be^8. The energy levels of this system are shown in figure 1 (23). The angular correlation in the center of mass system for either decay is shown to be:

$$W(\theta_{\beta\alpha}) = 1 + (10/7)^{1/2}\,\frac{4}{3}\,F_2(11, 22)\,a\,W_\beta P_2(\theta_{\beta\alpha})$$

$$\simeq 1 + a\,W_\beta \cos^2\theta_{\beta\alpha}$$

Since the sign of $\underline{a}$ changes between the Li^8 and B^8 decays, a comparison of the two correlations measures twice the effect. Indeed, it is imperative to make a comparison measurement in an experiment because there are many terms which can lead to a small asymmetry with the same sign in both decays (24, 25).

The M1 γ-ray transition rate has not been experimentally measured from the $J = 2^+$, $T = 1$ state in Be^8. Therefore Bernstein and Lewis (22) assumed an average value of $\Gamma_\gamma(M1) = 0.15\,\Gamma_W$, where Γ_W is the Weisskopf unit. For this estimate, $\Gamma_\gamma(M1)$ equals 8.2 ev. From the ft-value, 5×10^5, and the approximately known γ-ray energy, 13.7 Mev, the quantity, $\underline{a}$, is given by, $|a| = 0.0025\,[\Gamma_\gamma(M1)(ev)]^{1/2} =$ 0.0073 per Mev. Therefore, if δ is defined as the difference $(Li^8 - B^8)$ of the coefficients of the $\cos^2\theta_{\beta\alpha}$ term in the angular correlations, Bernstein and Lewis predict $\delta = (\pm 0.015)\,W_\beta$, ($W_\beta$ in Mev). The sign is undetermined since the sign of $\underline{a}$ cannot be determined from the ft-value.

At this point, chronologically, the first part of the experiment described in this thesis was performed by B. Povh, Dr. C. A. Barnes, and the author (26). The preliminary result then was $\delta = (0.002 \pm 0.004) W_\beta$ (statistical error only), which temporarily, at least, appeared to disagree with the C. V. C. theoretical prediction.

At this time Dr. H. Weidenmuller calculated the various wave functions and matrix elements by the intermediate coupling model of the nucleus (27). By fitting parameters so that the model gave the correct values of the energy splitting, the log ft-value, and the magnetic moment of the ground state of Li^8, Weidenmuller was able to put limits on the matrix elements in question. Since the magnetic dipole operator contains a contribution from the nucleons' orbital momenta which is not enhanced by the pion current terms, the older Fermi theory (i. e. with no π-corrections at all) may also lead to an appreciable asymmetry. If ℓ is the orbital angular momentum operator and σ the spin operator, the Fermi theory predicts an effect proportional to $< |\ell + \sigma| >$ and the C. V. C. theory predicts an effect proportional to $< |\ell + 4.7\sigma| >$. Quantitatively the calculation predicts:

Fermi theory	$(0.001) W_\beta < \delta < (0.004) W_\beta$
C. V. C. theory	$(0.005) W_\beta < \delta < (0.009) W_\beta$

The calculation can give the sign and predicts <u>a</u> is positive for Li^8, and thus δ, as defined above, is also predicted to be positive. The C. V. C. theoretical asymmetry is a factor of 2 smaller than the original estimate of Bernstein and Lewis (22), and the two theories predict similar effects differing in magnitude by about a factor of 2. Both of these facts make a positive test for the C. V. C. theory more difficult.

The limits for $\Gamma_\gamma(M1)$ in this calculation are 1 to 4 ev with the inclusion of estimates of the spin-orbit-coupling term in the Hamiltonian. The value of $\Gamma_\gamma(E2)$ is estimated to be negligible. Kurath has made a similar calculation and finds essentially the same result for $\Gamma_\gamma(M1)$ (28).

In view of this calculation no definite conclusion may be drawn from the small result of the first part of the experiment. Therefore it was decided to repeat the experiment to obtain better statistical accuracy and better control of possible systematic errors. This second experiment, which is described in this thesis , was carried out by the author, with F. B. Morinigo and Dr. C. A. Barnes (29). The result is $\delta = (0.0069 \pm 0.0011)W_\beta$ (statistical error plus estimates of systematic errors), which is a positive indication for the C. V. C. theory.

Various other experiments have been suggested, and some have been attempted in order to verify or disprove the C. V. C. theory (21, 22, 24, 30-34). An experiment at this laboratory measuring the B^{12} and N^{12} spectral shapes is so far inconclusive (32). A β-γ angular correlation experiment in the beta decay of F^{20} is consistent with the theory but is not definitive since the mirror decay cannot be used for comparison (33). Muon absorption experiments are also consistent with the theory but are not accurate enough to be considered positive evidence (34). More accurate comparisons of the O^{14} and muon coupling constants still do not resolve the few per cent discrepancy between them (18, 19). This may indicate a deficiency of the theory or may be resolved by refined calculations of other small effects that are involved. The experiment described here is perhaps the most positive experimental confirmation of the validity of the C. V. C. theory, which has been carried out up to the present time.

Figure 1 illustrates the pertinent energy levels of the mass-8 isotopic triplet. Li^8 decays by electron emission and B^8 decays by positron emission to the 2.90-Mev excited state of Be^8, with half lives of 0.85 and 0.77 second, respectively (23). The 2.90-Mev state is unstable and immediately breaks up into two α-particles. 16.1 Mev, in the case of Li^8, and 17.0 Mev, in the case of B^8, are the energies available to be shared by the electron, neutrino, and two α-particles. The α-particle energy spectrum peaks at 1.5 Mev and is about 0.8-Mev broad. Therefore the electron and positron spectra do not have simple allowed shapes, but approximate end points of 13.1 and 14.0 Mev are characteristic of the decays. The state in Be^8 analogous to the $J = 2^+$ ground states of Li^8 and B^8 is probably either the one at 16.94 Mev or the one at 16.63 Mev. The γ-ray widths of these states are not known, but experiments are proceeding in several laboratories in an attempt to measure these widths.

The present experiment involves measuring coincidences between α-particles in a fixed direction and electrons or positrons at an angle, $\theta_{\beta\alpha}$, relative to this direction. Some data were taken with three angles, $\theta_{\beta\alpha} = 0^\circ$, 90°, and 180° and the rest were taken with $\theta_{\beta\alpha} = 90^\circ$ and 180°. The general features of the first and second phases of the experiment are similar but they differ in detail. The discussion to follow will refer to the second phase of the experiment unless the first phase is specifically mentioned.

II. APPARATUS

The parent radioactive nuclei, Li^8 and B^8, are produced in the nuclear reactions:

$$Li^7(d,p)Li^8 \qquad Q = -0.192 \text{ Mev}, \; E_{th} = 0.247 \text{ Mev}$$

$$Li^6(He^3,n)B^8 \qquad Q = -1.976 \text{ Mev}, \; E_{th} = 2.966 \text{ Mev}$$

The beams of deuterons and He^3 ions are accelerated to 0.75 Mev and 3.2 Mev, respectively, in a Van de Graaff electrostatic generator, and are analyzed in a 90^o double focusing magnet. After passing through vertical and horizontal defining slits the beam hits the target. The horizontal slits, which define the vertical motion of the beam, also serve to regulate the Van de Graaff voltage. The beam energies are held constant to better than 1/2 %, although this is not an important parameter for the experiment.

Target Chamber

The target chamber consists of a 3"-diameter by 1/8"-wall lucite tube mounted vertically on an angular distribution table scribed with angle marks at 10^o intervals. The chamber and table are shown in figure 2. The β-detector is the plastic scintillator shown in the foreground and is mounted inside the lead shield during the experiment. The scintillator, lead shield, photomultiplier, and preamplifier can all be rotated precisely about the axis of the lucite target chamber and can be positioned by the scribed scale to within about $1/10^o$. The lucite vacuum chamber contains a concentric cylindrical liquid nitrogen cold trap, the target shield, and a lead container for the shield mounted from below. A 5-mil aluminum target backing is fastened to a movable 1/4"-diameter brass rod which is mounted from above. A tube containing the retractable lithium furnace is mounted 2-3/4" above the plane of the detectors. The target rod can be pulled up to allow the target backing directly to face the furnace for the lithium evaporation. The beam enters the target chamber through the lucite tube mounted from the rear right-hand side in figure 2.

Actually three different lucite chambers have been used in the course of the experiment. In the first two, where data can be taken only at $\theta_{\beta\alpha} = 90^\circ$ and 180°, the gold-silicon α-detectors are mounted through holes in the side of the chamber. In the third which is shown in figure 2, data can be taken at $\theta_{\beta\alpha} = 0^\circ$, 90°, and 180°, and the α-detectors are mounted from the top. The chamber is covered with black paper during the experiment since the detectors are slightly light sensitive.

As in all angular correlation experiments, symmetry is of prime importance. The target chambers have been designed with this in view. The walls of all chambers are milled to a uniform thickness to minimize the variation of electron energy loss with angle. In all cases the lithium evaporating furnace is positioned as symmetrically as possible to minimize variation in the number of scattered electrons with angle, although it is at a different height than the detectors and should have a negligible effect. The target has been placed at a 45° angle with respect to the detector positions except in the B^8 case of the first part of the experiment. Dummy α-detectors are symmetrically placed to prevent differences in the number of scattered or transmitted electrons. The beam entrance tube cannot be placed symmetrically. However it is a thin walled lucite tube and should produce a negligible number of scattered electrons.

The target consists of either natural lithium (92.6% Li^7 and 7.4% Li^6) for the Li^8 case or enriched Li^6 (99.7% Li^6) for the B^8 case. In both cases the lithium is evaporated in metal form on a 5-mil aluminum backing. In the first phase of the experiment the lithium was evaporated on the whole width of the aluminum backing and the target spot was thus defined by the width of the beam. The beam hit the target at an angle of 45° in the case of Li^8 and 30° in the case of B^8. This arrangement could allow some inaccuracy and possibly some systematic error in the position of the target spot. For this reason and also to minimize the recoil into the target backing (this will be discussed later), an improved arrangement is used in the second phase of the experiment. In this arrangement the beam hits the target at the glancing angle of 15°. Also the lithium is evaporated only on a 2-mm wide vertical strip. The 2-mm aperture of the furnace can be seen in figure 2. The projection of the lithium strip on the plane perpendicular to the direction of the beam ($2\text{ mm} \sin 15^\circ \approx 1/2\text{ mm}$) is narrower than the beam width. Therefore the target spot is defined by the evaporated lithium strip. This arrangement defines the target position more accurately than the previous arrangement and minimizes the possibility of systematic error arising from lateral motion of the beam. Also a signal from the vertical beam defining slits can be used to regulate a magnet which can hold the beam fixed in the center of these slits and thus in a well defined position on the target. The magnet has been used only during part of the experiment. No significant systematic beam movement is observed either with or without the magnet.

Counting Cycle

Several aspects of the experiment dictate certain features of the apparatus. For example, the 0.848-second Li^8 half life and the 0.77-second B^8 half life allow delayed counting while the beam is turned off. Two systems are common for this purpose, either synchronous motor choppers and gate signals phased with 60 cycle line voltage, or mechanically controlled choppers and gate signals phased with cam driven relays. The second system with a period of 1 second was chosen because it facilitates the operation of a target shield with a vertical solenoid-activated movement. This shield maintains symmetry within the sensitive target region during the counting period by dropping out of the way. As seen in figure 3 the chopping mechanism has four functions: (1) to gate the 100 channel analyzer, (2) to gate the scalers, (3) to activate the solenoid for the beam chopper, and (4) to activate the solenoid for the target shield. The chopping mechanism consists of the two solenoid power supplies and four switches driven by three cams on one shaft turning at 1 cycle per second. Both gate switches are driven by the same cam and are shorted except during the counting period. The beam chopper also has a vertical movement activated by a solenoid and is located about 20" ahead of the target. Starting with the beam cut off, the gates off and the target shield down, the complete counting cycle is the following:

at $t = 0$	the target shield rises to surround the target
$t = 0.05$ sec.	the beam is turned on
$t = 0.45$ sec.	the beam is cut off
$t = 0.50$ sec.	the shield drops
$t = 0.55$ sec.	the gates are turned on for the start of the counting period
$t = 0.95$ sec.	the gates are turned off
$t = 1.0$ sec.	the target shield rises.

α-Particle Detector

At the time of the start of this experiment it was not known whether a suitable gold-silicon semiconductor α-detector could be constructed. Gold-germanium semiconductor detectors (35, 36, 37) had been constructed and had operated satisfactorily when cooled to liquid nitrogen temperature. Therefore the first target chamber was designed to accommodate either type of semiconductor detector or a CsI(Tl) scintillator and photomultiplier, whichever proved the most satisfactory. A CsI(Tl) scintillator has the disadvantages of slow rise time, sensitivity to electrons, and extreme light sensitivity, thus requiring a light shield through which the α-particles have to pass. A silicon surface barrier detector was constructed (38) and found to operate satisfactorily at room temperature. (See Appendix A for a full description of the operation of semiconductor detectors.) A gold-silicon detector was compared with a CsI(Tl) scintillator by exposing both counters to the α-particles following the Li^8 beta decay. Both spectra showed pulses from electrons, and noise, at low pulse heights. However the silicon detector displayed a much cleaner spectrum and altogether was very well suited for the experiment. A typical response to the α-particles following the Li^8 decay is shown in figure 4 and the response to the 5.3 Mev α-particles of Po^{212} is shown in figure 5. The pulse height vs. energy of gold-silicon detectors was also measured and found to be quite linear. There is no evidence of an appreciable dead layer on the surface of the detectors. The noise of the silicon detectors increases with age and for this reason new detectors have to be constructed periodically. The usual size is a 5/16" wafer with a 1/4"-diameter aperture. The detectors are located approximately 7/8" from the target.

The most useful data have been taken with the system allowing the β-detector to be placed at all three angles, $\theta_{\beta\alpha} = 0^\circ, 90^\circ,$ and 180°. This system would not be possible without a semiconductor α-detector because at 0° the electrons pass directly through the α-detector before reaching the β-detector. The problem of light collection would make a similar scintillator and photomultiplier system very awkward. The silicon detector in this case consists of an etched wafer only about 3/4-mm thick in which the electrons lose a negligible amount of energy. The thin α-detectors, electrical leads, and apertures are visible in figure 2.

β-Detector

For the β-detector both a plastic and a NaI(Tl) scintillator were tested. It was known from a previous experiment that a plastic scintillator shows good β-spectra (13), but the plastic has the disadvantage of no convenient means of energy calibration with available γ-ray sources. Although the NaI(Tl) scintillator can be calibrated with γ-ray sources because of its sharper response, it produced a poorer β-spectrum of the Li^8 decay than the plastic scintillator. This was due to increased sensitivity to background radiation (mostly neutrons), slightly poorer crystal geometry, with higher Z which allowed more electrons to scatter out of the crystal, and to greater bremsstrahlung loss from the crystal. For this reason, and also to avoid the longer pulse rise time of NaI, the plastic scintillator has been used in the experiment. The response to the electrons from the Li^8 decay is shown in figure 6 and the response to the 2.6 Mev γ-ray from ThC" is shown in figure 7. The calibration of the energy scale by means of the β-spectrum is discussed in the next sections.

The plastic scintillator is fastened to a 2"-diameter RCA type 6655 photomultiplier with a 1"-long lucite light pipe. The scintillator which is shown in figure 2 is in the shape of truncated cones with a 2-3/4"-maximum diameter and a 2"-minimum diameter. The aperture in the lead shield is only 1-3/8" in diameter thus reducing the probability that electrons scatter out of the sides of the scintillator. The photomultiplier is shielded from stray magnetic fields by layers of high μ material and a steel case. The 3/4"-thick lead shield protects the scintillator from background γ-radiation.

Electronic Circuitry

A block diagram of the electronic system is shown in figure 3. The general system is that of a "slow-fast" coincident arrangement. The fast resolving time is 80 mμsec. and the slow resolving time is the 1 μsec. resolving time of the coincidence mixer of the 100 channel analyzer. The coincident α-spectrum is recorded in the 100 channel analyzer in order to extrapolate the spectrum to zero pulse height with reasonable confidence. This point is discussed in the next sections.

The preamplifiers used with the surface barrier detectors produce an output voltage pulse which is linearly dependent on the input charge. A low noise 417A triode on the input provides a gain of about 40. This is followed by a cathode follower and the signal is fed back to the input grid by a 20-$\mu\mu$f capacitor. The output voltage in this configuration is approximately the input charge from the detector divided by the feedback capacitor. A 1/2-Mev particle gives an output of only about 1 millivolt. Thus a large amount of amplification is needed in order to analyze the pulses. Therefore, in the slow system, another preamplifier with a stabilized voltage gain of about 40 is used. This is followed by a standard laboratory type 10T2 linear amplifier of gain up to about 5000, the output of which goes to the input of the 100 channel analyzer. In the fast system five Hewlett-Packard delay line amplifiers are used to provide the necessary gain. Special precautions, such as extra shielding on the connecting cables and separation of the amplifiers, are needed to prevent this system from oscillating when the gain is turned up.

Several pulse shaping and coincidence mixer systems have been used in the course of the experiment. In the first part of the experiment the pulses were clipped and limited after the Hewlett-Packard amplifiers by a delay line plate load on an E180F pentode. A 40-mμsec. resolving time was used in the case of Li^8 and 80-mμsec. in the case of B^8. The limiters were followed by a 6BN6 coincidence mixer.

In the second part of the experiment the pulses are clipped by a shorted cable following the second Hewlett-Packard amplifier as in figure 3. The resolving time with a 16' cable is about 80 mμsec. for both Li^8 and B^8. The E180F limiters and 6BN6 mixer have been used in collecting about half of the data. For the remaining data a circuit employing tunnel-diode limiters and coincidence mixer has been used. This circuit has the advantage of increased sensitivity which allows use of somewhat less gain in the chain of Hewlett-Packard amplifiers. The output of the coincidence mixer goes into the "gate" of the 100 channel analyzer.

The electronic circuits for the β-detector are similar to those for the α-detector except that the extra preamplifier is not needed and only 2 or 3 (depending on the β-energy) Hewlett-Packard amplifiers are needed. Following the linear amplifier is a single channel differential discriminator. This is used to select the portion of the β-spectrum desired to be in coincidence with the α-particles, such as the shaded portion of figure 6. The output of this discriminator goes to the "delayed coincidence" input of the 100 channel analyzer.

Both an electron sensitive plastic scintillator and an α-particle sensitive gold-silicon detector have been used at different times as a monitor counter. The monitor is used only as a check on the consistency of the α-detector counts. The electronic circuits for the monitor consist of a preamplifier, a 10T2 linear amplifier and a scaler.

Scalers are used to count the α-pulses, the β-pulses, the β-pulses passed by the single channel discriminator, the monitor pulses, and the output pulses of the fast coincidence mixer. These scalers and the 100 channel analyzer are gated on and off by the gating mechanism described previously.

The 100 channel analyzer requires the presence of four conditions in order to register a coincident count: (1) the gating switch is open for the 0.4 sec. counting period, (2) the fast coincidence mixer produces an output pulse, (3) the β-discriminator produces an output pulse, and (4) the α-amplifier produces an output pulse. The presence of (2) would indicate the presence of (4) if it were not for excess noise in the fast amplifiers. In such a case the 100 channel analyzer records a count in channel 1, 2, or 3. These counts are discarded in analyzing the data.

III. PROCEDURE

Several tests have been carried out to insure the proper operation of the various components of the equipment. Estimates of the possible systematic errors based on these tests are summarized in the next section. This section outlines the procedure of accumulating and analyzing the data after the apparatus has been adjusted and is operating properly.

Measurement

The first step at the beginning of a group of runs is to evaporate a fresh Li^6 or Li^7 target in metal form on the aluminum backing. The evaporation is done inside the target chamber under high vacuum. New spots of the 2-mm strip are bombarded periodically in taking data.

Next, the beam is aligned by adjusting the defining slits so that the beam enters the target chamber at the correct vertical position and precisely on the chamber axis. The beam spot and the shadow of the target backing on a quartz disc can be viewed for this adjustment. This disc is pulled out of the way for taking data. At this stage of the second part of the experiment, care has been taken not to expose the silicon α-detectors to sputtered material from the target or quartz. However, in the first part of the experiment some material may have sputtered on the detectors during the beam alignment for the B^8 decay, and thus caused a further degradation of the α-particle energies.

The intensity of the 0.75-Mev deuteron beam for the Li^8 decay is adjusted to about 0.1 μa average value in order to limit the random rate to 2-5%. For the B^8 decay randoms are not a problem and the 3.2-Mev He^3 beam is adjusted to about 1 μa average value which is nearly the maximum the 5-mil aluminum backing will stand without distortion. The beam is purposely not sharply focused on the target so that it uniformly bombards the width of the 2-mm lithium target strip. In the third target chamber where the β-detector can be positioned at all three angles, the target is grounded since the α-detectors are mounted from the brass top which also holds the target rod. Thus the beam current cannot be read directly. For this case the target shield is biased 300 volts positively and is connected to ground through a microammeter. The shield collects the secondary electrons knocked out of the target by the beam and indirectly monitors the beam intensity. A secondary emission factor of about 20 is observed for the 3.2 Mev He^3 beam on the Li^6 target, for the geometrical arrangement of this experiment.

With the system aligned and operating, the spectra of the various detectors are inspected on the 100 channel analyzer, and the counter voltages and amplifier gains are adjusted. The scaler biases are set to correspond to definite channels of the 100 channel analyzer spectrum. The β-single channel discriminator bias is set by observing the cutoff of the β-spectrum in coincidence with the discriminator output. Then the various spectra are recorded. The recorded spectra include those of (1) the β-detector, (2) background in the β-detector found by reversing the target so that the beam hits the bare aluminum, (3) the β-detector in coincidence with the single channel discriminator, (4) the monitor detector, (5) the α-detector, and (6) the α-detector with the α-limiter pulses going to both inputs of the fast coincidence mixer and its output gating the 100 channel analyzer. The last spectrum, called "α-α gate," checks on the proper operation of the fast circuit. These spectra are recorded occasionally throughout each group of data runs and again at the end of the group.

Finally coincident data are recorded. Runs of either a definite charge collected on the target or a fixed time are recorded for each angle of the β-detector. The time of a run is usually about 10 to 20 minutes and about 2 minutes are required to record the scalers and to print out the memory of the 100 channel analyzer. The β-detector is rotated to a new position while the memory is printing out. The order of angles in positioning the β-detector is varied frequently throughout a group of runs so that sequential or time-dependent effects do not appear as angle-dependent effects. For part of the three angle data the β-detector is set in the 90° position twice as often as at the other angles since the error in the coefficient, B, is more dependent on the error in the number of 90° coincidences. In the Li^{8} decay about one out of four runs measures random coincidences from the fast coincidence mixer. For these runs 120' of extra RG-114/U cable is put in the β-side of the fast coincidence mixer to delay the β-pulses beyond the resolving time. For the B^{8} decay random coincidences are neglected but an occasional random coincidence run is taken in which zero counts insures the proper operation of the equipment. With the β-detector at the 0° position runs are also taken with the target reversed so that the aluminum backing stops the α-particles which would normally reach the α-detector. The backing only minutely affects the β-spectrum. In this way a coincident spectrum is obtained from the electrons which produce a small pulse in the α-detector and a normal large pulse in the β-

scintillator. This spectrum is called "$0^{\circ}\beta$."

Analysis

The primary data of the experiment consist of the scaler readings, the non-coincident 100 channel analyzer spectra, and the coincident 100 channel analyzer spectra. A systematic procedure has been adopted to analyze this data. Roughly one day's set of runs is grouped together for the analysis. A group consists of 5 to 10 runs with a total of about 2×10^3 B^8 coincidences or 2×10^4 Li^8 coincidences at each angle.

The coincident α-spectra and the scalar readings of all the runs with the β-detector at a particular angle are added together. Since there are relatively few counts per channel in the coincident spectra, the channels are grouped together by threes for the analysis. The coincident α-spectra at each angle of the β-detector are normalized by dividing by the corresponding total number of β-single channel discriminator output counts. The normalization corrects the number of coincidences for differences in the total amount of Li^8 or B^8 produced in the target, for variations in the β-detector solid angle or gain, and for some counting rate effects. Normalization in this fashion is right if the solid angle of the α-detector is a constant independent of the position of the β-detector. This is discussed in the next section. The resulting coincident α-spectra are illustrated by figures 8, 9, 10, and 11. The curve for $\theta_{\beta\alpha} = 0^{\circ}$ is extrapolated to zero pulse height by subtracting the "$0^{\circ}\beta$"-spectrum. The "$0^{\circ}\beta$"-coincidences are arbitrarily normalized because the usual normalization would produce a negative net number of counts in the 0° spectrum below channel 10. This means that the α-detector is slightly more sensitive to the electrons when the flux of α-particles is not present than when it is. No explanation has yet been discovered for this behavior of the α-detector.

In the decay of Li^8 the number of random coincidences from the fast coincidence mixer, N_R, is calculated for each data run from the formula:

$$N_R = \frac{N_\alpha N_\beta \text{"}\tau\text{"}}{t}$$

where:
t = the net time of the run
N_α = the number of counts in the α-scaler
N_β = the number of counts in the β-discriminator scaler
"τ" = the effective resolving time.

For each group a best value of "τ" is found from the random runs with all angles of the β-detector. Essentially "τ" is defined by the same formula from those cases where N_R is known. It is not the true resolving time since it depends on the fraction of the whole α-spectrum which is counted by the α-scaler. "τ" is used to calculate the random coincidences in each data run separately. These numbers of random coincidences are summed and normalized in the same way as the real coincident spectra, and subtracted from the totals of the real coincident spectra. The result is a set of three numbers of coincidences, $n(0^\circ)$, $n(90^\circ)$, and $n(180^\circ)$, or two numbers for those runs where the β-detector could not also be placed at 0°. The statistical uncertainties of the random runs add small contributions to the statistical errors of $n(0^\circ)$, etc. Other effects which depend on the counting rate are neglected in the analysis of the data. These effects can be categorized as random coincidences from the slow coincidence mixer, pile up of pulses in the β-discriminator, and dead time in the β-discriminator. They are discussed more fully in the next section.

Also all the non-coincident spectra of a particular type, such as β-detector, background in the β-detector, etc., are added together and plotted. Plots of the α- and β-spectra are shown in figures 4, 6, 12, and 13. The spectra of the β-detector in coincidence with the single channel discriminator are also summed for each group of runs. The sum spectrum is similar to the shaded portion of figure 6 or 13 for the case where W_β is approximately 11 Mev. For the cases where $W_\beta \simeq 5$ and $W_\beta \simeq 8$ Mev, this spectrum consists of the portion from channel 25 to 40 or 40 to 55, respectively. In order to estimate the actual average energy of this spectrum, the average channel is first calculated. This is compared to the channel corresponding to the half maximum point of the whole β-spectrum, for example, channel 61.5 in figure 6. From the Li^8 β-spectrum obtained by Hornyak and Lauritsen in a magnetic spectrometer (39, 40), the half maximum point is known to be 9.5 Mev kinetic energy. Their spectrum is also plotted in figure 6. In the absence of a similar standard for the B^8 spectrum, the corresponding point is considered to be the ratio of end points times 9.5 Mev,or 10.2 Mev. With the assumption of a linear scale, the average channel is easily converted to kinetic energy or total energy with the addition of 1/2 Mev. Slight corrections are applied to the $W_\beta \simeq 5$ and 8 Mev data. The accuracy of this procedure is discussed in the next section.

At this point, the data has been reduced to the value of W_β and either the three numbers $n(0^\circ)$, $n(90^\circ)$, and $n(180^\circ)$ or the two numbers $n(90^\circ)$ and $n(180^\circ)$. Tables I and II list all of the data in this form for Li^8 and B^8 respectively. The number of coincidences are normalized to 200,000 electrons analyzed by the single channel differential discriminator. The numbers are corrected for randoms in the fast coincidence mixer and for the "0° β"-spectrum due to electrons. The variations in the numbers in a particular column are caused by the variations in the sizes of the various α-detectors which have been used.

The three numbers of coincidences are sufficient to find both coefficients, A and B, of the angular correlation function, W.

$$W(\theta_{\beta\alpha}) = 1 + A \cos \theta_{\beta\alpha} + B \cos^2 \theta_{\beta\alpha}$$

The number of normalized coincidences at any angle is proportional to the integral of W over the detector solid angles with the detector arrangement at that angle. In the experimental apparatus the β- and α-solid angles are fixed by circular apertures of $19^\circ 40'$ and 9° half angle, respectively. The integration over these solid angles is carried out in Appendix B. There result three equations in three unknowns, where one unknown is a proportionality factor.

$$\begin{aligned} n(0^\circ) &= n'(1 + f_1 A + f_2 B) \\ n(90^\circ) &= n'(1 \qquad\quad + f_3 B) \\ n(180^\circ) &= n'(1 - f_1 A + f_2 B) \end{aligned}$$

where $f_1 = 0.965$, $f_2 = 0.932$, and $f_3 = 0.034$. These equations are solved in Appendix C for the coefficients, A and B. Also the standard deviations of A and B found in terms of the statistical errors of the

TABLE I

Normalized and Corrected Number of Coincidences for Li^8

Group No.	Date (1960)	$n(0^\circ)$	$n(90^\circ)$	$n(180^\circ)$	W_β (Mev)
1	Feb 27		2061 ± 18	2286 ± 18	11.4
2	Feb 27		2013 ± 16	2258 ± 16	11.1
3	Mar 15		2493 ± 14	2768 ± 20	11.1
4	Mar 18		2406 ± 15	2669 ± 17	10.7
5	Mar 15	2397 ± 20	2502 ± 21	2813 ± 20	10.7
6	Mar 16	2247 ± 19	2384 ± 20	2713 ± 20	10.9
7	Mar 18	2239 ± 25	2409 ± 25	2780 ± 20	11.1
8	Mar 19	2311 ± 32	2367 ± 32	2637 ± 32	10.9
9	Apr 28	2660 ± 45	2789 ± 34	3051 ± 41	11.0
10	Jun 25	2305 ± 25	2480 ± 25	2738 ± 27	10.4
11	Jun 28	2341 ± 30	2445 ± 24	2804 ± 31	10.8
12	Jun 28	2227 ± 23	2433 ± 22	2744 ± 24	10.5
13	Jun 30	2376 ± 27	2482 ± 23	2750 ± 29	10.5
14	Jul 1	2372 ± 20	2535 ± 15	2791 ± 22	10.4
15	Jul 1	2371 ± 20	2459 ± 14	2664 ± 19	8.1
16	Jul 22	2341 ± 18	2410 ± 12	2601 ± 16	8.2
17	Jul 21	2271 ± 14	2355 ± 10	2469 ± 15	5.8
18	Jul 25	2373 ± 12	2427 ± 8	2552 ± 12	5.5

TABLE II

Normalized and Corrected Number of Coincidences for B^8

Group No.	Date (1960)	n(0°)	n(90°	n(180°)	W_β (Mev)
1	Feb 17		1935 ± 31	1953 ± 30	10.9
2	Feb 28		1848 ± 42	1949 ± 44	11.0
3	Feb 29		1854 ± 39	1986 ± 39	11.2
4	Feb 29		1790 ± 33	1942 ± 35	10.8
5	Mar 1		1848 ± 30	1943 ± 31	10.7
6	May 4	1820 ± 47	2003 ± 45	2213 ± 50	11.9
7	May 5	1866 ± 42	2127 ± 40	2287 ± 46	11.6
8	Jun 3	2079 ± 45	2394 ± 45	2564 ± 53	10.9
9	Jun 4	2090 ± 56	2456 ± 56	2536 ± 63	11.1
10	Jun 4	2095 ± 53	2469 ± 56	2487 ± 66	11.1
11	Jul 15	2148 ± 53	2413 ± 39	2554 ± 60	11.4
12	Jul 17	2031 ± 42	2381 ± 29	2485 ± 48	10.6
13	Jul 19	2089 ± 40	2426 ± 32	2547 ± 43	10.6

numbers of coincidences.

$$A = \frac{n(0^{\circ}) - n(180^{\circ})}{2f_1 n(90^{\circ})}$$

$$\Delta A = \frac{1}{2f_1 n(90^{\circ})}\left[\Delta^2 n(0^{\circ}) + \left[\frac{n(180^{\circ}) - n(0^{\circ})}{n(90^{\circ})}\right]^2 \Delta^2 n(90^{\circ}) + \Delta^2 n(180^{\circ})\right]^{1/2}$$

$$B = \frac{n(0^{\circ}) + n(180^{\circ}) - 2n(90^{\circ})}{2f_2 n(90^{\circ}) - f_3 n(0^{\circ}) - f_3 n(180^{\circ})}$$

$$\Delta B = \frac{1}{2(f_2 - f_3) n(90^{\circ})}\left[\Delta^2 n(0^{\circ}) + 4\Delta^2 n(90^{\circ}) + \Delta^2 n(180^{\circ})\right]^{1/2}$$

For each group of runs with data at all three angles, the quantities, A, B, ΔA, and ΔB, are calculated with these formulas. For the groups of runs with data at only two angles, only the quantity, B - A, may be calculated. Therefore, these groups are analyzed for B by using the average value of A from the three angle data. The formulas in this case are the following:

$$B = \frac{n(180^{\circ}) - (1 - f_1 A) n(90^{\circ})}{f_2 n(90^{\circ}) - f_3 n(180^{\circ})}$$

$$\Delta B = \frac{1}{f_2 n(90^{\circ}) - f_3 n(180^{\circ})}\left[(1 + f_3 B)^2 \Delta^2 n(180^{\circ}) + (1 - f_1 A + f_2 B)^2 \Delta^2 n(90^{\circ})\right]^{1/2}$$

Results

The coefficients, A and B, are both divided by W_β in order to average together the several groups of data and for comparison with theory. Although the theoretical predictions are that A is proportional to the β-momentum, p, and B is proportional to p^2/W_β, the approximation, $W_\beta = p$, is adequate for these purposes since it is accurate to within 1/2% even at $W_\beta = 5$ Mev. In the averaging procedure the coefficients, A/W_β and B/W_β, are weighted with the inverse square of the statistical error. Possible systematic errors are not considered in the averaging procedure. The results from the three angle data are listed in the top entries of table III.

The two angle data are analyzed with the assumption that $A = (-0.0087) W_\beta$, as indicated by the three angle data. The weighted averages are listed in the middle entries of table III.

Attempts to take data in the B^8 decay at lower β-energies are frustrated by the large amount of background which is present in the β-spectrum, as is evident in figure 13. This background makes the normalization procedure unreliable at the lower energies. The possibility of allowing coincidences over the lower energy portion of the β-spectrum but normalizing to the high energy portion was considered but was discarded as unreliable. The best values for comparing the difference of the Li^8 and B^8 beta decays of the coefficient, B/W_β, are the weighted averages of the three angle and the two angle data with $W_\beta \simeq 11$ Mev. These are listed in the bottom entries of table III. Also the difference, $\frac{B(Li^8) - B(B^8)}{W_\beta} = \frac{\delta}{W_\beta}$, is given. No valid comparison with the B^8 data can be made of the lower energy Li^8 data.

TABLE III

Weighted Averages of the Coefficients, A/W_β and B/W_β

Beta Decay	W_β (Mev)	Coefficient	Weighted Average	Statistical Error	Number of Groups
Li^8	5	A/W_β	-0.0073	±0.0006	2
		B/W_β	0.0023	±0.0008	
Li^8	8	A/W_β	-0.0072	±0.0006	2
		B/W_β	0.0033	±0.0008	
Li^8	11	A/W_β	-0.0087	±0.0002	10
		B/W_β	0.0034	±0.0004	
B^8	11	A/W_β	-0.0088	±0.0005	8
		B/W_β	-0.0039	±0.0008	
Li^8	11	B/W_β	0.0020	±0.0006	4
B^8	11	B/W_β	-0.0044	±0.0012	5
Li^8	11	B/W_β	0.0029	±0.0003	14
B^8	11	B/W_β	-0.0040	±0.0007	13
Li^8-B^8	11	δ/W_β	0.0069	±0.0008	

A histogram of all the results is given in figure 14. For comparison purposes, normal distribution curves are drawn with the averages of the $W_\beta \simeq 11$ Mev data. The widths are equal to $\sqrt{n}\Delta$, where n is the number of groups and Δ is the standard deviation of the weighted mean. The histograms of the Li^8 data also contain $W_\beta \simeq 5$ and 8 Mev groups. Also some data which may be inaccurate because of known faulty operation of the equipment or other known reasons has been included in the histogram but not in the averaging procedure.

The β-α angular correlation of the beta decay of Li^8 has been studied for asymmetries of the $\cos^2\theta_{\beta\alpha}$ form by other workers. In general they have not obtained data with comparable statistical accuracy. In 1953 D. StP. Bunbury measured the correlation with a proportional counter and β-spectrometer (41). He found the asymmetries:

$$(0.004 \pm 0.020) W_\beta \quad \text{for } W_\beta = 9.8 \text{ Mev}$$

$$(0.016 \pm 0.012) W_\beta \quad \text{for } W_\beta = 7.5 \text{ Mev}$$

Since he does not mention compensation for the $\cos\theta_{\beta\alpha}$ term and he only took data for angles greater than 90°, these results are probably equivalent to the difference, B - A, in this experiment. In 1954 S. S. Hanna, E. C. LaVier, and C. M. Class measured the correlation with scintillation detectors (42). They made measurements at $\theta_{\beta\alpha}$ and $\pi - \theta_{\beta\alpha}$ in order to compensate for the $\cos\theta_{\beta\alpha}$ term. Their average result is:

$$B = (0.002 \pm 0.006) W_\beta,$$

with the assumption of an average energy of about 6 Mev. In 1959 K. Krebs, H. Riesenberg, and V. Soergel measured the correlation with a proportional counter and a β-spectrometer (43). Their experiment measures B - A and they correct for A with its first order theoretical form in order to find B. The results are:

$$B = (0.0057 \begin{smallmatrix} +\ 0.0029 \\ -\ 0.0019 \end{smallmatrix}) W_\beta \qquad \text{for} \quad W_\beta = 7.0 \text{ Mev}$$

$$B = (0.0054 \begin{smallmatrix} +\ 0.0074 \\ -\ 0.0066 \end{smallmatrix}) W_\beta \qquad \text{for} \quad W_\beta = 3.5 \text{ Mev}$$

These results, although less accurate, are generally consistent with the present experiment and all give a positive sign of the coefficient, B, for the Li^8 correlation.

IV. DISCUSSION

Since the statistical errors of the coefficients, A and B, are less than $(0.001) W_\beta \simeq 0.01$, it is imperative to consider effects of similar size in the data arising from the apparatus or method of analysis. These can be subdivided into effects associated with the β-spectrum, with the α-spectrum, with counting rate, and with symmetry.

β-Spectrum

The coefficients are divided by W_β in order to average the groups together and to compare the results with theory. Therefore, some estimate of the accuracy of W_β, or in other words of the calibration of the β-spectrum, is called for. As described previously, the β-detector is a plastic scintillator and does not have particularly good resolution for γ-rays. Figure 7 shows the spectrum of the 2.6-Mev γ-ray from ThC". There is no particularly sharp feature of this curve which "a priori" can be associated with the energy, 2.6 Mev. A calibration accuracy of only about 10% can be expected from this spectrum. Therefore the β-spectrum itself is used as the calibration by comparison with the Li^8 β-spectrum measured by Hornyak and Lauritsen in a magnetic spectrometer (39, 40). A convenient calibration point is the upper half maximum point, which occurs at an energy of 9.5 Mev kinetic energy on their curve. The spectrum from the β-spectrometer is compared to one from the scintillation counter in figure 6. The experimental and standard curves are normalized to have the same area and the half maximum points have the same abscissa. For the B^8 spectrum, the half maximum energy is considered to be

9.5 Mev times the ratio of the end points, or 10.2 Mev. (The end points for production of 2.90 Mev excitation energy in Be^{8*} are used.) Negligible distortion of the shape arises from Coulomb corrections at these high β-energies. Vedder has measured both the Li^8 and B^8 spectra and finds both half maximum points about 3% lower in energy (44).

In the analysis of the data, the average β-energy of the spectrum passed by the single channel discriminator is found by the comparison with the point of half maximum. For the cases where $W_\beta \simeq 11$ Mev, the discriminator passes all pulses above a fixed height. (See figure 6 or 13.) In these cases an independent but approximate procedure is available to calculate the average energy from the number of pulses above the fixed height and also the total number. If one assumes an allowed fermi spectral shape of known end point and a one-to-one correspondence of pulse height to energy, there is a definite, calculable energy associated with the fraction of pulses in the upper end of the spectrum. In several cases the mean energies have been calculated by both methods and on the averages are equal within 4%. The differences are not always in the same direction. From a similar comparison with the integral of the Hornyak and Lauritsen curve, the average energy may also be found and again agrees within about 4%, but this method is not completely independent of the first. From these comparisons it is estimated that the systematic error in W_β is less than 5% for the high energy groups, when the energy is calculated by the procedure used in the analysis of the data.

The correspondence between the standard and experimental curves of figure 6 is not unreasonable, but there is a definite difference of slope in the upper portion. To try to account for this difference in shape, and also to try to estimate the number of small pulses originating from high energy electrons, an attempt has been made to fold in the resolution function of the plastic scintillator. It is assumed that the scintillator used in the equipment has the same resolution function as a different 2" x 3" plastic scintillator. Figure 15 shows the response of the latter scintillator to 7.1 Mev monoenergetic electrons as obtained by Dr. H. Hilton and Dr. V. Soergel in a β-spectrometer (45). This and similar curves at other energies are approximated by the triangular areas shown in the figure. A graphical analysis has been made by dividing the standard spectrum into 1/2 Mev intervals and for each interval plotting a curve like that of figure 15 of equal area. The smoothed over sum spectrum is shown in figure 16 along with the experimental and standard spectra. It is normalized to the same peak height as the standard. As seen in this figure, the derived curve has nearly the shape of the experimental curve in the upper energy region. The important feature is that the half maximum point of the derived curve is very nearly equal to that of the standard, which would indicate the calibration procedure is valid. The shape at lower pulse height indicates an excess number of counts.

From a similar graphical analysis, the contamination of the 5 and 8 Mev groups by higher energy electrons is determined. The result is to raise the average energies of these groups by 15% and 5%, respectively. Since the derived spectrum contains too many low pulses to fit the experimental spectrum, this may be an over estimate. Therefore, the data are analyzed with energies corrected by 10% and 5%, respectively. The limits of systematic error for these cases can reasonably be set at 10%, but this is not as important as in the cases of the higher β-energy groups since the statistical accuracy of the data is poorer.

An improved β-detector system could have been achieved with the use of an anticoincidence scintillator around the β-detector scintillator. This would prevent the counting of electrons which scatter out of the scintillator and also would cut the background rate.

α-Spectrum

The accuracy of the integration over the whole coincident α-spectrum is possibly the severest limitation on the accuracy of the results. This problem arises from two intrinsic features of the Be^{8*} breakup and one feature of the experimental arrangement: the 2.90 Mev state is quite broad, the energy distribution of the α-particles changes with angle, and the α-particles lose some energy in the target and dead layers on the detectors.

The fact that the α-particles lose some energy in the target is the most serious because this energy loss is different for the Li^8 and B^8 decays. The spectra from an infinitesimally thin target would contain essentially no α-particles below about 1/2 Mev and there would be little difficulty in detecting all energies with 100% efficiency. The B^8 or Li^8 ions recoil into the target backing from the momentum of the incident 3.2-Mev He^3 beam or the 0.75-Mev d beam. Therefore, the α-particles must lose some energy in travelling back out of the target. The mean recoil energies are approximately $\frac{8}{9} \times \frac{3}{9} \times 3.2$ Mev = 0.95 Mev for B^8 and $\frac{8}{9} \times \frac{2}{9} \times 0.75$ Mev = 0.15 Mev for Li^8. Since the beam enters at 15° to the target and the α-particles leave at 45°, the α-particles must penetrate a distance corresponding to the range of the 0.95 Mev B^8 ions or the 0.15 Mev Li^8 ions times the quantity, $\sin 15^\circ/\sin 45^\circ = 0.36$. Although the α-particle energy loss depends on the energy, the energy loss is approximately 100 to 300 kev for the B^8 decay and 0 to 50 kev for the Li^8 decay. In the first part of the experiment there was even a greater loss since the target was at a 30° angle to the beam and the α-detector may have had a dead layer on the surface during the measurements of the B^8 correlation. Figure 17 shows a comparison of the 90° coincident spectra of the first and second parts of the experiment. The second spectrum has been greatly improved by placing the target at 15° to the beam and protecting the α-detector during the beam alignment procedure. However, even in the second part of the experiment the spectrum extends down to zero pulse height because of the energy losses and the limited resolution of the α-detectors.

The change in the energy distribution of the α-particles with the angle of the β-detector stems from the recoil of the Be^{8*} nucleus from the beta decay. The electron-neutrino correlation has been indirectly measured from this effect and shows that the form of the interaction for the Li^8 decay is axial vector (13, 46). The effect prevents one from using a fixed lower cutoff of the α-spectrum because the fraction of the total counts above the cutoff is dependent on the angle. Therefore in this experiment the entire α-spectrum is recorded on the 100 channel analyzer.

Nevertheless, the problem still exists of recognizing an electronic cutoff of the α-spectrum at low pulse heights. The problem is aggravated by noise produced in the silicon detector which causes an increase in the spectrum at low pulse heights, as in figures 4 and 12. This noise is not passed by the α-α coincidence gate because the frequency of the noise spectrum is generally much lower than that required by the 80 mμsec. fast resolving time. Yet it is the fast coincidence mixer that is most suspect as producing an electronic cutoff. Several methods have been used to test the coincidence mixer. The spectrum of a pulser in place of the α-detector can be displayed on the 100 channel analyzer. With the α-α gate, the pulser registers down to channel 8 with about 100% efficiency and counts below that with reduced efficiency. Full limiting occurs for pulses larger than channel 12. A criticism might be offered that the pulser produces better shaped pulses than the α-detector, and therefore these are detected more easily by the coincidence mixer. However, no difference can be seen in the shape of large pulses from the α-detector and pulser. The shape of the small pulses from the α-detector cannot be seen accurately because of the great number of larger pulses. On the other hand, the α-α gate system may be a too stringent test of small pulse performance because it requires the coincidence mixer to sense two small pulses, whereas in the actual experiment the β-pulses are all fully limited.

Another check has been made by reducing the α-detector output by shunting it with a small capacitor. Then the α-spectrum with the α-α gate is recorded and the gain of the fast amplifiers lowered. A factor of two lowering in gain is needed to reduce appreciably the coincidences in channel 10. Thus with reasonable certainty, the system can be considered 100% efficient down to channel 10 under normal operating conditions. Less than 1% of the total counts of the 90° and 180° curves are of smaller pulse height. About 2% of the 0° curves lie in this region. However the 0° curve is complicated by the fact that some electrons passing through the α-detector produce small pulses. These small pulses from the α-detector are naturally in coincidence with the β-detector output. Therefore the small "$0^{\circ}\beta$"-spectrum must be subtracted from the 0° curve. The "$0^{\circ}\beta$"-spectrum is arbitrarily adjusted in size because normalization by the usual procedure consistently produces a negative number in the subtraction. The general shape of the "$0^{\circ}\beta$"-spectrum and the shapes of the 90° and 180° curves are used to extrapolate the 0° spectrum to zero pulse height.

The error in the coefficient, B, associated with this extrapolation is in the same direction for both Li^8 and B^8. Thus the difference, δ, should be less susceptible to this extrapolation. The three angle data with $W_\beta \simeq 11$ Mev has been treated as two angle data in an attempt to estimate the possible errors involved. The result is that B for Li^8 increases by $(0.0003) W_\beta$ and B for B^8 increases by $(0.0005) W_\beta$ giving only a net decrease in δ of $(0.0002) W_\beta$. The fact that two different coincidence mixer and limiter systems have been used with no noticeable change in results is also an indication that the low energy portions of the α-spectra are reliable.

The data taken with Li^8 β-energies of ~5 and ~8 Mev are much less susceptible to error in the extrapolation to zero pulse height because the Be^{8*} recoil is less. Figures 8 and 9 show the spectra in these cases. They also show an interesting change in shape at the high energy portion of the spectrum. Figure 18 shows a comparison of the 90° data at all three energies normalized to the same area. As seen in this figure, the high energy region of the α-spectrum in coincidence with electrons of ~11 Mev is much lower. This can be explained by the conservation of energy. The mass difference of Li^8 and two α-particles is 16.1 Mev. If the electron is required to take 10 or more Mev there is left 6 or less Mev to be shared between the two α-particles and neutrino. Thus there should be a cutoff at about 3 Mev in the α-spectrum. On the other hand, 5 Mev is less energy than the average of the whole β-spectrum and so one expects a higher than average number of counts at the high energy portion of the corresponding α-spectrum. The ~3 Mev α-energy cutoff associated with the ~11 Mev β-group does have the advantage of few counts over channel 100. For part of the runs the counts have been summed from channel 100 to 120 and stored in channel 0 of the analyzer. Above this the counts are discarded. For the rest of the ~11 Mev runs and all of the ~5 and ~8 Mev runs the counts are summed up to channel 160. For the ~11 Mev data the extension to channel 160 adds less than 1% to the number of coincidences and the error in A or B from neglecting these counts is less than $(0.0001)W_{\beta}$. For the lower β-energies, 8 to 12% of the total number of counts are over channel 100, which makes the extension to channel 160 imperative.

The α-spectra of random coincidences do not show the high energy cutoff which is evident in the coincident α-spectra. Figure 19 represents the sum of several groups of random coincident spectra from the data with $W_{\beta} \cong 11$ Mev. The coincident curve of figure 10 and the non-coincident curve of figure 4 are drawn for comparison. The random coincidences fit the non-coincident curve. This is to be expected because random coincidences are caused by the association of an electron from one Li^8 beta decay with an α-particle from another, unrelated decay.

Counting Rate Effects

Effects associated with the counting rate are appreciable only for the Li^8 decay since for the B^8 decay the counting rate is at least ten times smaller. The major effect is that of random coincidences in the fast coincidence mixer. These random coincidences are experimentally measured and subtracted from the real coincidences for the Li^8 measurements as discussed previously, but other effects are neglected. For the B^8 measurements all counting rate effects are neglected.

The other effects dependent on counting rate are (1) random coincidences in the slow coincidence mixer, (2) pile up of pulses into the β-discriminator, and (3) dead time in the β-discriminator circuit. All three sources are present in the measurement of coincidences, while the last two are also present in the measurements of the electron counts to which the coincidences are normalized. These effects can be expressed in the following equation for the ratio of real coincidences to non-coincident electrons of the correct energy:

$$\frac{N_c(\text{true})}{N_\beta(\text{true})} = \frac{N_c(\text{measured})[1-(\text{RCS})-(\text{PUP})+(\text{DTL})] - N_R}{N_\beta(\text{measured})[1-(\text{PUP})'+(\text{DTL})']}$$

$$\frac{N_c(\text{true})}{N_\beta(\text{true})} \simeq \frac{N_c(\text{measured})}{N_\beta(\text{measured})} [1 - (\text{RCS}) - (\text{PUP}) + (\text{PUP})' + (\text{DTL}) - (\text{DTL})'] - \frac{N_R}{N_\beta(\text{measured})}$$

where:

(RCS) = Random Coincidences in the Slow coincidence mixer, expressed as a fraction of the real coincidences

(PUP) = Pile Up of two Pulses into the β-discriminator, one of which is also in fast coincidence with an α-particle

(DTL) = Dead Time Losses of coincidences because the β-discriminator did not have sufficient time to recover from a previous pulse

(PUP)' = Pile Up of two Pulses into the β-discriminator, expressed as a fraction of the non-coincident electrons of correct energy. In this case neither pulse must be in coincidence with an α-particle

(DTL)' = Dead Time Losses of non-coincident electrons because of dead time in the β-discriminator circuit

N_R = Number of random coincidences from the fast coincidence mixer (not a fraction)

The fractional dead time losses are necessarily equal (and thus cancel) for the coincidences and normalization numbers since the dead time is caused by the same group of pulses in the same circuit. Fractional pile up can be slightly different in the two cases since the fast coincidence requirement imposes additional restrictions on some of the pulses, but they approximately cancel.

For the case of $W_\beta \simeq 11$ Mev, estimates of these fractions have been developed from the experimental parameters ($\tau_s = 1.2$ μsec.,

τ_{DT} = 6 μsec., N_β = 1000 per sec.) and approximations to the β-spectrum and β-pulse shape (the spectrum is assumed trapezoidal and the pulse shape is assumed a pure exponential with 1 μsec. decay constant). The results are the following:

$$\begin{array}{rcr} (\mathrm{RCS}) & = & 0.006 \\ (\mathrm{PUP}) & = & 0.030 \\ -(\mathrm{PUP})' & = & -0.032 \\ -(\mathrm{DTL})' & = & -0.006 \\ (\mathrm{DTL}) & = & \underline{0.006} \\ & & 0.004 \end{array}$$

Since N_R is about 0.03 times N_c, the neglected effects, (RCS), etc., add up to less than 20% of the measured randoms. However, neglecting these effects can also be justified for another reason. The reason is that the fractions, (RCS), etc., are only dependent on counting rate and thus, the numbers of spurious coincidences, $N_c \times$ (RCS), etc., have the same angular dependence as N_c alone. On the other hand, the number, N_R, is only dependent on counting rate and thus, the angular dependence of N_R is isotropic. This means that for a fixed counting rate, ignoring the effects, (RCS), etc., would have no effect on the measurements of the angular correlation of N_c, whereas ignoring N_R would make the angular correlation of N_c appear more nearly isotropic than it actually is. Of course in the experimental measurements, the counting rate is not fixed but the variations with angle of the β-detector in general are less than 5%.

The smallness of these effects does not justify a detailed estimate for the cases with $W_\beta \simeq 5$ Mev or 8 Mev. Qualitatively, it can be seen that (RCS) would remain about the same for the same counting rate, (PUP) would decrease, and (DTL) would increase. The net result would be about the same as for the case with $W_\beta \simeq 11$ Mev so that corrections for only the measured numbers of random coincidences is quite adequate.

Second order effects such as a simultaneous random coincidence in both slow and fast coincidence mixers are truly negligible. Also the dead time of the 100 channel analyzer produces a negligible effect ($N_c \simeq 10$ per sec., $\tau \simeq 50$ μsec.). Pile up of two α-particle pulses during the time scale of the slow coincidence mixer may exist, but would not add nor subtract from the recorded number of coincidences. However, it could produce a slight distortion of the coincident α-spectrum.

Symmetry of the Counting Arrangement

Symmetry conditions are of prime importance in this experiment. Four sources of asymmetry may be present: (1) variation in the number of scattered electrons with angle, (2) variation in the β-detector gain with angle, (3) Li^8 or B^8 ions recoiling out of the target and decaying on the walls of the target chamber, and (4) variation in the α-detector solid angle with the position of the β-detector.

The first source has been minimized by the design of the target chamber. It should be negligible, especially for the 11-Mev electrons. Electrons which scatter out of the solid angle of the β-detector do not affect the results.

The second source of asymmetry would arise from the sensitivity of the photomultiplier to stray magnetic fields. The gain has been checked with the ThC" γ-ray source. The source is fastened to the β-detector and the number of counts above a fixed bias is recorded as the detector assembly is rotated. The bias is equivalent to about channel 65 in figure 7, so that a small change in gain shows up as a larger change in the number of counts. With the beam analyzing magnet turned on, the variation in the number of counts with angle is less than 1/2%. Also with the detector in a fixed position, the variation in counts is less than 1/2% while turning the magnet off and on. These measurements would indicate that the systematic change in gain with angle is negligible for the purposes of the experiment. Any effects on the number of counts because of gain changes are compensated by the normalization procedure.

The third source of asymmetry, Li^8 or B^8 ions recoiling out of the target, makes the target shield a necessity. The half angle of the cone of recoiling Li^8 ions is 33^o, of the B^8 ions 8^o. With the target at 15^o some of the Li^8 ions recoil out of the target while the B^8 ions do not. These Li^8 ions are caught by the target shield which drops into its lead container during the counting period. To test this system, the target is fastened to the shield and the ratio of electrons detected with the shield moving up and down in its normal cycle to the number of electrons with the shield always up is measured. This ratio is about 0.1%, and there is small variation in the ratio with the angle of the β-detector. This indicates that the shield is completely effective in catching the escaping Li^8 ions.

The fourth point, variation in the α-detector solid angle, is potentially the most serious. A variation in solid angle could occur if the weight of the β-detector assembly warped the table enough to cause a change in relative position of α-detector and target or of the beam position and target. Mounting the target and α-detector in the same mount should reduce the chance of relative motion between them and evaporating the lithium targets in the form of a narrow strip should reduce the possibility of motion of the target spot caused by lateral motion of the beam. The purpose of the monitor counter, which in part of the experiment is an electron detector and in the other part is an α-particle detector, is to check on this point. From the ratio of its counts to the non-coincident α-particles the solid angle of the α-detector varies on the average less than 0.2%. This would indicate that the α-detector solid angle is suitably constant, and that the correct procedure is to normalize the coincidences by the number of electrons analyzed by the β-discriminator, as has been done in the experiment. There is one indication that signifies that the system is slightly asymmetrical. The difference in the Li^8 and B^8 cases of the variation with angle of the ratio of α-particles to electrons analyzed by the differential discriminator averages over all groups to about 0.01. This means that the final result for δ would be decreased by about $(0.001)\,W_\beta$ if the coincidences were normalized to the single α-particle counts instead of to the electron counts. However, the β-detector can have a different efficiency at the different angles for various reasons. For example, the dummy α-detectors may be slightly different in thickness or the target may not be exactly on the axis of rotation of the β-detector. If the α-detector solid angle is constant, the normalization procedure compensates the data for changes in the β-detector efficiency.

Discussion of Results

The sources of systematic error discussed above must be quantitatively estimated in a form compatible with the stated statistical errors, in order to evaluate the overall reliability of the results, and especially of the quantity, δ. Although this is a somewhat arbitrary procedure, table IV lists estimates of the limits of possible errors associated with (1) statistics, (2) calibration of the β-spectrum, (3) integration over the α-spectrum, (4) counting rate effects, and (5) symmetry conditions. The column marked "RMS Sum" is the square root of the sum of the squares of the numbered columns. In the cases where $W_\beta \simeq 11$ Mev, a significant number of groups of data are averaged together to give the final results. The groups are illustrated in the histogram of figure 14. It is instructive to compare the experimental RMS deviation of these groups with the other errors. The RMS deviation of the mean, found by weighting the data samples in the same way as they are weighted to calculate the mean, is given in the column marked "Exp. RMS." The numbers in this column are very nearly equal to the statistical errors alone. This is an indication that the systematic errors are relatively constant for all groups of data or that the systematic errors average out to zero over the number of runs in a group.

In the previous sections, the angular correlation has been discussed in its general form:

$$W(\theta_{\beta\alpha}) = 1 + A \cos \theta_{\beta\alpha} + B \cos^2\theta_{\beta\alpha}$$

where A and B are functions of the momentum of the α-particle and electron. The actual functional dependence of A or B contains terms

TABLE IV

Estimates of Errors of the Coefficients, A/W_β and B/W_β

Beta Decay	W_β (Mev)	Coef-ficient	Exp. Result	Errors[*]						
				Exp. RMS	(1)	(2)	(3)	(4)	(5)	RMS Sum
Li^8	5	A/W_β	-0.0073		0.0006	0.0008	0.0001	0.0001	0.0004	0.0011
		B/W_β	0.0023		0.0008	0.0004	0.0001	0.0001	0.0004	0.0010
Li^8	8	A/W_β	-0.0072		0.0006	0.0008	0.0002	0.0001	0.0003	0.0011
		B/W_β	0.0033		0.0008	0.0004	0.0002	0.0001	0.0003	0.0010
Li^8	11	A/W_β	-0.0087	0.0003	0.0002	0.0004	0.0003	0.0001	0.0002	0.0006
		B/W_β	0.0029	0.0003	0.0003	0.0002	0.0003	0.0001	0.0002	0.0005
B^8	11	A/W_β	-0.0088	0.0003	0.0005	0.0005	0.0004	--	0.0004	0.0009
		B/W_β	-0.0040	0.0007	0.0007	0.0002	0.0004	--	0.0004	0.0009
Li^8-B^8	11	δ/W_β	0.0069		0.0008	0.0004	0.0003	0.0001	0.0006	0.0011

[*] For detailed description of the various errors listed, see accompanying text.

arising from kinematic considerations of the transformation from the Be^{8*} rest system to the laboratory system and from interference of forbidden transition matrix elements with the allowed axial vector matrix element. The complete transformation has been carried to second order in the electron momentum. A description of the transformation is given in Appendix D. This transformation was first worked out by F. B. Morinigo after B. Stech and J. Eichler (47) pointed out the form employed in the reduction of the data for the first part of the experiment was inaccurate. Only the interference terms of interest with respect to the C. V. C. theory are included in the correlation. The result from Appendix D is:

$$W(\theta_{\beta\alpha}) = 1 - [p < \frac{1}{p_\alpha}(90^\circ) > + \frac{3}{2} ap^2 < \frac{1}{p_\alpha}(90^\circ) >] \cos \theta_{\beta\alpha}$$

$$+ [ap + \frac{5}{8} p^2 < \frac{1}{p_\alpha}(90^\circ) >^2] \cos^2 \theta_{\beta\alpha}$$

where $\underline{a}$ is the quantity defined in the introduction which is enhanced in the C. V. C. theory relative to the Fermi theory. It changes sign in the Li^8 and B^8 decays. If the terms arising from interference of forbidden axial vector with allowed axial vector matrix elements were included, they would be similar to the terms with the quantity, $\underline{a}$, but would not change sign (21). Including all such terms into the completely unknown quantities, $\underline{b}$ and $\underline{b}'$, and with the approximation, $W_\beta \simeq p$, the coefficients, A and B, are the following:

$$A = - [< \frac{1}{p_\alpha}(90^\circ) > (1 + \frac{3}{2} ap) + b] W_\beta$$

$$B = [a + \frac{5}{8} p < \frac{1}{p_\alpha}(90^\circ) >^2 + b'] W_\beta$$

and therefore,

$$\delta = B(Li^8) - B(B^8) = |2a| W_\beta$$

Since the quantity, δ, is a difference, all of the small terms which do not change sign in the two decays cancel. Weidenmuller's calculation (27) of the quantity, δ, shows that it is given in the two theories of beta decay by:

Fermi theory $$\delta = 0.012 \frac{<|\ell + \sigma|>}{<|\sigma|>} \frac{p^2}{W_\beta W_o}$$

C. V. C. theory $$\delta = 0.012 \frac{<|\ell + 4.7\sigma|>}{<|\sigma|>} \frac{p^2}{W_\beta W_o}$$

where $<|\ell|>$ and $<|\sigma|>$ are dimensionless matrix elements of the orbital angular momentum and spin. With Weidenmuller's quantitative limits for these matrix elements the predictions are:

Fermi theory $(0.001) W_\beta < \delta < (0.004) W_\beta$

C. V. C. theory $(0.005) W_\beta < \delta < (0.009) W_\beta$

The experimental result, $\delta = (0.0069 \pm 0.0011) W_\beta$, definitely favors the C. V. C. theory. Even if all the estimates of systematic errors happened to be in the same direction, the estimated total error would be $(\pm 0.0022) W_\beta$, and the result would still slightly favor the C. V. C. theory. However, it must be emphasized that the theoretical predictions depend on a calculation of the analogous M1 γ-ray transition by an intermediate coupling model. It clearly would be advantageous to determine experimentally this γ-ray transition rate. If the C. V. C. theory is assumed valid, the present experiment predicts a width, $\Gamma_\gamma(M1) = (1.9 \pm 0.6)$ ev.

Although the errors of the experimental results are about the same size as the second order terms of the theoretical forms for A and B, a comparison may give some indication of the size of the terms arising from interference of forbidden axial vector with allowed axial vector matrix elements. From a previous magnetic analysis of the α-spectrum by C. A. Barnes, et al (13), the average of the reciprocal of the α-momentum is calculated to be $< \frac{1}{p_\alpha}(90^\circ) > = 0.0093 \left(\frac{\text{Mev}}{c} \right)^{-1}$ for a β-energy about 11 Mev. This times $(-)W_\beta$ is the leading term in the theoretical form of A. Therefore, to first order in $\frac{p}{p_\alpha}$, $A = (-0.0093)W_\beta$. The second order term, $[-\frac{3}{2}\,ap < \frac{1}{p_\alpha}(90^\circ)>]\,W_\beta$, changes sign in the two decays. For $p = 11$ Mev/c and $a = 0.0035$, this term is $(-0.0005)W_\beta$ for Li^8 and $(+0.0005)W_\beta$ for B^8. Thus, the theoretical values are $A = (-0.0098-b)W_\beta$ for Li^8 and $A = (-0.0088-b)W_\beta$ for B^8. These are to be compared with experimental values of $A = (-0.0087 \pm 0.0006)W_\beta$ for Li^8 and $A = (-0.0088 \pm 0.0009)W_\beta$ for B^8. The experimental errors are about the same size as the expected difference between the two determinations of A. Using an average value would indicate that b is about -0.0005.

The first order term in the theoretical expression for B is the quantity, aW_β, which is the major point of the experiment. The second order term, $[\frac{5}{8}\,p < \frac{1}{p_\alpha}(90^\circ) >^2]\,W_\beta$, equals $(+0.0006)W_\beta$ for $p = 11$ Mev/c. One half of the sum of the theoretical expressions for the B^8 and Li^8 cases is equal to the second order terms, $(+0.0006 + b')W_\beta$. One half of the sum of the experimental measurements, $B = (0.0029 \pm 0.0005)W_\beta$ for Li^8 and $B = (-0.0040 \pm 0.0009)W_\beta$ for B^8, is equal to $(-0.0005)W_\beta$.

This would indicate $\underline{b}'$ is about -0.001. Thus, the experiment, besides measuring the V-A interference ($\underline{a}$), suggests that A-A interference ($\underline{b}$ or $\underline{b}'$) is present but is smaller.

In the cases of the Li^8 data with the lower β-energies, the theoretical value of the coefficient, A, is slightly smaller because of the change in the shape of the α-spectrum, and resulting change in value of $<\frac{1}{p_\alpha}(90^\circ)>$. The changes in the spectra are illustrated in figure 18. A numerical integration of $\frac{1}{p_\alpha}$ over these spectra give the results, $<\frac{1}{p_\alpha}(90^\circ)> = 0.0083\ (\frac{Mev}{c})^{-1}$ for $W_\beta \simeq 5$ Mev and $<\frac{1}{p_\alpha}(90^\circ)> = 0.0088\ (\frac{Mev}{c})^{-1}$ for $W_\beta \simeq 8$ Mev, based on the value, $<\frac{1}{p_\alpha}(90^\circ)> = 0.0093\ (\frac{Mev}{c})^{-1}$ for $W_\beta \simeq 11$ Mev. The experimental results for A are both smaller than the values predicted by the theoretical forms using the above results for $<\frac{1}{p_\alpha}(90^\circ)>$. The experimental results are $A = (-0.0073 \pm 0.0011)\,W_\beta$ for $W_\beta \simeq 5$ Mev and $A = (-0.0072 \pm 0.0011)\,W_\beta$ for $W_\beta \simeq 8$ Mev. While the differences of these results from the theoretical values are statistically not very significant, they again are an indication of the term, $\underline{b}$, of order -0.001.

The main reason for taking data at the various β-energies is to show that the coefficient, B, is linear in energy, W_β. The experimental results do show this within the experimental errors.

$$B = (0.0023 \pm 0.0010)\,W_\beta \qquad \text{for } W_\beta \simeq 5 \text{ Mev}$$

$$B = (0.0033 \pm 0.0010)\,W_\beta \qquad \text{for } W_\beta \simeq 8 \text{ Mev}$$

$$B = (0.0029 \pm 0.0005)\,W_\beta \qquad \text{for } W_\beta \simeq 11 \text{ Mev}$$

This checks that the measurement is of the quantity, aW_β, since $\underline{a}$ is independent of energy. The size of the experimental errors does not warrant any statement about the second order terms in the theoretical form of B at the lower β-energies.

To improve the accuracy of the present experiment would require redesign of the experiment in almost every detail, in view of the comparable size of the various estimated systematic errors. For any particular run the statistics are the major source of error. However, when many runs are averaged together, the other effects become relatively more important. The statistical error can be improved only by taking more data. The energy calibration of the β-spectrum possibly could be improved by a more elaborate scintillation counter and certainly by use of a β-spectrometer. Ideally the integration over the α-spectrum would be no problem if a really thin target could be made, and noiseless, electron insensitive α-detectors were available. Counting rate effects already are small but can be reduced to any desired degree by slower counting rates. Symmetry is possibly the hardest point to improve and is also very difficult to check. It may be that with a thin enough target, the α-detector could be rotated relative to a fixed β-detector to achieve more nearly symmetrical conditions. Most of the suggested improvements would require a sacrifice of counting rate, which in the present experiment is already rather low.

APPENDIX A

Semiconductor Surface Barrier Detectors (35-38, 48-54)

The operation of a semiconductor detector is based on the creation of electron-hole ion pairs in the semiconductor by an energetic charged particle. In an applied field these ion pairs are free to drift and they result in a sudden charge at the contacts of the detector after the passage of the particle. The detectors' usefulness arises from the facts (1) that the region of applied field is thick enough to stop particles of a few Mev, (2) that the output charge is linearly dependent on the particle energy, (3) that the output pulse rise time is of the order of one mμ sec., and (4) that the number of ion pairs created is of an order of magnitude greater than the number in a gas ionization chamber. For the generation of the high field region two techniques are available: surface barriers and diffused p-n junctions. Both silicon and germanium are used to construct detectors of large sensitive areas. Germanium detectors must be cooled to near liquid nitrogen temperature while silicon detectors operate well at temperatures up to at least 45°C.

The present experiment was performed with gold-silicon surface barrier detectors but both gold-silicon and gold-germanium detectors have been constructed and tested. This Appendix outlines the general properties of semiconductor detectors, compares measurement with theory, and describes the steps in their construction.

The particles to be detected enter the surface barrier detector after passing through the thin gold surface contact. This gold layer is deposited by evaporation and can be made thin enough (less than 0.1

micron) so that a negligible amount of energy is lost in it. In n-type material the particle-sensitive depletion layer is formed by biasing the gold surface negative with respect to the bulk material. If its range is less than the thickness of the depletion layer, a particle of energy, E, produces a charge, Q, on the contacts, where $Q = eE/\epsilon$. e is the electron charge and ϵ is the mean energy required to create an electron-hole pair. The effective value of ϵ in silicon and germanium has been measured with 5.3 Mev α-particles. It is plotted in figure 20 as a function of the applied bias voltage. For a bias above a certain voltage the depletion layer thickness is greater than the range of the α-particles and negligible recombination of the electron-hole pairs occurs. In this region ϵ is constant, and is measured to be 3.0 ev for germanium and 3.8 ev for silicon with estimated errors of 5%. The accepted values are 3.0 ev and 3.6 ev (54). Experimentally it has been shown that ϵ is independent of the value of dE/dx for the particle, even for particles of extremely different dE/dx such as fission fragments and electrons (54).

The result of ϵ being constant is that the output pulse height is proportional to the incident energy. Figure 21 shows the general form of results obtained with various silicon detectors for protons and α-particles. For a particle energy up to the point where its range equals the depletion layer depth the curve is linear. The pulse height shows a further increase as the range exceeds the depletion layer depth because of diffusion of the electron-hole pairs in the bulk semiconductor back to the high field depletion layer. This portion of the curve is sensitive to the decay time of the electronic circuitry since the diffusion is a relatively slow process. Above a certain energy the pulse height falls because of the decreasing stopping power with increasing energy.

Two properties of interest, the thickness of the depletion layer and the capacitance of the surface barrier detector, are satisfactorily described by a theory devised by W. Schottky (55, 56, 57, 35). Because the surface and bulk fermi levels must adjust to the same level, the surface charge is compensated by a region of opposite charge extending into the semiconductor. This region is called the depletion layer since it is devoid of free electrons and is thus left with a net density of charged donor impurities. The thickness of the depletion layer, x, is given by:

$$x = \left(\frac{2K\epsilon_o}{eN}\right)^{1/2} (\psi_s + V)^{1/2} = (2K\epsilon_o \rho \mu_n)^{1/2} (\psi_s + V)^{1/2}$$

where:

ψ_s = the difference of the surface and bulk fermi potentials (approximately half the band gap)

V = the applied bias voltage

N = the net density of donor impurities

K = the dielectric constant

ϵ_o = the permittivity of free space

μ_n = the electron mobility

ρ = the resistivity = $\frac{1}{eN\mu_n}$

For silicon detectors at bias voltages large enough to neglect ψ_s, the thickness, x, is approximately given in microns by:

$$x \simeq 0.5(\rho V)^{1/2}$$

This result shows that thicker depletion layers can be obtained with higher bias voltages, higher resistivity material, or both.

The small signal behavior of a surface barrier detector is approximately that of a capacitor. The capacitance is that of a parallel plate capacitor with plate separation, x, and dielectric constant, K. The capacitance per unit area is given by:

$$C = \frac{K\epsilon_o}{x} = \left(\frac{K\epsilon_o}{2\rho\mu_n}\right)^{1/2} \frac{1}{(\psi_s + V)^{1/2}}$$

and thus:

$$1/C^2 = \frac{2\rho\mu_n(\psi_s + V)}{K\epsilon_o}$$

In figure 22 measured values of $1/C^2$ for a silicon detector are plotted vs the bias voltage, V. The slope of the line is calculated with a resistivity of 170 Ωcm. For this sample of silicon 10 volts bias results in about 500 μμf per cm^2.

The above formula indicates that the energy in the output pulse, which equals $Q^2/2C$, increases approximately as $(\rho V)^{1/2}$ for high bias voltages. However the bias voltage cannot be increased indefinitely without causing a large leakage current which produces increased noise. Also the resistivity, ρ, cannot be increased indefinitely because the maximum available resistivity in silicon is about 10,000 Ωcm, although intrinsic silicon would have a resistivity of about 230,000 Ωcm (58).

Some useful quantities for germanium and silicon are given in the following table.

TABLE V

Properties of Silicon and Germanium

Property	Unit	Silicon	Germanium
Dielectric Constant, K	--	12	16
Band Gap Energy, E_g	ev	1.1	0.7
Electron Mobility, μ_n	cm^2/volt-sec.	1300	3900
Hole Mobility, μ_p	cm^2/volt-sec.	480	1900
Energy Loss per Ion Pair	ev	3.6	3.0
Density	gm/cm^3	2.33	5.32

The order of magnitude of the rise time of the pulse produced by an incident particle can be calculated from the electron and hole mobilities and the depletion layer thickness and field in which the ion pairs are created.

$$\tau \simeq \frac{x}{v} \simeq \frac{x}{\mu_n(V/x)} \simeq \frac{x^2}{\mu_n V} \simeq 2K\epsilon_o\rho$$

Note that this expression is independent of bias voltage. For silicon τ is approximately given by:

$$\tau \simeq 2 \times 10^{-3}\rho \ \text{m}\mu\text{sec.}$$

Although high resistivity materials have the advantage of thicker depletion layers and smaller capacitance, they have the disadvantage of longer rise times. Also the situation is more complicated for high resistivity material because of the rise time associated with the series resistance of the bulk material and the input capacitance of the preamplifier. When the range of the incident particle is greater than the depletion layer thickness, a slowly rising pulse is superimposed on the fast pulse. The slower rise time is of the order of several hundred mμsec.

Figure 5 shows the response to 5.3 Mev α-particles of a typical detector used in this experiment and also that of a smaller detector. Since the number of generated electron-hole pairs is large ($n = E/\epsilon = 5.3 \times 10^6/3.6 = 1.47 \times 10^6$), the statistics of this process do not determine the resolution ($n/\Delta n = n/\sqrt{n} = \sqrt{n} = 1.2 \times 10^3$). If the response is gaussian, the full width at half maximum is given by 2.35σ and the resolution is defined as the energy of the peak divided by σ. Other workers have obtained resolutions of 0.7×10^3 for gold-silicon barriers (49). It is mainly the noise in the counter generated by excess surface current which limits the resolution. Amplifier noise also contributes but is of an order of magnitude smaller than the noise of the detector with 5% full width at half maximum. Crystal inhomogeneities and defects also tend to reduce the resolution.

Figure 23 shows the direct current characteristics of several silicon and germanium detectors. The reverse current is mainly surface leakage except at low bias voltages. A qualitative relationship has been observed that a detector with lower reverse current exhibits a higher resolution. The reverse current and the resolution vary with time. Generally a detector deteriorated in vacuum but sometimes could be improved temporarily by washing the surface, heating slightly, or just standing in air. When a detector became too noisy to use it exhibited a large amount of noise with a low frequency spectrum. The noise passed by the 80 mμsec. clipping time did not increase so much.

No particular routine has been rigorously adhered to in the construction of gold-silicon detectors, but the general procedures are listed below.

(1) A sample of silicon is sliced to ~ 1 mm thickness with a diamond embedded saw. The wafers are cut into squares of the desired size. (5/16" is usual for the present experiment.)

(2) The wafers are lapped with # 600 carborundum. A few detectors have been further polished with fine garnet but no definite improvement in results is found.

(3) The lapped wafers are etched in a polyethylene beaker of CP-4 for about 1 minute. The beaker is agitated to remove bubbles from the silicon. The CP-4 heats up from the reaction with silicon. CP-4 consists of the following:

1 part concentrated hydrofluoric acid by volume
1 part glacial acetic acid
1-1/2 parts concentrated nitric acid.

(4) The etch is diluted with distilled water before removing the silicon wafer. The wafer is then washed in distilled water and dried on tissue paper. After etching, care is taken not to handle the wafer with the fingers.

(5) The crystal is mounted. Generally silver conducting paint is used to make the back contact for silicon detectors and indium solder is used for germanium. Some detectors have been

potted in epoxy resin and others have been left exposed to air.

(6) The gold surface is evaporated onto the crystal through a mask. The thickness of the gold roughly cuts the transmission of light by 1/2. For the epoxy mounted detectors the gold is also evaporated on the epoxy and thus makes contact to a pin beside the wafer. For the open detectors the contact is made by a narrow strip of 1-mil gold foil stuck to the gold surface with silver conducting paint.

APPENDIX B

Integration Over Detector Solid Angles

In the laboratory system the β-α angular correlation can be written as:

$$W(\theta_{\beta\alpha}) = 1 + A \cos \theta_{\beta\alpha} + B \cos^2 \theta_{\beta\alpha}$$

where the coefficients, A and B, are functions of the electron and α-particle momenta. The experimentally measured distribution represents the average of this correlation over the finite solid angles of the β- and α-detectors. Hence, in order to relate A and B to the experimental data, $W(\theta_{\beta\alpha})$ must be integrated over the solid angles. Both detectors have solid angles defined by circular apertures. The finite size of the target spot also tends to smear the experimental angular correlation, but this effect is negligible compared to that from the detector apertures. For each position, $\theta_{\beta\alpha} = 0^\circ, 90^\circ$, and 180°, the number of coincidences is proportional to the value of the normalized double integral:

$$\frac{\int_{\Omega_\beta} \int_{\Omega_\alpha} W(\theta_{\beta\alpha})\, d\Omega_\alpha d\Omega_\beta}{\int_{\Omega_\beta} \int_{\Omega_\alpha} d\Omega_\alpha d\Omega_\beta}$$

Figure 24(a) illustrates the geometry and defines the appropriate angles for the 0° and 180° configurations. Let σ be the azimuthal angle and η be the polar angle of the infinitesimal solid angle $d\Omega_\alpha$ in the α-detector, which has a maximum polar angle θ_α. Let λ be the azimuthal angle and δ be the polar angle of the infinitesimal solid angle $d\Omega_\beta$ in the β-detector, which has a maximum polar angle θ_β. Then

$$d\Omega_\alpha = -d\sigma\, d(\cos\eta); \qquad d\Omega_\beta = -d\lambda\, d(\cos\delta)$$

From a theorem of spherical trigonometry:

$$\cos\theta_{\beta\alpha}(0^\circ) = -\cos\theta_{\beta\alpha}(180^\circ) = \cos\delta\cos\eta + \sin\delta\sin\eta\cos(\lambda+\sigma)$$

$$= \cos\delta\cos\eta + \sin\delta\sin\eta(\cos\lambda\cos\sigma - \sin\lambda\sin\sigma)$$

where $\cos\theta_{\beta\alpha}(0^\circ)$ means $\cos\theta_{\beta\alpha}$ measured in the 0°-detector arrangement. Thus for the 0° and 180° arrangements:

$$\int_{\Omega_\beta}\int_{\Omega_\alpha} W(\theta_{\beta\alpha})\, d\Omega_\alpha d\Omega_\beta = \int_0^{\theta_\beta}\int_0^{2\pi}\int_0^{\theta_\alpha}\int_0^{2\pi} \{1 \pm A[\cos\delta\cos\eta$$

$$+ \sin\delta\sin\eta(\cos\lambda\cos\sigma - \sin\lambda\sin\sigma)] + B[\cos^2\delta\cos^2\eta$$

$$+ 2\cos\lambda\cos\eta\sin\delta\sin\eta(\cos\lambda\cos\sigma - \sin\lambda\sin\sigma)$$

$$+ \sin^2\delta\sin^2\eta(\cos^2\lambda\cos^2\sigma - 2\cos\lambda\cos\sigma\sin\lambda\sin\sigma$$

$$+ \sin^2\lambda\sin^2\sigma)]\}\, d\sigma\, d(\cos\eta)\, d\lambda\, d(\cos\delta)$$

where the + sign applies to 0° and the - sign applies to 180°. The integration over σ and λ yields:

$$\int_{\Omega_\beta}\int_{\Omega_\alpha} W(\theta_{\beta\alpha})\, d\Omega_\alpha d\Omega_\beta = (2\pi)^2\int_0^{\theta_\beta}\int_0^{\theta_\alpha} \{1 \pm A[\cos\delta\cos\eta]$$

$$+ B[\cos^2\delta\cos^2\eta + \frac{1}{2}\sin^2\delta\sin^2\eta]\}\, d(\cos\eta)\, d(\cos\delta)$$

and the integration over η and δ yields:

$$\int_{\Omega_\beta}\int_{\Omega_\alpha} W(\theta_{\beta\alpha})\, d\Omega_\beta d\Omega_\alpha = (2\pi)^2(1 - \cos\theta_\beta(1 - \cos\theta_\alpha) \{1$$

$$\pm \frac{A}{4}[(1 + \cos\theta_\beta)(1 + \cos\theta_\alpha)]$$

$$+ \frac{B}{6}[\cos\theta_\beta \cos\theta_\alpha(1 + \cos\theta_\beta)(1 + \cos\theta_\alpha) + 2]\}$$

Dividing by the solid angles of the detectors gives the following expression for the normalized integral:

$$\frac{\int_{\Omega_\beta}\int_{\Omega_\alpha} W(\theta_{\beta\alpha}) d\Omega_\alpha d\Omega_\beta}{\int_{\Omega_\beta}\int_{\Omega_\alpha} d\Omega_\alpha d\Omega_\beta} = 1 \pm \frac{A}{4}[(1 + \cos\theta_\beta)(1 + \cos\theta_\alpha)]$$

$$+ \frac{B}{6}[\cos\theta_\beta \cos\theta_\alpha(1 + \cos\theta_\beta)(1 + \cos\theta_\alpha) + 2]$$

Figure 24(b) illustrates the angles involved in the 90° configuration. The angles, σ, η, λ, and δ, are defined as before. Also ϕ is defined as the angle between (1) the line joining the target and the center of the α-detector and (2) the line joining the target and the infinitesimal solid angle $d\Omega_\beta$. Then:

$$\cos\phi = \cos\delta \cos 90^\circ + \sin\lambda \sin 90^\circ \sin\lambda = \sin\delta \cos\lambda$$

Also define ζ as the projection of the angle δ on the plane parallel to the surface of the α-detector. It can be shown:

$$\cos\zeta = \frac{\cos\delta}{(1 - \sin^2\delta \cos^2\lambda)^{1/2}} \; ; \; \sin\zeta = \frac{\sin\delta \sin\lambda}{(1 - \sin^2\delta \cos^2\lambda)^{1/2}}$$

Applying the theorem of spherical trigonometry a second time yields:

$$\cos\theta_{\beta\alpha} = \cos\phi\cos\eta + \sin\phi\sin\eta\cos(\sigma-\zeta)$$

$$= \sin\delta\cos\lambda\cos\eta + \sin\eta(\cos\sigma\cos\delta + \sin\sigma\sin\delta\sin\lambda)$$

Thus, for the 90° arrangement:

$$\int_{\Omega_\beta}\int_{\Omega_\alpha} W(\theta_{\beta\alpha})d\Omega_\alpha d\Omega_\beta = \int_0^{\theta_\beta}\int_0^{2\pi}\int_0^{\theta_\alpha}\int_0^{2\pi} \{1 + A[\sin\delta\cos\lambda\cos\eta$$

$$+ \sin\eta(\cos\sigma\cos\delta + \sin\sigma\sin\delta\sin\lambda)] + B[\sin^2\delta\cos^2\lambda\cos^2\eta$$

$$+ 2\sin\delta\cos\lambda\cos\eta\sin\eta(\cos\sigma\cos\delta + \sin\sigma\sin\delta\sin\lambda)$$

$$+ \sin^2\eta(\cos^2\sigma\cos^2\delta + 2\cos\sigma\cos\delta\sin\sigma\sin\delta\sin\lambda$$

$$+ \sin^2\sigma\sin^2\delta\sin^2\lambda)]\}\, d\sigma\, d(\cos\eta)\, d\lambda\, d(\cos\delta)$$

The integration over σ and λ yields:

$$\int_{\Omega_\beta}\int_{\Omega_\alpha} W(\theta_{\beta\alpha})\, d\Omega_\beta d\Omega_\alpha = (2\pi)^2\int_0^{\theta_\beta}\int_0^{\theta_\alpha}\{1$$

$$+ \frac{B}{4}[1 + \cos^2\eta + \cos^2\delta - 3\cos^2\eta\cos^2\delta]\}\, d(\cos\eta)\, d(\cos\delta)$$

And the integration over η and δ yields:

$$\int_{\Omega_\beta}\int_{\Omega_\alpha} W(\theta_{\beta\alpha})d\Omega_\alpha d\Omega_\beta = (2\pi)^2(1 - \cos\theta_\beta)(1 - \cos\theta_\alpha)\{1$$

$$+ \frac{B}{12}[4 - \cos\theta_\beta\cos\theta_\alpha(1 + \cos\theta_\beta)(1 + \cos\theta_\alpha)]\}$$

Normalization gives the following expression for the 90° configuration:

$$\frac{\int_{\Omega_\beta}\int_{\Omega_\alpha} W(\theta_{\beta\alpha})\,d\Omega_\alpha\,d\Omega_\beta}{\int_{\Omega_\beta}\int_{\Omega_\alpha} d\Omega_\alpha\,d\Omega_\beta} = 1 + \frac{B}{12}\left[4 - \cos\theta_\beta \cos\theta_\alpha (1+\cos\theta_\beta)(1+\cos\theta_\alpha)\right]$$

In the experimental apparatus, $\theta_\beta = 19^{\circ}40'$ and $\theta_\alpha = 9^{\circ}$. Using these values results in the following numbers for the integrals of $W(\theta_{\beta\alpha})$ over the detector solid angles:

0°: $1 + 0.965\,A + 0.932\,B$

90°: $1 + 0.034\,B$

180°: $1 - 0.965\,A + 0.932\,B$

APPENDIX C

Solution for the Coefficients, A and B

The number of β-α coincident counts in each configuration (0°, 90°, 180°) is proportional to the angular distribution function, $W(\theta_{\beta\alpha})$, integrated over the detector solid angles, as in Appendix B. This is a function of the unknowns, A and B, which are to be determined, and also an unknown proportionality factor, n'. Let $n(0^\circ)$, $n(90^\circ)$, and $n(180^\circ)$ be the normalized number of coincidences measured at each angle. Then:

$$(1) \qquad n(0^\circ) = n'(1 + f_1 A + f_2 B)$$

$$(2) \qquad n(90^\circ) = n'(1 + f_3 B)$$

$$(3) \qquad n(180^\circ) = n'(1 - f_1 A + f_2 B)$$

where $f_{1,2,3}$ are the integrals of Appendix B, $f_1 = 0.965$, $f_2 = 0.932$, $f_3 = 0.034$. Rewriting equation (2):

$$n' = \frac{n(90^\circ)}{1 + f_3 B}$$

Adding and subtracting equations (1) and (3) yields equations for B and A respectively:

$$B = \frac{n(0^\circ) + n(180^\circ) - 2n(90^\circ)}{2f_2 n(90^\circ) - f_3 n(0^\circ) - f_3 n(180^\circ)}$$

$$A = \frac{n(0^\circ) - n(180^\circ)}{2f_1 n(90^\circ)} \left[1 + f_3 \frac{n(0^\circ) + n(180^\circ) - 2n(90^\circ)}{2f_2 n(90^\circ) - f_3 n(0^\circ) - f_3 n(180^\circ)} \right]$$

$$A \simeq \frac{n(0^\circ) - n(180^\circ)}{2f_1 n(90^\circ)}$$

For the purpose of calculating the standard deviations of the coefficients, A and B, arising from the statistical errors in $n(0^\circ)$, $n(90^\circ)$, and $n(180^\circ)$, the various partial derivatives are needed:

$$\frac{\partial B}{\partial n(0^\circ)} = \frac{\partial B}{\partial n(180^\circ)} = \frac{2(f_2 - f_3)n(90^\circ)}{[2f_2 n(90^\circ) - f_3 n(0^\circ) - f_3 n(180^\circ)]^2}$$

$$\frac{\partial B}{\partial n(90^\circ)} = \frac{-2(f_2 - f_3)[n(0^\circ) + n(180^\circ)]}{[2f_2 n(90^\circ) - f_3 n(0^\circ) - f_3 n(180^\circ)]^2}$$

The approximation, $n(90^\circ) \simeq \frac{1}{2}[n(0^\circ) + n(180^\circ)]$, is accurate enough for this purpose and simplifies the partial derivatives to the following:

$$\frac{\partial B}{\partial n(0^\circ)} = \frac{\partial B}{\partial n(180^\circ)} = \frac{1}{2(f_2 - f_3)n(90^\circ)}$$

$$\frac{\partial B}{\partial n(90^\circ)} = \frac{-1}{(f_2 - f_3)n(90^\circ)}$$

The standard deviation of B is found by using the general rule for the combination of independent errors:

$$\Delta B = \left\{ \left[\frac{\partial B}{\partial n(0^\circ)} \right]^2 \Delta^2 n(0^\circ) + \left[\frac{\partial B}{\partial n(90^\circ)} \right]^2 \Delta^2 n(90^\circ) + \left[\frac{\partial B}{\partial n(180^\circ)} \right]^2 \Delta^2 n(180^\circ) \right\}^{1/2}$$

$$\Delta B = \frac{1}{2(f_2 - f_3)n(90^\circ)} \left[\Delta^2 n(0^\circ) + 4\Delta^2 n(90^\circ) + \Delta^2 n(180^\circ) \right]^{1/2}$$

Similarly for A:

$$\frac{\partial A}{\partial n(0^{\circ})} = \frac{-\partial A}{\partial n(180^{\circ})} = \frac{1}{2f_1 n(90^{\circ})}$$

$$\frac{\partial A}{\partial n(90^{\circ})} = \frac{n(180^{\circ}) - n(0^{\circ})}{2f_1 n^2(90^{\circ})}$$

$$\Delta A \simeq \frac{1}{2f_1 n(90^{\circ})} \left\{ \Delta^2 n(0^{\circ}) + \left[\frac{n(180^{\circ}) - n(0^{\circ})}{n(90^{\circ})} \right]^2 \Delta^2 n(90^{\circ}) + \Delta^2 n(180^{\circ}) \right\}^{1/2}$$

These expressions for the standard deviations, ΔA and ΔB, take into account only the statistical accuracy of the data. However, $\Delta n(0^{\circ})$, etc. cannot be replaced simply by $[n(0^{\circ})]^{1/2}$, etc. since each number of coincidences is normalized by the corresponding number of non-coincident β-counts.

For the data with the β-detector placed only in the 90° and 180° positions there result only equations (2) and (3). In this case A is considered a known quantity. Then:

$$B = \frac{n(180^{\circ}) - (1 - f_1 A) n(90^{\circ})}{f_2 n(90^{\circ}) - f_3 n(180^{\circ})}$$

The partial derivatives in this case are the following:

$$\frac{\partial B}{\partial n(180^{\circ})} = \frac{f_2 n(90^{\circ}) - f_3 n(180^{\circ}) - (-f_3)[n(180^{\circ}) - (1 - f_1 A) n(90^{\circ})]}{[f_2 n(90^{\circ}) - f_3 n(180^{\circ})]^2}$$

$$= \frac{1 + f_3 B}{f_2 n(90^{\circ}) - f_3 n(180^{\circ})}$$

$$\frac{\partial B}{\partial n(90^\circ)} = \frac{-(1-f_1A)[f_2n(90^\circ)-f_3n(180^\circ)] - f_2[n(180^\circ)-(1-f_1A)n(90^\circ)]}{[f_2n(90^\circ) - f_3n(180^\circ)]^2}$$

$$= \frac{-(1 - f_1A + f_2B)}{f_2n(90^\circ) - f_3n(180^\circ)}$$

Therefore:

$$\Delta B = \frac{1}{f_2n(90^\circ) - f_3n(180^\circ)} [(1+f_3B)^2\Delta^2 n(180^\circ)$$

$$+ (1 - f_1A + f_2B)^2\Delta^2 n(90^\circ)]^{1/2}$$

The dependence of the error in B on the error in A has been neglected. It is an order of magnitude smaller than the statistical errors.

APPENDIX D

The Transformation From the Be^{8^*} Rest System to the Laboratory System

The angular correlation in the rest system of the daughter nucleus, Be^{8^*}, of the electron, neutrino, and α-particles in the decays of Li^8 or B^8 can be derived from the theory of beta decay. In order to calculate the angular correlation in the laboratory system of the electron and α-particle, one must multiply the correlation in the Be^{8^*} rest system by the purely geometric solid angle transformation and then integrate over all directions of the unobserved neutrino.

Figure 25 shows superimposed diagrams of the directions of the electron, neutrino, and α-particles in the two systems. In the Be^{8^*} rest system the particles are denoted by $\underline{e}$, $\underline{n}$, $\underline{a}$ and the angles between them by $\underline{en}$, $\underline{ea}$, $\underline{na}$. Similarly in the laboratory system the particles and angles are denoted by $\underline{\beta}$, $\underline{\nu}$, $\underline{\alpha}$ and $\underline{\beta\nu}$, $\underline{\beta\alpha}$, $\underline{\nu\alpha}$. Then the following general identity can be written:

$$
\begin{aligned}
&W(en, ea, na)\,d\Omega_e d\Omega_n d\Omega_a \\
&= W[\,en(\beta\nu, \beta\alpha, \nu\alpha), ea(\beta\nu, \beta\alpha, \nu\alpha), na(\beta\nu, \beta\alpha, \nu\alpha)]\,\frac{d\Omega_e d\Omega_n d\Omega_a}{d\Omega_\beta d\Omega_\nu d\Omega_\alpha}\, d\Omega_\beta d\Omega_\nu d\Omega_\alpha
\end{aligned}
$$

Thus the problem is to express the angles $\underline{en}$, $\underline{ea}$, and $\underline{na}$ in terms of the angles $\underline{\beta\nu}$, $\underline{\beta\alpha}$, and $\underline{\nu\alpha}$, to solve for the ratio of solid angles, and finally to integrate over the neutrino solid angle.

First the ratio of solid angles is solved. Since the neutrino has velocity, c, and the electron has a velocity nearly equal to c, while the Be^{8^*} recoil velocity is very much less than c, the angles and momenta of the electron and neutrino are very nearly equal in both the Be^{8^*} rest system and the laboratory system. Thus to a very good approximation: $d\Omega_e/d\Omega_\beta = 1$, $d\Omega_n/d\Omega_\nu = 1$, $\underline{en} = \underline{\beta\nu}$. The remaining ratio,

$d\Omega_a/d\Omega_\alpha$, can be solved with the aid of equations for the conservation of momentum. In figure 25 the electron defines the polar axis and the neutrino defines the $y = 0$ plane. Then: $d\Omega_a = -d(\cos \underline{ea})d\psi$, $d\Omega_\alpha = -d(\cos \underline{\beta\alpha})d\phi$. Writing the ratio of solid angles in terms of the Jacobian:

$$\frac{d\Omega_a}{d\Omega_\alpha} = \frac{\partial(\cos \underline{ea}, \psi)}{\partial(\cos \underline{\beta\alpha}, \phi)} = \frac{\partial(\cos \underline{ea})}{\partial(\cos \underline{\beta\alpha})} \frac{\partial\psi}{\partial\phi} - \frac{\partial(\cos \underline{ea})}{\partial\phi} \frac{\partial\psi}{\partial(\cos \underline{\beta\alpha})}$$

Define p as the momentum of the electron, q as the momentum of the neutrino, p_a as the momentum in the Be^{8*} rest system of the detected α-particle and p_α as the momentum in the laboratory system of the detected α-particle. A second α-particle is emitted with equal and opposite momentum in the Be^{8*} rest system. An approximation is made by neglecting the conservation of energy equation and using only the conservation of momentum (3). This neglects the kinetic energy of the recoiling Be^{8*}, which is at most 15 kev. In this approximation q is independent of the direction of the α-particle. The momentum equations for the three directions of figure 25 are:

$$\frac{1}{2} q \sin \underline{\beta\nu} = - p_\alpha \sin \underline{\beta\alpha} \cos \phi + p_a \sin \underline{ea} \cos \psi$$

$$p \sin \underline{\beta\alpha} \sin \phi = p_a \sin \underline{ea} \sin \psi$$

$$\frac{1}{2} q \cos \underline{\beta\nu} + \frac{1}{2} p = -p_\alpha \cos \underline{\beta\alpha} + p_a \cos \underline{ea}$$

Solving for the variables of the Be^{8*} rest system in terms of the laboratory variables yields:

$$\cos \underline{ea} = [\cos \underline{\beta\alpha} + p' + q'\cos \underline{\beta\nu}]\ [1 + p'^2 + q'^2 + 2p'\cos \underline{\beta\alpha}$$
$$+ 2p'q'\cos \underline{\beta\nu} + 2q'\cos \underline{\beta\nu}\cos \underline{\beta\alpha}$$
$$+ 2q'\cos\phi \sin \underline{\beta\nu} \sin \underline{\beta\alpha}]^{-1/2}$$

$$\cot\psi = \cot\phi + q'\sin \underline{\beta\nu} \csc\phi \csc \underline{\beta\alpha}$$

where, $p' = p/2p_\alpha$, $q' = q/2p_\alpha$. Then $p' \simeq 1/20$ and $q' \simeq 1/100$ for the experimental case with $W_\beta \simeq 11$ Mev. Taking the partial derivatives yields to first order in q':

$$\partial\psi/\partial\phi \simeq 1 - q' \sin \underline{\beta\nu} \cos\phi \csc \underline{\beta\alpha}$$

$$\partial\psi/\partial(\cos \underline{\beta\alpha}) \simeq -q'\sin \underline{\beta\nu} \sin\phi \cos \underline{\beta\alpha} \csc^3 \underline{\beta\alpha}$$

$$\partial(\cos \underline{ea})/\partial\phi \simeq [q'\sin\phi \sin \underline{\beta\nu} \sin \underline{\beta\alpha}(\cos \underline{\beta\alpha} + p')][1 + p'^2 + q'^2$$
$$+ 2p'\cos \underline{\beta\alpha} + 2p'q'\cos \underline{\beta\nu} + 2q'\cos \underline{\beta\nu}\cos \underline{\beta\alpha}$$
$$+ 2q'\cos\phi \sin \underline{\beta\nu} \sin \underline{\beta\alpha}]^{-3/2}$$

$$\partial(\cos \underline{ea})/\partial(\cos \underline{\beta\alpha}) \simeq [1 + q'^2 + p'\cos \underline{\beta\alpha} + p'q'\cos\phi \sin \underline{\beta\nu}\cos \underline{\beta\alpha}$$
$$+ q'\cos \underline{\beta\nu}\cos \underline{\beta\alpha} + 2q'\cos\phi \sin \underline{\beta\nu} \sin \underline{\beta\alpha}$$
$$+ q'\cos\phi \sin \underline{\beta\nu} \cot \underline{\beta\alpha} \cos \underline{\beta\alpha}][1 + p'^2 + q'^2$$
$$+ 2p'\cos \underline{\beta\alpha} + 2p'q'\cos \underline{\beta\nu} + 2q'\cos \underline{\beta\nu}\cos \underline{\beta\alpha}$$
$$+ 2q'\cos\phi \sin \underline{\beta\nu} \sin \underline{\beta\alpha}]^{-3/2}$$

Ideally the procedure would be to multiply these partial derivatives together to form $d\Omega_a/d\Omega_\alpha$ and then multiply this by the function, W, and integrate over $d\Omega_\nu$. The algebra of this procedure is forbiddingly complicated. Instead, the procedure used here is to carry out the multiplication and integration for the simplified case with $q = 0$ and then show that all of the integrals in which q appears to first order are identically zero.

Next the correlation function of the Be^{8^*} rest system is expressed in terms of laboratory coordinates. As derived by Dr. H. Weidenmuller, the correlation in the Be^{8^*} rest system is (59):

$$W(ea, en, na) = (1 - \frac{1}{3} ap) - (\frac{p}{W_\beta} - \frac{1}{3} ap) \cos \underline{ea} \cos \underline{na}$$

$$- ap \cos \underline{en} + ap \cos^2 \underline{ea}$$

where the quantity, a, is the interference term arising from the vector M1 type matrix element in the two theories of beta decay. Terms of order $(\alpha Z)^2$ have been neglected for the allowed transition and the approximations, $m_e = 0$ and $\alpha Z = 0$, have been assumed for the forbidden transition.

In the $q = 0$ approximation:

$$\cos \underline{ea} \simeq \frac{p' + \cos \underline{\beta\alpha}}{(1 + p'^2 + 2p' \cos \underline{\beta\alpha})^{1/2}} \quad , \cos \psi \simeq \cos \phi$$

From a theorem of spherical trigonometry:

$$\cos \underline{na} = \cos \underline{en} \cos \underline{ea} + \sin \underline{en} \sin \underline{ea} \cos \psi$$

Therefore, the correlation function in terms of the laboratory variables is:

$$W = (1 - \frac{1}{3}ap) - ap\cos\underline{\beta\nu} + \left[\frac{p' + \cos\underline{\beta\alpha}}{1 + p'^2 + 2p'\cos\underline{\beta\alpha}}\right]\left[-(\frac{p}{W_\beta} - \frac{1}{3}ap)\right.$$

$$\times\ \cos\underline{\beta\nu}(p' + \cos\underline{\beta\alpha}) + ap(p' + \cos\underline{\beta\alpha})$$

$$\left.- (\frac{p}{W_\beta} - \frac{1}{3}ap)\sin\underline{\beta\nu}\sin\underline{\beta\alpha}\cos\phi\right]$$

This is to be multiplied by the ratio of solid angles, which in the $q = 0$ approximation is:

$$d\Omega_a/d\Omega_\alpha = \frac{1 + p'\cos\underline{\beta\alpha}}{(1 + p'^2 + 2p'\cos\underline{\beta\alpha})^{3/2}}$$

This ratio is independent of the neutrino direction and thus is a constant for the integration over the neutrino solid angle. The laboratory angular distribution function of the electron and α-particle is the normalized integral:

$$W(\theta_{\beta\alpha}) = W(\beta\alpha) = \frac{\int_{\Omega_\nu}(W\, d\Omega_a/d\Omega_\alpha)d\Omega_\nu}{\int_{\Omega_\nu} d\Omega_\nu}$$

$$= \frac{1}{4\pi}\int_0^{2\pi}\int_{-1}^{+1}(W\, d\Omega_a/d\Omega_\alpha)\, d(\cos\underline{\beta\alpha})\, d\phi$$

The only variable terms in the integral are $\cos\underline{\beta\nu}$ and $\sin\underline{\beta\nu}\cos\phi$. However, the integrals of these functions are identically zero.

$$\int_{-1}^{+1}\cos\underline{\beta\nu}\, d(\cos\underline{\beta\nu}) = 0, \qquad \int_0^{2\pi}\cos\phi\, d\phi = 0$$

Thus

$$W(\beta\alpha) = [(1 - \tfrac{1}{3}\,ap) + \frac{ap(p' + \cos \underline{\beta\alpha})^2}{1 + p'^2 + 2p'\cos \underline{\beta\alpha}}][\frac{1 + p'\cos \underline{\beta\alpha}}{1 + p'^2 + 2p'\cos \underline{\beta\alpha})^{3/2}}]$$

This is approximated by expanding the denominators, keeping only terms up to order p'^2, combining the $\cos^3 \underline{\beta\alpha}$ term with the $\cos \underline{\beta\alpha}$ term, and renormalizing the constant term to be 1. Also the quantity, p', is replaced by its definition, $p/2p_\alpha$.

$$W(\beta\alpha) \simeq 1 - (\frac{p}{p_\alpha} + \frac{3ap^2}{2p_\alpha})\cos \underline{\beta\alpha} + (ap + \frac{9p^2}{8p_\alpha^2})\cos^2 \underline{\beta\alpha}$$

Next, it is shown that this same result also applies when $q \neq 0$. This can be seen from the expressions for the angles of the Be^{8^*} rest system in terms of the laboratory variables, and also from the expressions for the partial derivatives. Note that q' appears in these expressions only when multiplied by either $\cos \underline{\beta\nu}$ or $\sin \underline{\beta\nu} \cos \phi$. Thus the general form of the product, $W\,d\Omega_a/d\Omega_\alpha$, indicating only the first order dependence on q' and the dependence on the neutrino angles, is the following:

$$(Uq'\cos \underline{\beta\nu} + Vq'\sin \underline{\beta\nu} \cos \phi)(X + Y\cos \underline{\beta\nu} + Z\sin \underline{\beta\nu}\cos \phi)$$

For each product of two terms at least one of the integrals over the neutrino angles, $\underline{\beta\nu}$ and ϕ, is equal to zero. Thus there are no first order terms in q'. Second order terms are negligible.

Another effect large enough to be considered is the variation of p_α with angle, arising from the recoil of Be^{8^*}. The Be^{8^*} recoil averaged over the neutrino direction is:

$$p_{recoil} = p - q/3$$

Half of this momentum is received by each α-particle. If the 90° α-spectrum is used as an approximation to the spectrum in the Be^{8^*} rest system, the 180° and 0° spectra are replicas of the 90° spectrum but shifted by $\pm \frac{1}{2} p_{recoil}$. Therefore, averaging a function of the momentum, p_α, over the α-spectrum at angle, $\underline{\beta\alpha}$, is approximately equivalent to averaging the same function of $p_\alpha - \frac{1}{2}(p - \frac{q}{3})\cos \underline{\beta\alpha}$ over the 90° α-spectrum. The angular distribution, $W(\beta\alpha)$, contains the function $1/p_\alpha$, which is to be averaged over the α-spectrum. Using the approximation, $1/(1-x) \simeq 1 + x$, where x is small, gives the following average of the function, $1/p_\alpha(\beta\alpha)$:

$$< \frac{1}{p_\alpha} (\beta\alpha)> \simeq < \frac{1}{p_\alpha} (90^{\circ})> \left[1 + \frac{1}{2} < \frac{1}{p_\alpha} (90^{\circ})>(p - \frac{q}{3})\cos \underline{\beta\alpha} \right]$$

This correction is appreciable only for the leading $\cos \underline{\beta\alpha}$ term in $W(\beta\alpha)$.

The final expression for the angular correlation in the laboratory system is the following:

$$W(\beta\alpha) \simeq 1 - \left[p<\frac{1}{p_\alpha}(90^{\circ})> + \frac{3}{2} ap^2 <\frac{1}{p_\alpha}(90^{\circ})> \cos \underline{\beta\alpha} \right]$$
$$+ \left[ap + \frac{5}{8} p^2 < \frac{1}{p_\alpha}(90^{\circ})>^2 \right] \cos^2 \underline{\beta\alpha}$$

The quantity, $\underline{a}$, as discussed in section I, includes the interference effect of the vector M1 type matrix element. It is expected to be about a factor of 2 larger in the C. V. C. theory than in the Fermi theory of beta decay, and it changes sign in the Li^8 and B^8 decays. Coefficients arising from interference of forbidden axial vector matrix elements have not been included, but they would not change sign in the two decays. The significance of this distribution is discussed in Section IV.

REFERENCES

1. J. J. Sakurai, Progress in Nuclear Physics, 7, 243 (1959).
2. M. Gell-Mann, Lecture Notes by W. G. Wagner (1959).
3. J. M. Blatt and V. F. Weisskopf, Theoretical Nuclear Physics, John Wiley and Sons (1952).
4. M. E. Rose, Nuclear Spectroscopy, edited by Ajzenberg-Selove 811 (1960).
5. Invited Papers from the Conference on Weak Interactions, Rev. Mod. Phys. 31, 782 (1959).
6. T. D. Lee and C. N. Yang, Phys. Rev. 104, 254 (1956).
7. C. S. Wu, E. Ambler, R. W. Hayward, and D. D. Hoppes, Phys. Rev., 105, 1413 (1957).
8. R. L. Garwin, L. M. Lederman, and M. Weinrich, Phys. Rev. 105, 1415 (1957).
9. J. I. Friedman and V. L. Telegdi, Phys. Rev. 105, 1681 (1957).
10. R. P. Feynman and M. Gell-Mann, Phys. Rev. 109, 193 (1958).
11. E. C. G. Sudarshan and R. E. Marshak, Phys. Rev. 109, 1860 (1958).
12. J. J. Sakurai, Nuovo Cimento 7, 649 (1958).
13. C. A. Barnes, W. A. Fowler, H. B. Greenstein, C. C. Lauritsen, and M. E. Nordberg, Phys. Rev. Letters 1, 328 (1958).
14. L. Grodzins, Progress in Nuclear Physics 7, 163 (1959).
15. T. D. Lee and C. N. Yang, Phys. Rev. 105, 1671 (1957).
16. L. Landau, Nuclear Physics 3, 127 (1957).
17. A. Salam, Nuovo Cimento 5, 299 (1957).
18. R. K. Bardin, C. A. Barnes, W. A. Fowler, and P. A. Seeger, Phys. Rev. Letters 5, 323 (1960).
19. R. K. Bardin, Thesis, Kellogg Radiation Laboratory (1961).
20. S. S. Gershtein and J. B. Zel'dovich, Zhur. Eksptl. i. teort. Fiz. U. S. S. R. 29, 698 (1955) Soviet Physics J. E. T. P. 2, 576 (1957).

21. M. Gell-Mann, Phys. Rev. 111 , 362 (1958).

22. J. Bernstein and R. R. Lewis Phys. Rev. 112, 232 (1958).

23. F. Ajzenberg-Selove and T. Lauritsen, Nuclear Physics 11, 1 (1959).

24. M. Morita, Phys. Rev. 113, 1584 (1959).

25. M. Morita and H. Yamada, Progr. Theoret. Phys. 13, 114 (1955).

26. M. E. Nordberg, B. Povh, and C. A. Barnes, Phys. Rev. Letters 4, 23 (1960)

27. H. A. Weidenmuller, Phys. Rev. Letters, 4, 299 (1960).

28. D. Kurath, Phys. Rev. Letters 4, 180 (1960).

29. M. E. Nordberg, F. B. Morinigo, and C. A. Barnes, Phys. Rev. Letters 5, 321 (1960).

30. J. Dreitlein and H. Primakoff, Washington U. Tech. Rept. No. 34 (1959).

31. J. F. Dreitlein, Phys. Rev. 116, 1604 (1959).

32. H. Hilton, Thesis, Kellogg Radiation Laboratory (1960).

33. F. Boehm, V. Soergel, and B. Stech, Phys. Rev. Letters 1, 77 (1958).

34. J. G. Fetkovich, T. H. Fields, and R. L. McIlwain, Phys. Rev. 118, 319 (1960).

35. F. J. Walter, J. W. T. Dabbs, and L. D. Roberts, O. R. N. L. Rept. No. CF-58-11-99 (1958).

36. F. J. Walter, J. W. T. Dabbs, and L. D. Roberts, Rev. Sci. Instr. 31, 756 (1960).

37. J. M. McKenzie and D. A. Bromley, Phys. Rev. Letters 2, 203 (1959).

38. E. Nordberg, Bull. Am. Phys. Soc. Series II, 4, 457 (1960).

39. W. F. Hornyak and T. Lauritsen, Phys. Rev. 77, 160 (1950).

40. W. F. Hornyak, Thesis, Kellogg Radiation Laboratory (1949).

41. D. StP. Bunbury, Phys. Rev. 90, 1121 (1953).

42. S. S. Hanna, E. C. LaVier, and C. M. Class, Phys. Rev. 95, 110 (1954).

43. K. Krebs, H. Rieseberg, and V. Soergel, Zeitr. F. Physik 159, 232 (1960).

44. J. F. Vedder, U. C. R. L. Rept. No. 8324 (1958).

45. H. Hilton and V. Soergel (private communication).

46. T. Lauritsen, C. A. Barnes, W. A. Fowler, and C. C. Lauritsen, Phys. Rev. Letters 1, 326 (1958).

47. B. Stech and J. Eichler (private communication).

48. G. Dearnaley and A. B. Whitehead, A. E. R. E. Rept. No. 3437 (1960).

49. M. L. Halbert and J. L. Blankenship, Nuclear Instr. and Methods, 8, 106 (1960).

50. J. D. Van Putten, Jr. and J. C. Vander Velde, Bull. Am. Phys. Soc. Series II, 5, 197 (1960).

51. S. S. Friedland, J. W. Mayer, and J. S. Wiggins, Nucleonics, 18, No. 2, 54 (1960).

52. P. F. Donovan, G. L. Miller, and B. M. Foreman, Bull. Am. Phys. Soc. Series II, 5, 355 (1960).

53. Proceedings of the Seventh Scintillation Counter Symposium, Transactions on Nuclear Science 7, No. 2-3, 178 (1960).

54. Proceedings of the Semiconductor Detector Conference, Transactions on Nuclear Science 8, No. 1, 1 (1961).

55. W. Schottky, Zeitr. F. Physik 113, 367 (1939).

56. J. Bardeen, Handbook of Physics, Edited by Condon and Odishaw 8-52 (1958).

57. E. Spenke, Electronic Semiconductors, McGraw-Hill (1958).

58. E. M. Conwell, Proc. I. R. E. 46, 1281 (1958).

59. H. A. Weidenmuller (private communication).

60. W. B. Herrmannsfeldt, R. L. Burman, P. Stahelin, J. S. Allen, and T. H. Braid, Phys. Rev. Letters 1, 61 (1958).

Figure 1 illustrates the energy levels of the mass-8 isotopic triplet. Either electrons from the beta decay of Li^8 or positrons from the beta decay of B^8 are detected in coincidence with α-particles from the breakup of the 2.90-Mev state of Be^8 as a function of the angle, $\theta_{\beta\alpha}$. Both beta decays are primarily allowed axial vector but second forbidden vector matrix elements affect the angular distribution of coincidences by an amount depending on the magnitude of the analogous M1 γ-ray transition rate shown dashed in the figure. The effect on the angular distribution may be used as a check of the validity of the conserved vector current theory of beta decay. Li^8 is produced in the $Li^7(d, p)Li^8$ reaction by a deuteron beam of 0.75 Mev. B^8 is produced in the $Li^6(He^3, n)B^8$ reaction by a He^3 beam of 3.2 Mev. Figure 1 is discussed in Section I, pages 7 and 10.

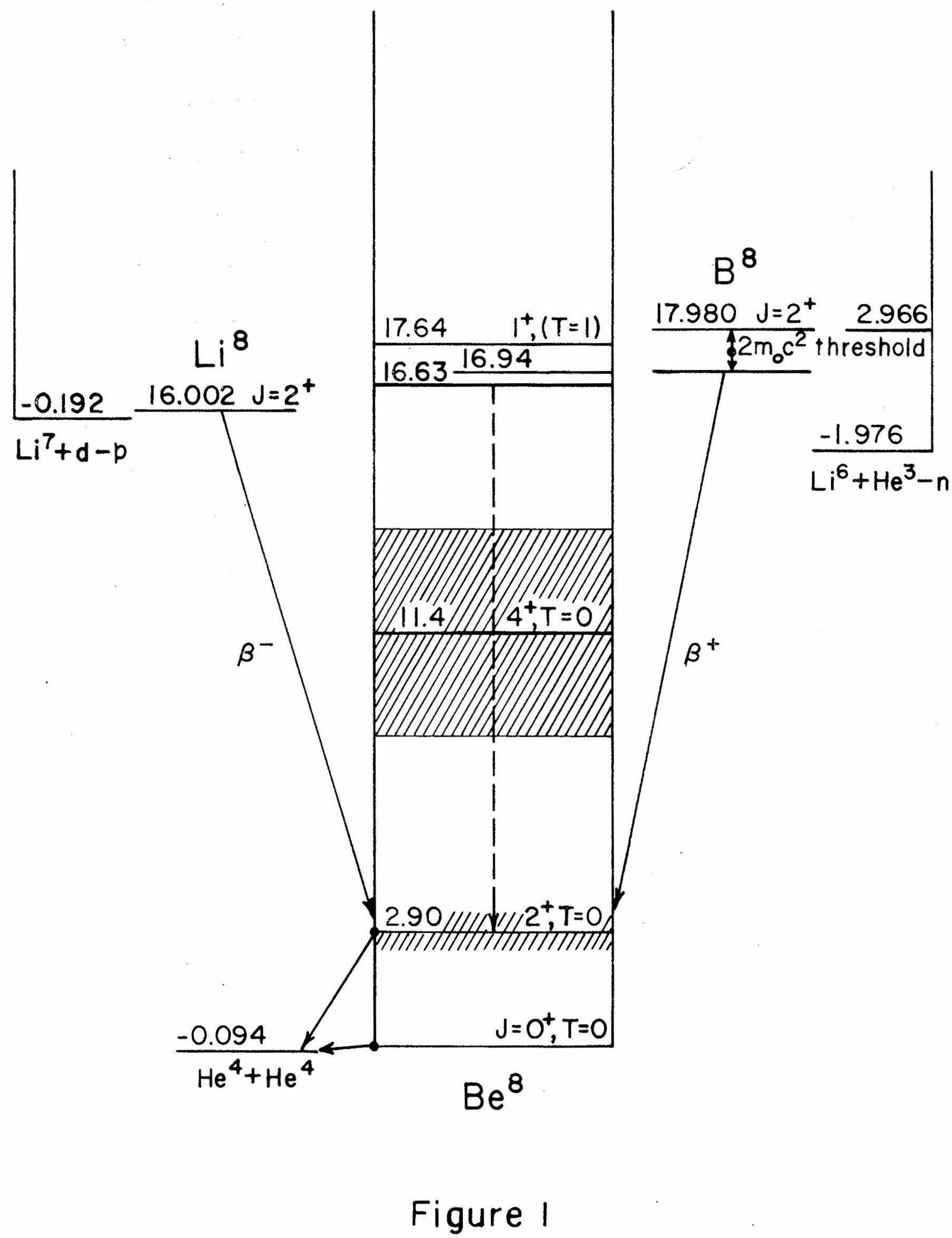
Li^8
16.002 J=2$^+$
-0.192
Li^7+d−p
B^8
17.980 J=2$^+$
2.966
2m$_o$c^2 threshold
-1.976
Li^6+He^3−n
17.64
1$^+$,(T=1)
16.63
16.94
11.4
4$^+$,T=0
β$^-$
β$^+$
2.90
2$^+$,T=0
J=0$^+$,T=0
-0.094
He^4+He^4
Be^8

Figure 1

Figure 2 illustrates the 3"-diameter target chamber and associated apparatus. The incident beam from the Van de Graaff generator enters the tube at the right rear and strikes the target at a 15° angle. Four gold-silicon surface barrier α-particle detectors are placed at 45° angles to the target. The α-detector furthest to the right in the figure is used as a monitor, the one towards the right foreground detects α-particles in coincidence with electrons, and the other two detectors are dummy detectors for the purpose of symmetry. A furnace, which is used to evaporate thin, 2-mm wide, Li^7 or Li^6 targets on the 5-mil aluminum backing is shown in the rear of the chamber about 3" above the plane of the detectors. A tantalum cup with a cut through which the beam enters is shown surrounding the target backing. This shield drops into the 1-1/2"-diameter lead container during the counting period. The lead container is supported by the cold trap which can be filled with liquid nitrogen from below. The plastic scintillator which detects electrons is shown in the foreground. It is mounted inside the movable lead shield to the left during the course of the experiment. Figure 2 is discussed in Section II, pages 11-17.

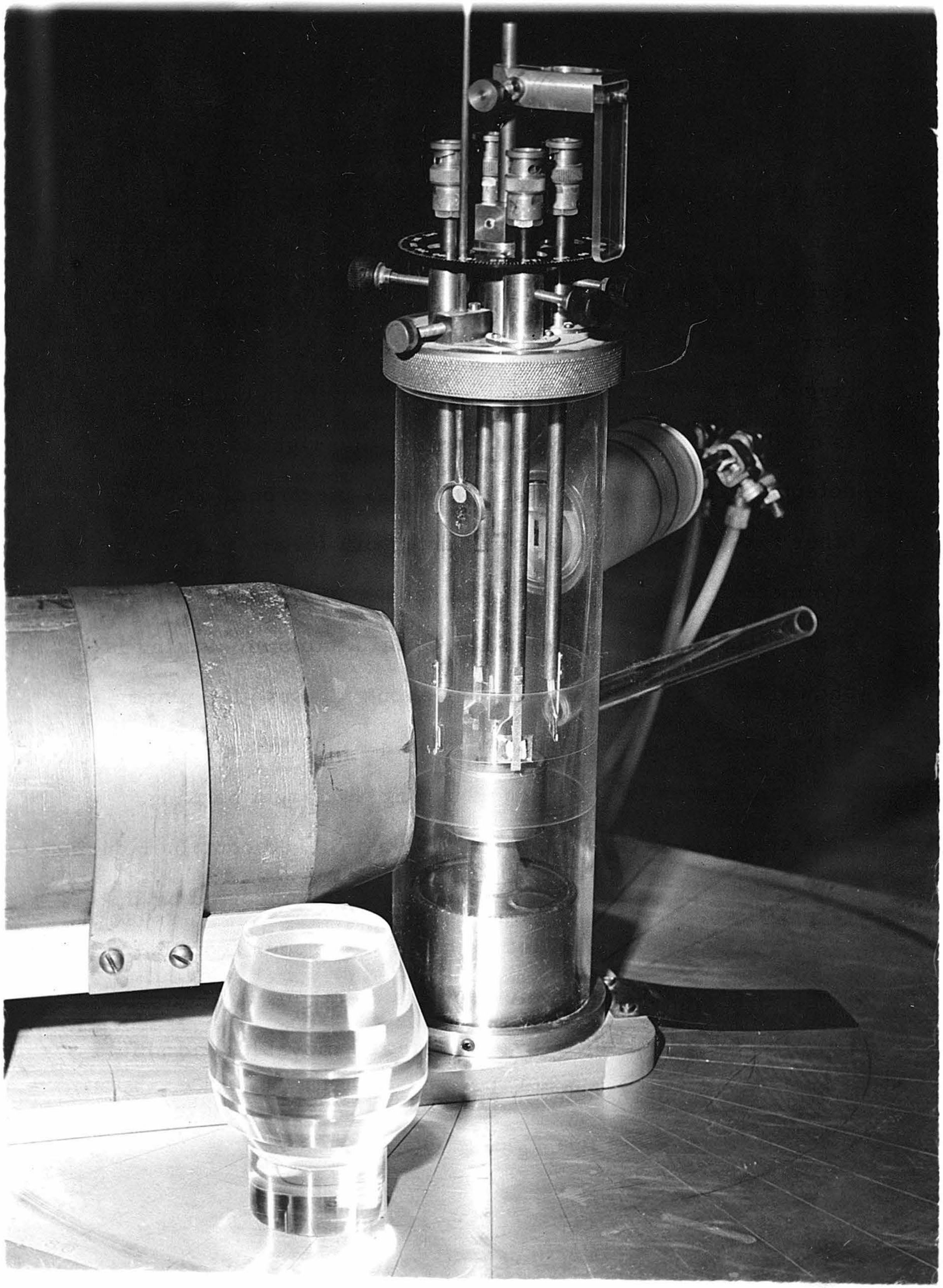

TARGET CHAMBER

Figure 2

Figure 3 outlines a block diagram of the electronic circuitry used in this experiment. A "fast-slow" coincidence system is used with a fast resolving time of about 80mμ sec. and a slow resolving time of about 1.2 μ sec. The coincident α-spectra are displayed on the 100 channel analyzer. A single channel discriminator selects the β-energy. The gating supply regulates the 1 sec. delayed counting cycle: the beam is on the target 40% and off 60% of the time, the scalers and 100 channel analyzer are off 60% and on 40% of the time, the target shield is up 50% and down 50% of the time. Figure 3 is discussed in Section II, pages 14 and 17-20.

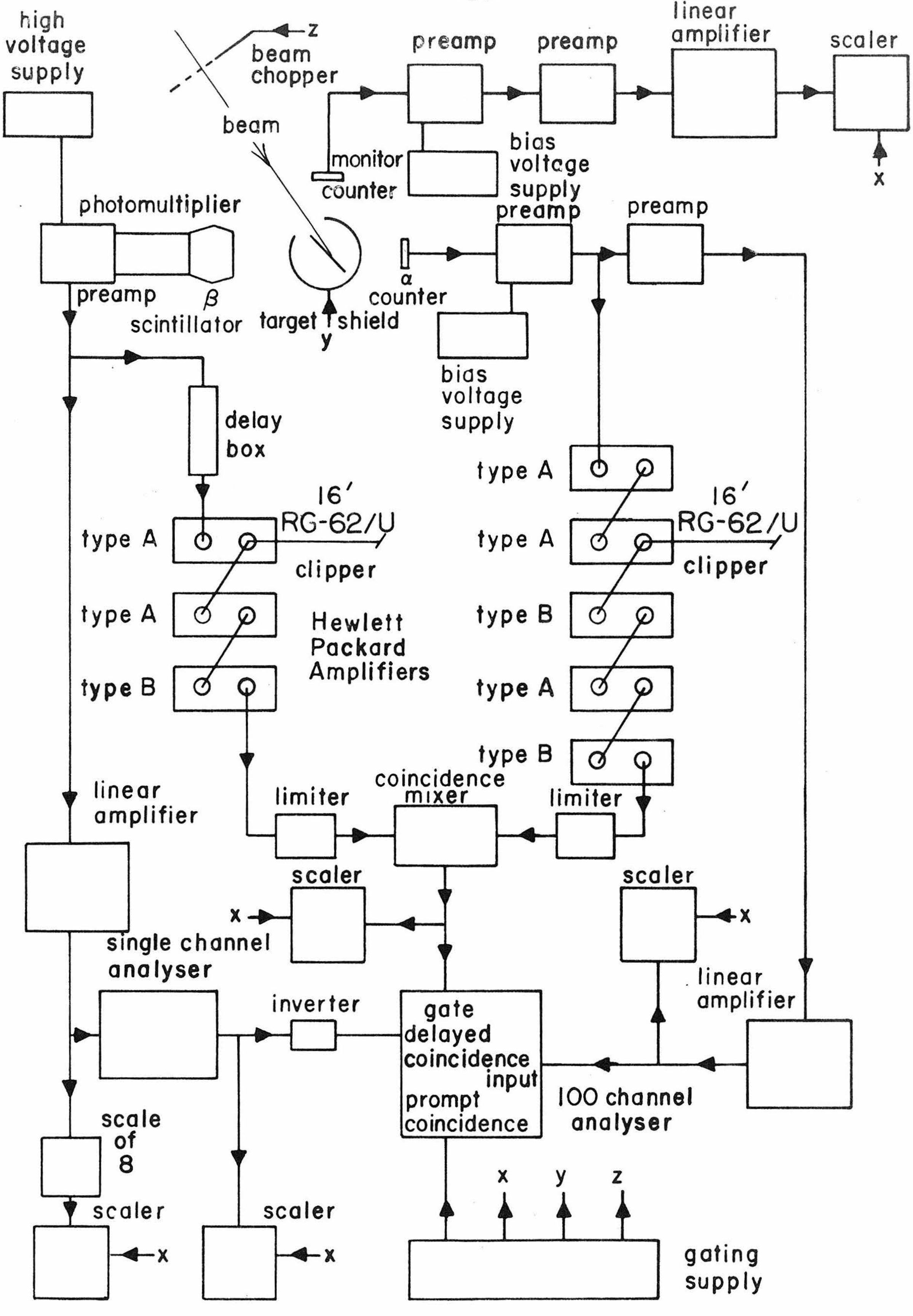

ELECTRONIC CIRCUITRY

Figure 3

Figure 4 is a spectrum from the 100 channel analyzer showing the response of a gold-silicon surface barrier detector to the α-particles following the Li^8 beta decay. From an ideally thin target the peak would occur at about 1.5 Mev and be about 0.8-Mev wide. Actually the peak is lowered and broadened by the α-particle loss in the target and the limited resolution of the detectors. Noise and pulses from electrons appear in the low channels. The points marked "α-α coincidence gate" represents the same spectrum but with the 100 channel analyzer being gated by the fast coincidence mixer with the same α-particle pulses in both inputs. This mode of operation is less sensitive to noise but the spectrum indicates that the fast coincidence mixer reliably detects pulses from α-particles to somewhat below channel 10. (See Section II, page 15; Section III, page 26; and Section IV, page 40.)

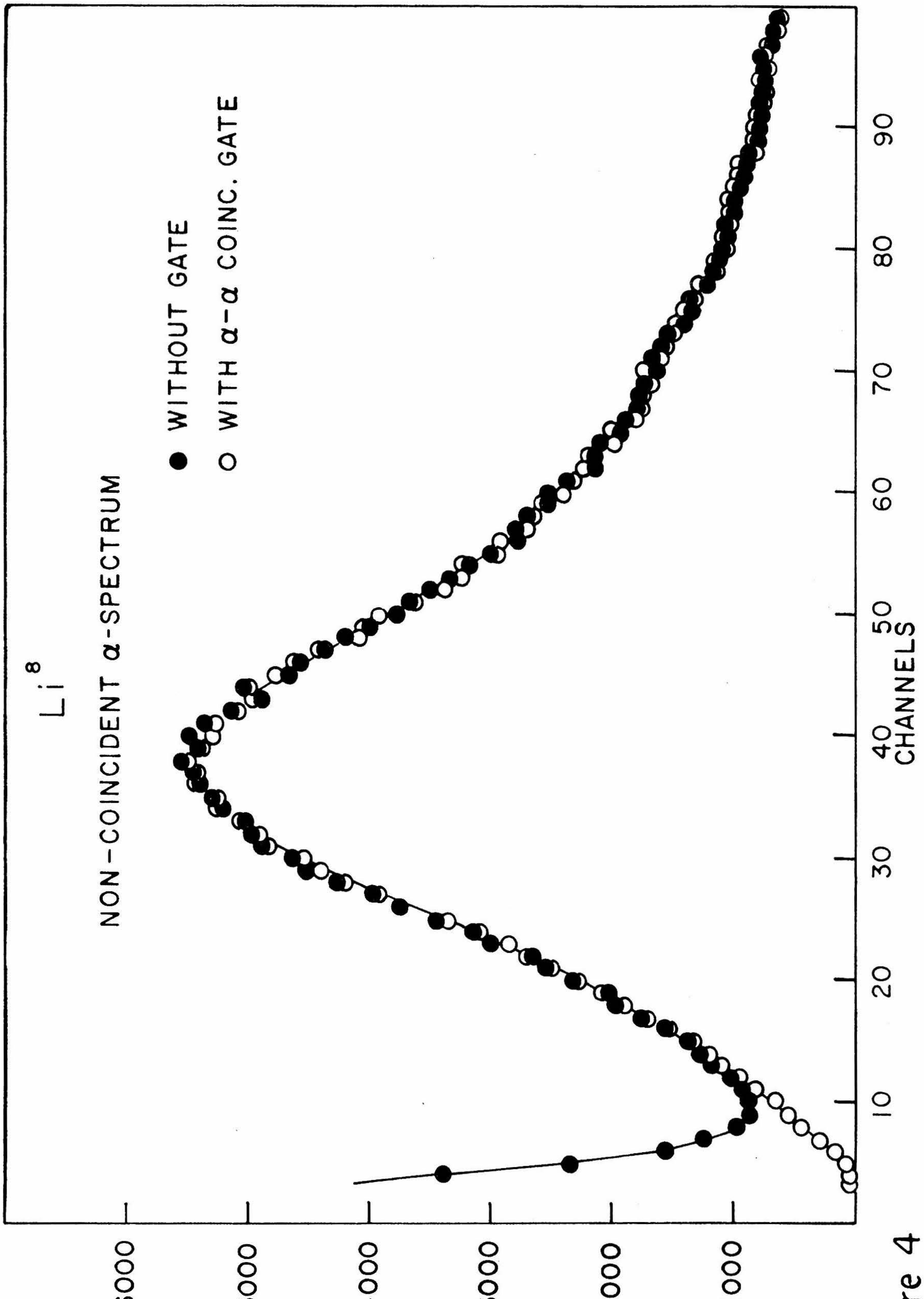
Li^8
NON-COINCIDENT α-SPECTRUM
● WITHOUT GATE
○ WITH α-α COINC. GATE
COUNTS PER CHANNEL
6000
5000
4000
3000
2000
1000
10
20
30
40
50
60
70
80
90
CHANNELS

Figure 4

Figure 5 shows the pulse height response of two gold-silicon surface barrier detectors to monoenergetic α-particles from a polonium source. The wider curve is from a typical detector used in this experiment while the narrower curve is from a smaller, selected counter of superior resolution. The amplifier gain used for obtaining figure 5 is about half of that for figure 4. At the lower energies of figure 4, the full width at half maximum for monoenergetic α-particles is greater than for the case of 5.3 Mev α-particles. A discussion related to figure 5 can be found in Section II, page 16 or Appendix A, page 61.

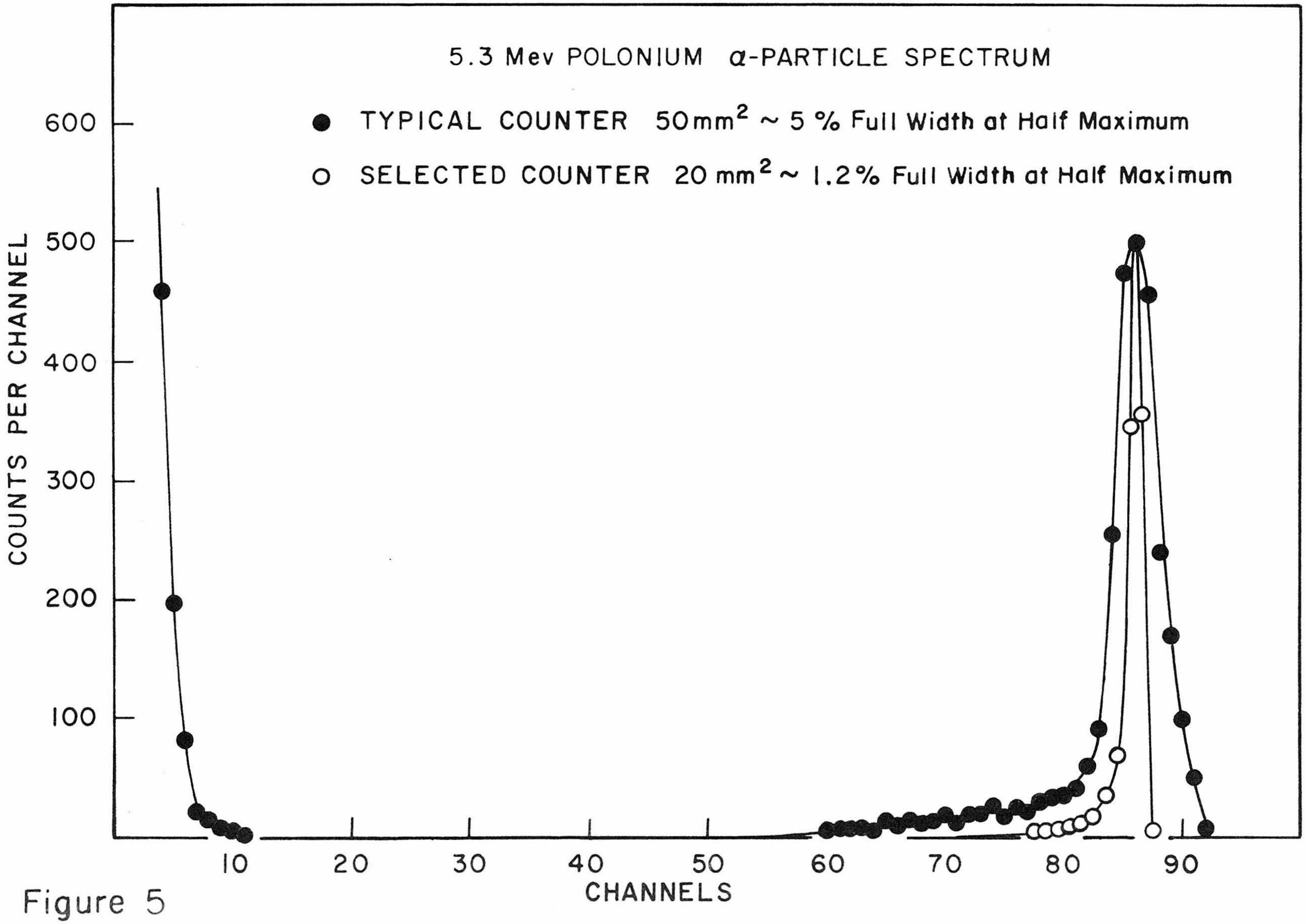
5.3 Mev POLONIUM α-PARTICLE SPECTRUM
● TYPICAL COUNTER 50mm² ~ 5 % Full Width at Half Maximum
○ SELECTED COUNTER 20 mm² ~ 1.2% Full Width at Half Maximum
COUNTS PER CHANNEL
600
500
400
300
200
100
10
20
30
40
50
60
70
80
90
CHANNELS

Figure 5

Figure 6 illustrates the relation of the β-spectrum from the Li^8 decay to the analysis of the pulse height response of the plastic scintillator. To obtain the solid points, background, measured with the beam on only the aluminum backing, is subtracted from the open points. A magnetic spectrometer β-spectrum of equal area is plotted with equal abscissa for the point of half maximum. This abscissa is equivalent to 9.5 Mev, kinetic energy, thus converting channels (lower scale) to kinetic energy (upper scale). The shaded portion of the spectrum represents pulses selected by the single channel analyzer for the case of an average β-energy about 11 Mev. Figure 6 is also discussed in Section II, page 17; Section III, page 26; and Section IV, page 35.

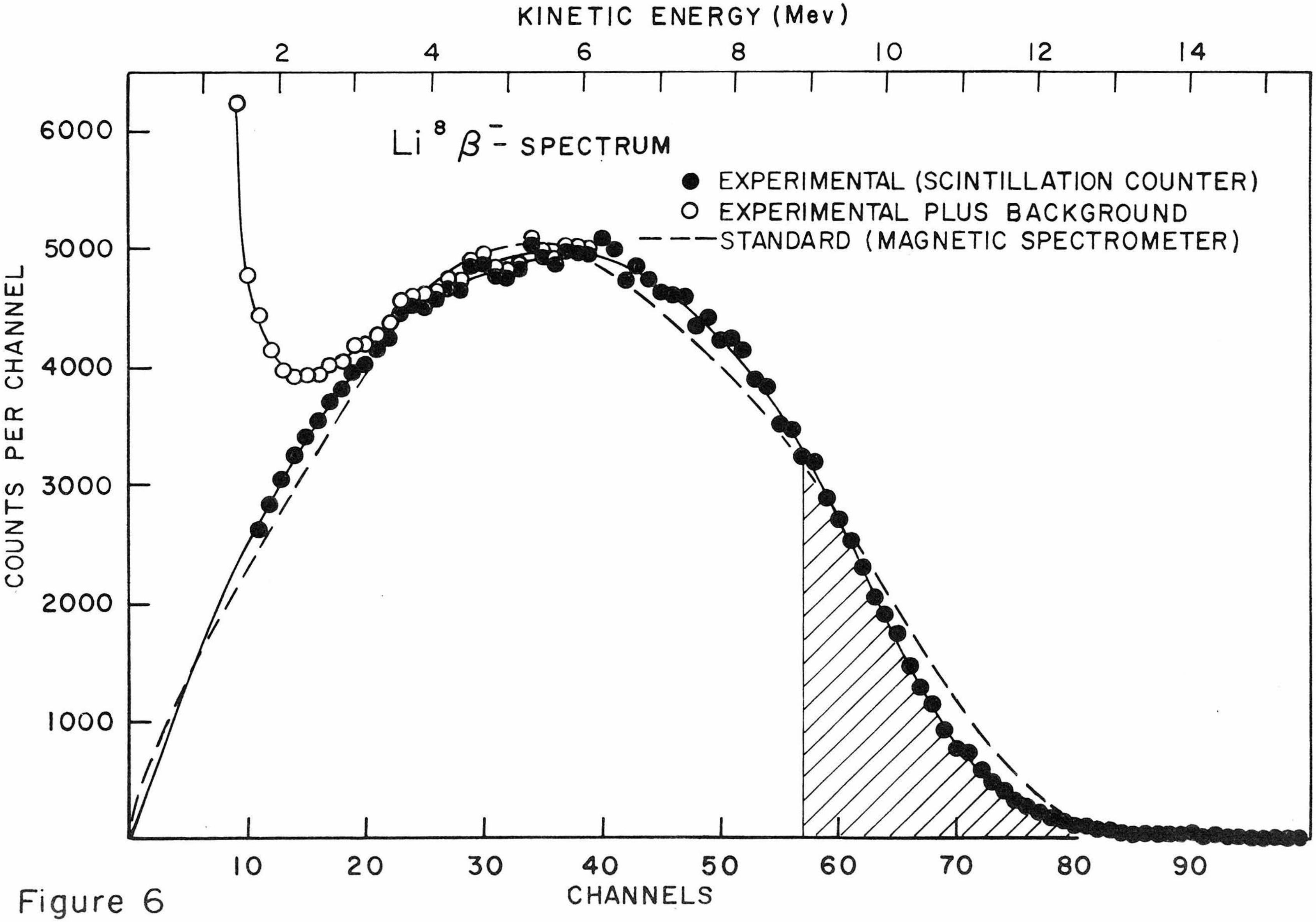
KINETIC ENERGY (Mev)
2
4
6
8
10
12
14
$Li^8\ \beta^-$ - SPECTRUM
● EXPERIMENTAL (SCINTILLATION COUNTER)
○ EXPERIMENTAL PLUS BACKGROUND
— — STANDARD (MAGNETIC SPECTROMETER)
COUNTS PER CHANNEL
6000
5000
4000
3000
2000
1000
10
20
30
40
50
60
70
80
90
CHANNELS

Figure 6

Figure 7 illustrates the response of the plastic scintillator β-detector to 2.62 Mev γ-rays. As is evident the response is quite poor and therefore this spectrum is not used to calibrate the β-energy scale. This figure is mentioned in Section II, page 17 and Section IV, page 35.

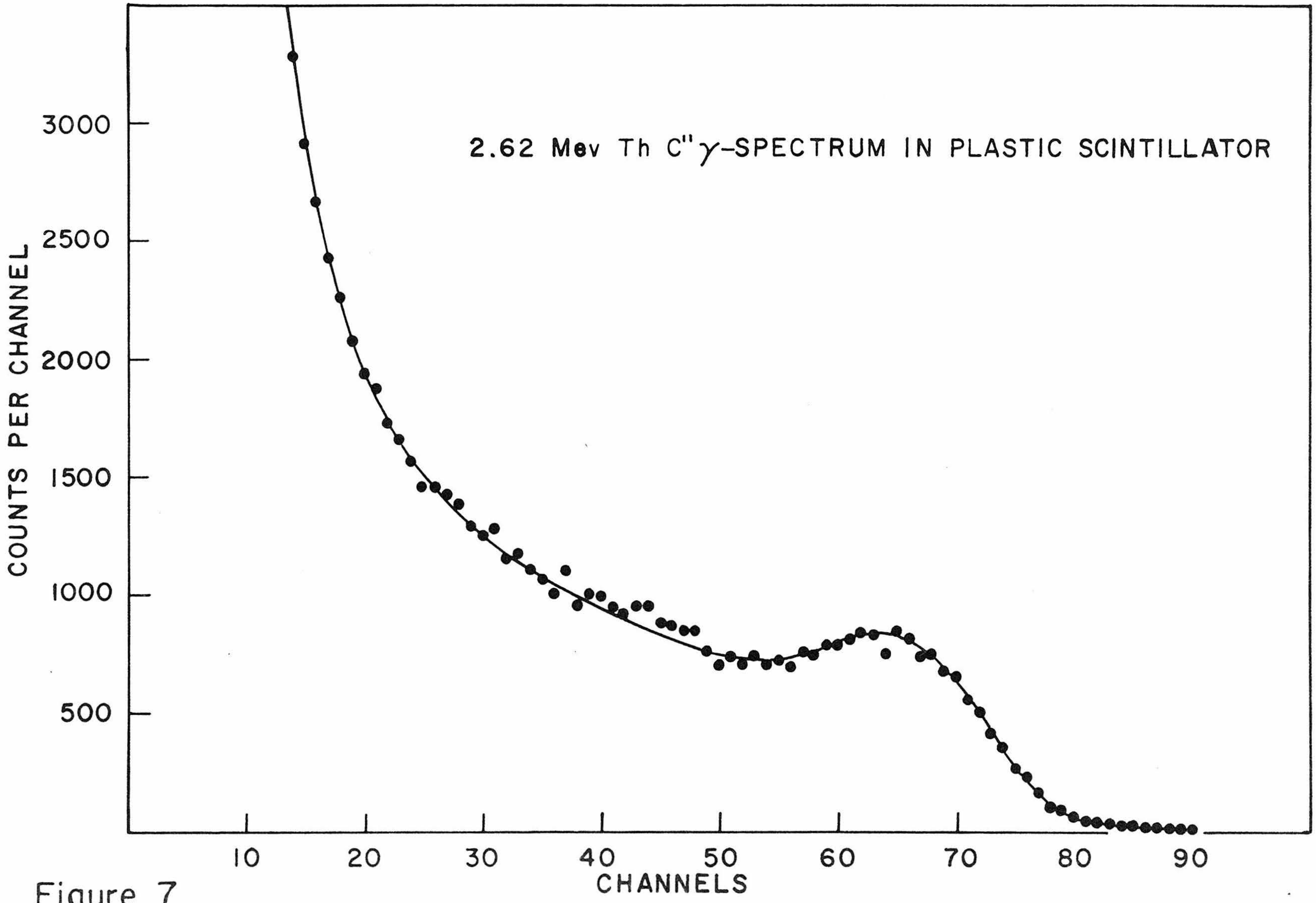
2.62 Mev Th C''γ-SPECTRUM IN PLASTIC SCINTILLATOR
COUNTS PER CHANNEL
3000
2500
2000
1500
1000
500
10
20
30
40
50
60
70
80
90
CHANNELS

Figure 7

Figure 8 is an example of the essential data of the experiment. It represents the sum of the coincident α-spectra from two groups of data as a function of the angle, $\theta_{\beta\alpha}$, for the particular case of coincidences with electrons from the Li^8 decay of total energy about 5 Mev. The curves are normalized to a fixed number of non-coincident β-counts. The integrals of the curves are used to calculate the coefficients of the angular distribution function. The total numbers of coincidences of pulse height greater than 100 channels are also known. For the case of $\theta_{\beta\alpha} = 0^o$, electrons traverse the α-detector and produce small pulses, called the "$0^o\beta$" spectrum which must be subtracted from the measured numbers of coincidences to yield the true numbers. This is done in the dashed extrapolation to zero pulse height. The shift in the position of the peaks is caused by the recoil of the Be^8 nucleus from the momentum of the electron and neutrino. This shift aggravates the problem of accurately measuring the areas under the curves. Figure 8 is discussed in Section III, page 24. (Also compare figures 9, 10 and 11.)

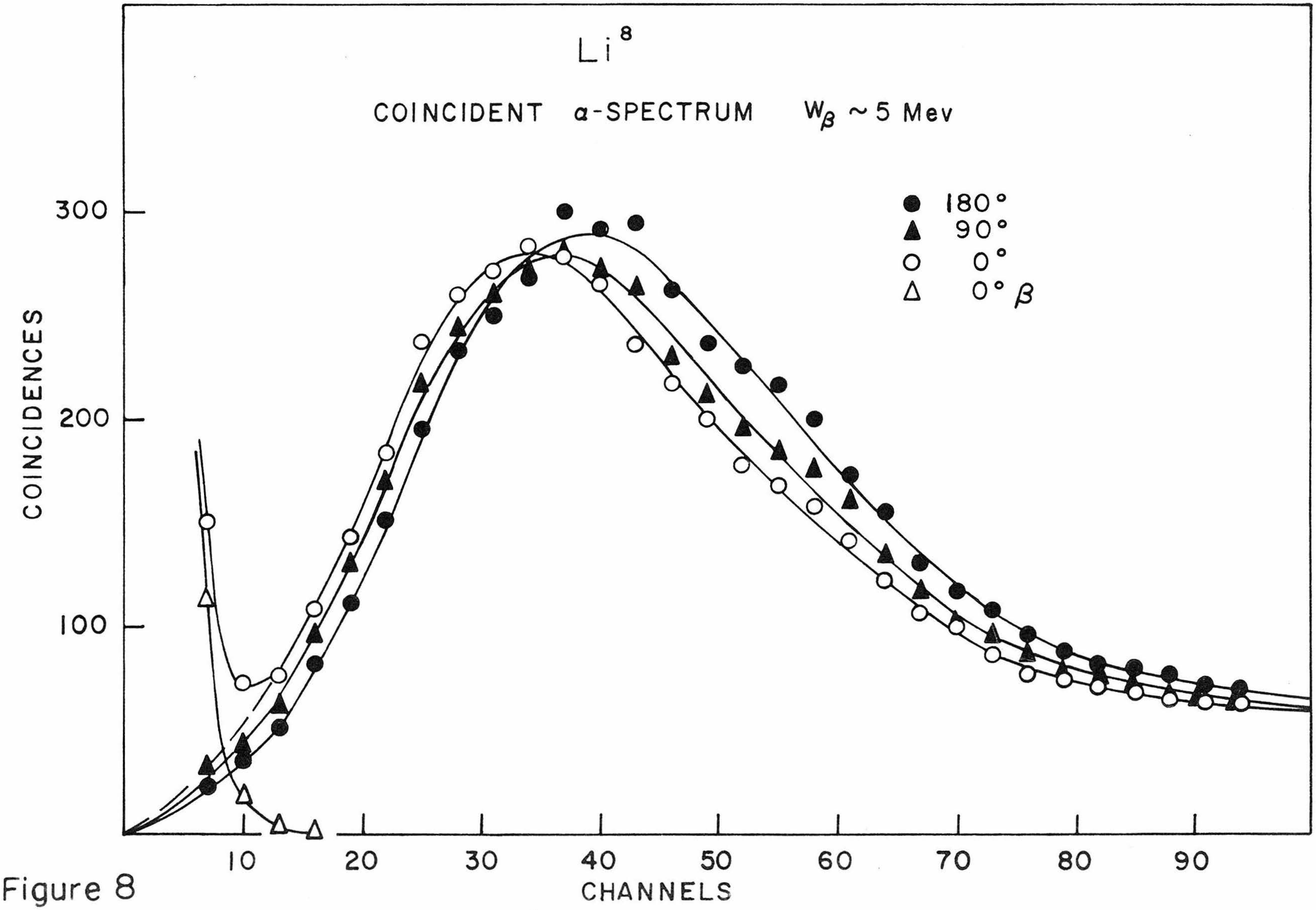
Li^8
COINCIDENT α-SPECTRUM $W_\beta \sim 5$ Mev
● 180°
▲ 90°
○ 0°
△ 0° β
COINCIDENCES
100
200
300
10
20
30
40
50
60
70
80
90
CHANNELS

Figure 8

Figure 9 illustrates the coincident α-spectra as a function of the angle, $\theta_{\beta\alpha}$, for the case of electrons from the Li^8 decay of total energy about 8 Mev. The details are essentially the same as in figure 8. (Compare figures 10 and 11, and see the discussion in Section III, page 24.)

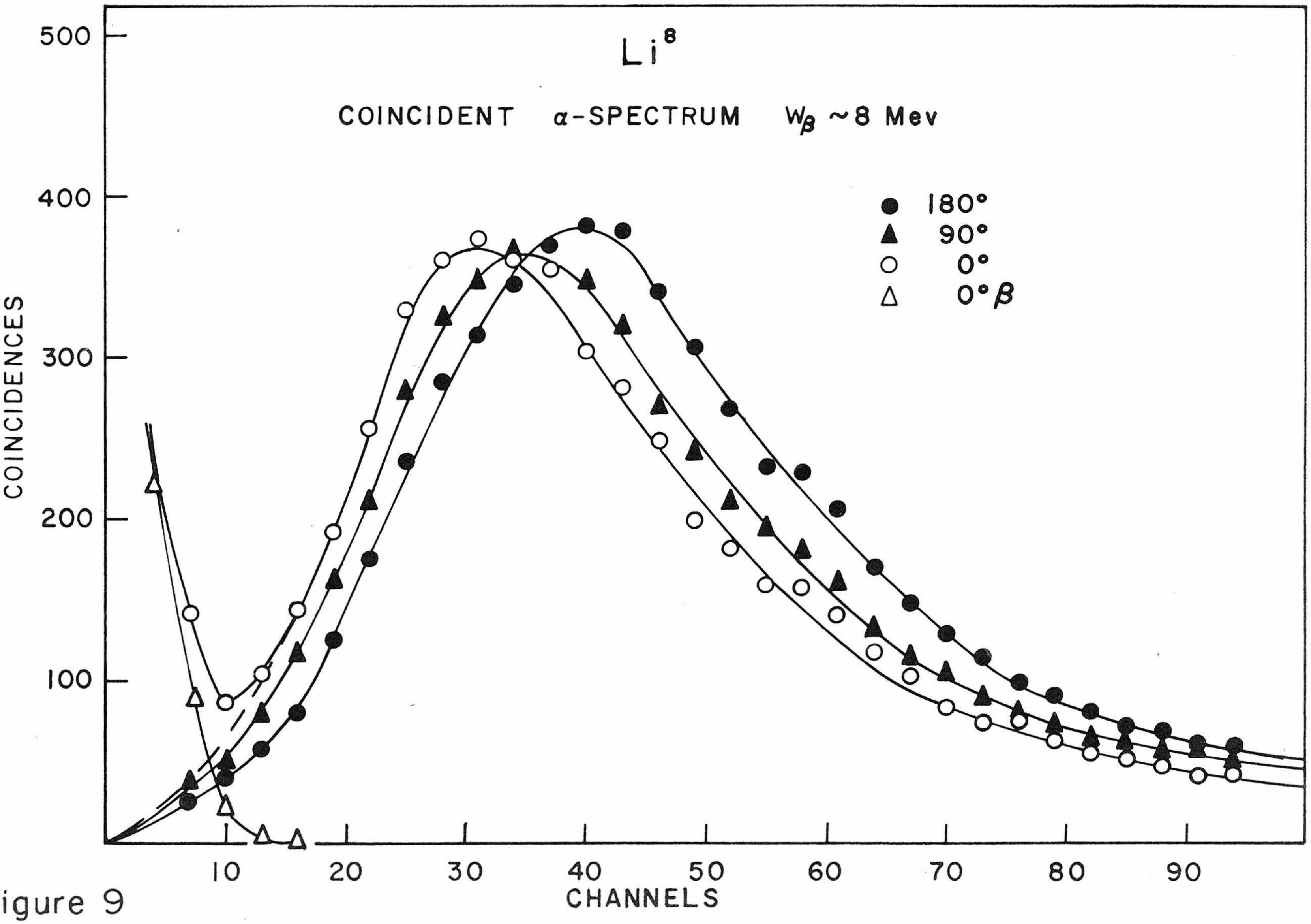
Li^8
COINCIDENT α-SPECTRUM $W_\beta \sim 8$ Mev
● 180°
▲ 90°
○ 0°
△ 0° β
COINCIDENCES
500
400
300
200
100
10
20
30
40
50
60
70
80
90
CHANNELS

Figure 9

Figure 10 shows the coincident α-spectra for the case of electrons from the Li^8 decay of average total energy about 11 Mev. The shift of the peaks caused by the recoil of Be^8 from the momentum of the electron and neutrino is greater in this case than in figure 8, since the electron momentum is greater. Figure 10 represents the sum of the data from two groups out of a total of 14 similar groups of data. Figure 10 should be compared to figure 11, which is the analogous data from the B^8 decay. (Also see Section III, page 24.)

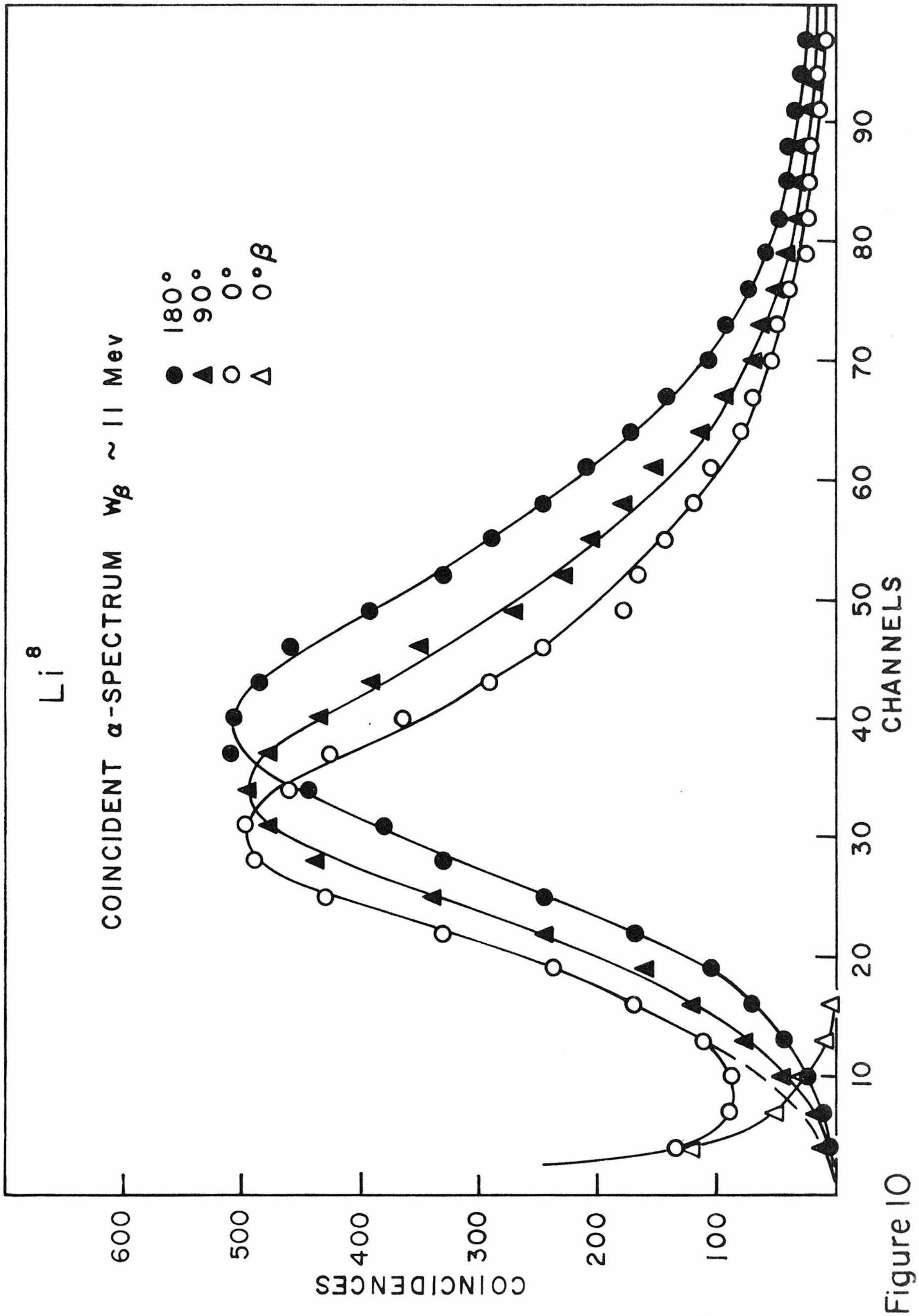
Li8
COINCIDENT α-SPECTRUM Wβ ~ 11 Mev
● 180°
▲ 90°
○ 0°
△ 0°β
COINCIDENCES
600
500
400
300
200
100
CHANNELS
10
20
30
40
50
60
70
80
90

Figure 10

Figure 11 is analogous to figure 10, where figure 11 applies to positrons of about 11 Mev total energy from the B^8 decay and figure 10 applies to electrons from the Li^8 decay. The increased widths of the spectra of figure 11 are caused by the additional energy loss of the α-particles in the target. The B^8 nuclei recoil from the 3.2-Mev He^3 beam deeper into the target than do the Li^8 nuclei from the 0.75-Mev deuteron beam. The description of figure 8 also applies to figure 11. Figure 11 is discussed in Section III, page 24.

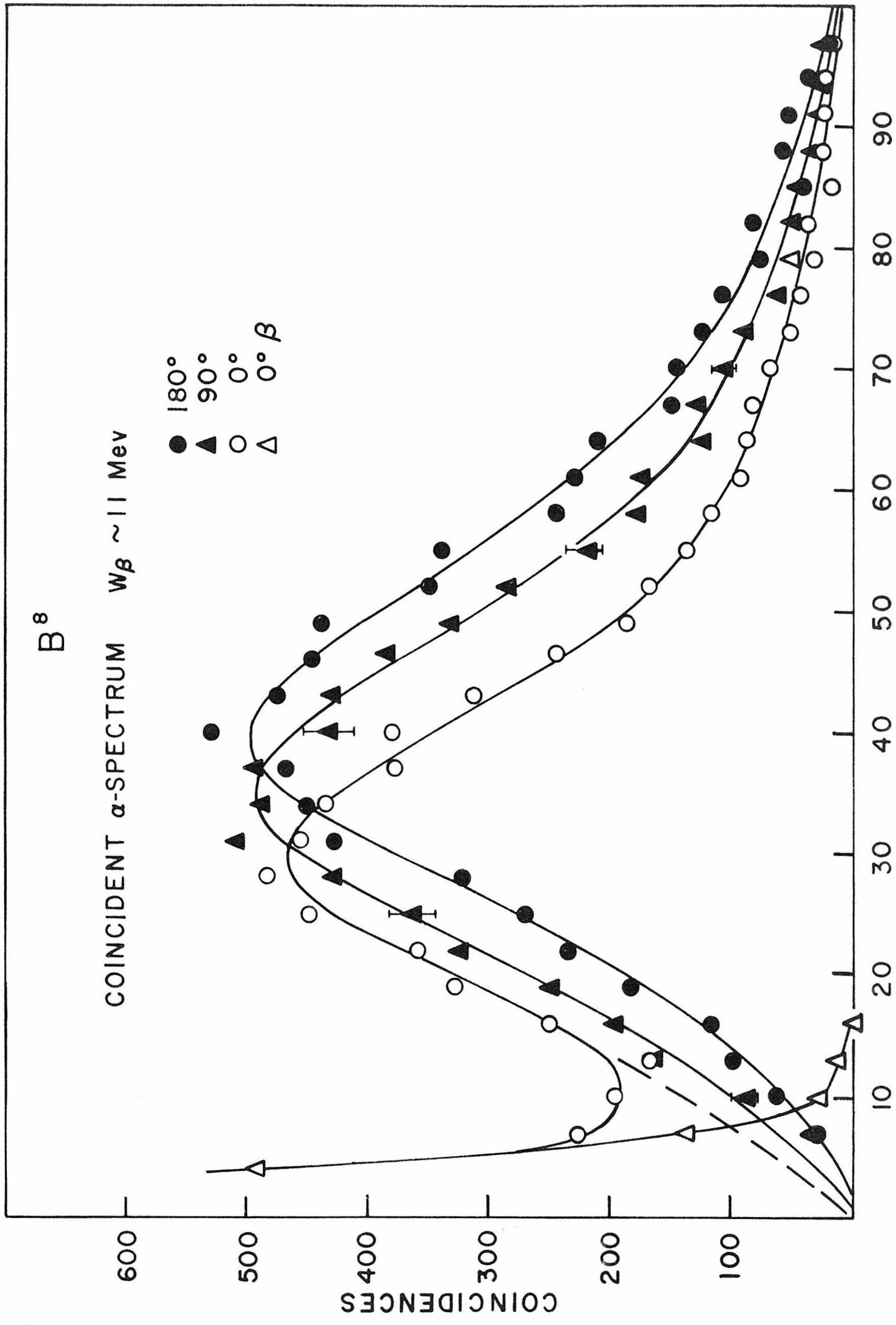
B⁸
COINCIDENT α-SPECTRUM
W_β ~ 11 Mev
● 180°
▲ 90°
○ 0°
△ 0° β
COINCIDENCES
100
200
300
400
500
600
CHANNELS
10
20
30
40
50
60
70
80
90

Figure 11

Figure 12 represents the pulse height analysis of the response of the gold-silicon detector to α-particles following the B^8 beta decay. This spectrum can be compared with figure 4 which is the α-spectrum following the Li^8 decay. In figure 12 there is a larger contribution from noise since the counting rate of α-particles is lower. Also the curve is broadened by the energy loss in the target. The points marked "α-α coincidence gate" represent the operation of the 100 channel analyzer gated by the **fast** coincidence mixer with α-particle pulses in both inputs. This spectrum indicates that the fast coincidence mixer is sensitive to pulses from α-particles as small as channel 6 to 10. (See Section III, page 26 and Section IV, page 40.)

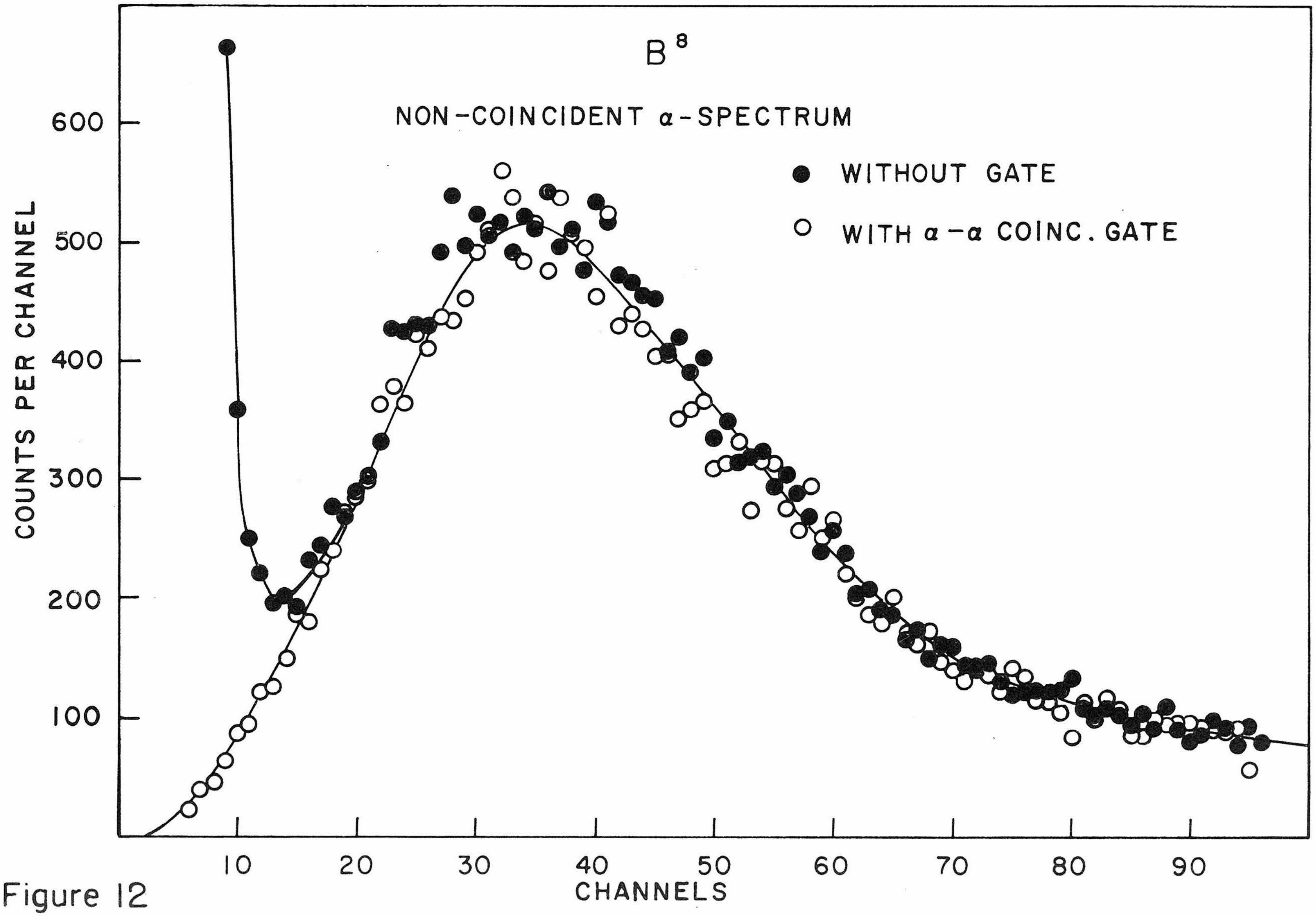
B^8
NON-COINCIDENT α-SPECTRUM
● WITHOUT GATE
○ WITH α−α COINC. GATE
COUNTS PER CHANNEL
600
500
400
300
200
100
10
20
30
40
50
60
70
80
90
CHANNELS

Figure 12

Figure 13 is the positron spectrum of the B^8 beta decay obtained with the plastic scintillator. The solid points are obtained from the open points by subtracting background measured with the beam striking only the aluminum target backing. The abscissa of the half maximum point is taken to be 10. 2 Mev, to determine the kinetic energy scale. The background of this spectrum is much greater than that of the Li^8 electron spectrum in figure 6. This is caused by the greater incident beam energy and much lower yield of B^8. The shaded portion of the spectrum represents the pulses selected by the single channel analyzer and corresponds to a total energy of about 11 Mev. The increased background does not permit reliable coincidence data with low energy positrons. Figure 13 is discussed in Section III, pages 26 and 31; and Section IV, page 35.

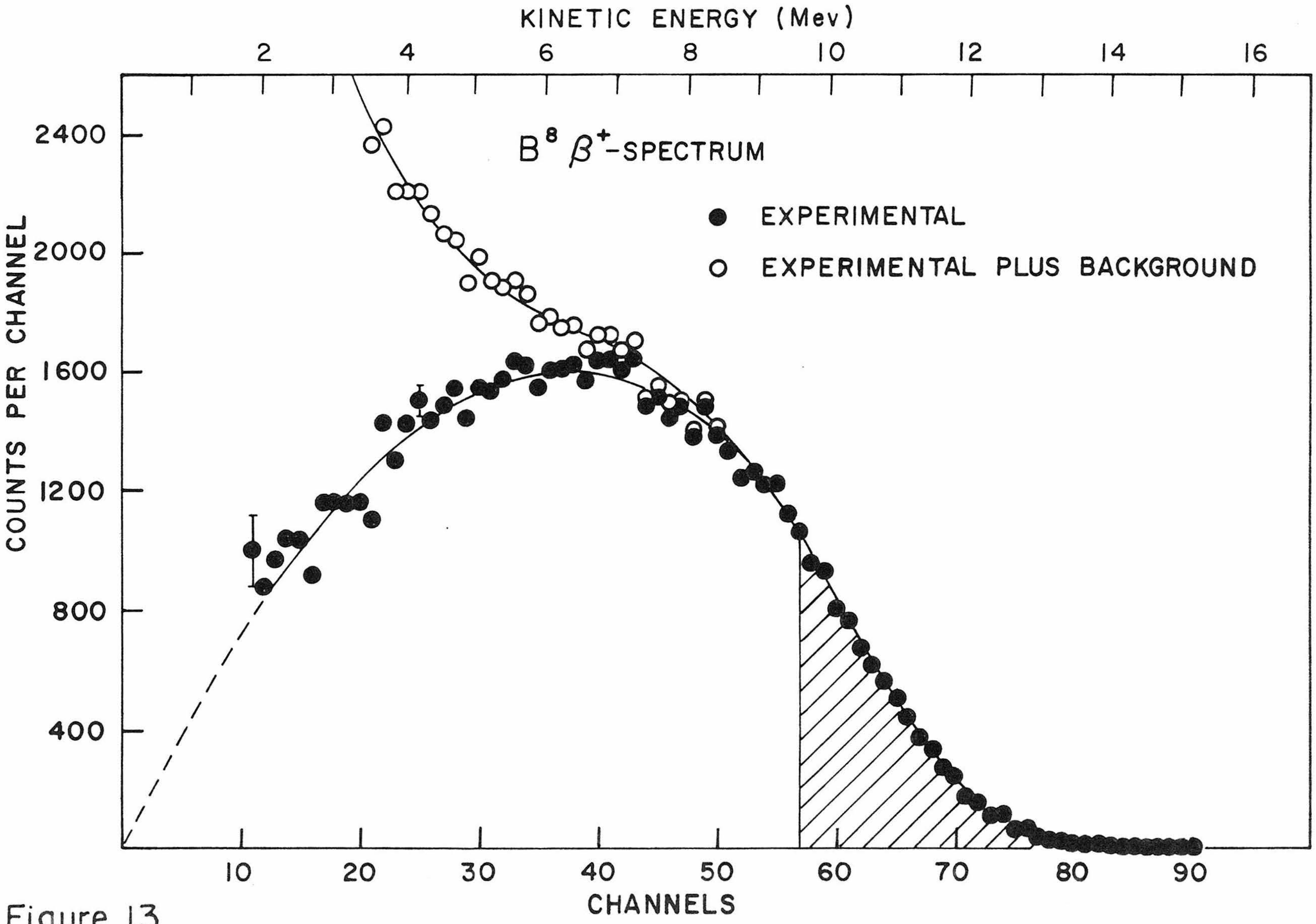
KINETIC ENERGY (Mev)
2
4
6
8
10
12
14
16
COUNTS PER CHANNEL
2400
2000
1600
1200
800
400
B^8 β^+-SPECTRUM
● EXPERIMENTAL
○ EXPERIMENTAL PLUS BACKGROUND
10
20
30
40
50
60
70
80
90
CHANNELS

Figure 13

Figure 14 is a histogram of all the data reduced to the values of the coefficients of the angular distribution function, $W(\theta_{\beta\alpha}) = 1 + A \cos \theta_{\beta\alpha} + B \cos^2 \theta_{\beta\alpha}$. Since the theoretical forms of the coefficients are proportional to the electron total energy, W_β, the coefficients are divided by W_β in order to average the various groups of data together. Each group of data is represented by a rectangle whose height is proportional to the inverse square of the statistical error of that group. Normal distribution curves are plotted about the mean of each coefficient. The data marked unreliable are not used in computing the mean values. The widths of the normal curves are equal to the square root of the number of groups times the statistical error of the mean. The coefficients, A, for the Li^8 and B^8 decays are very nearly equal. The coefficients, B, for the two decays are different. The magnitude of this difference is a positive indication for the conserved vector current theory of beta decay. The histogram is discussed in Section III, page 33; and Section IV, page 49.

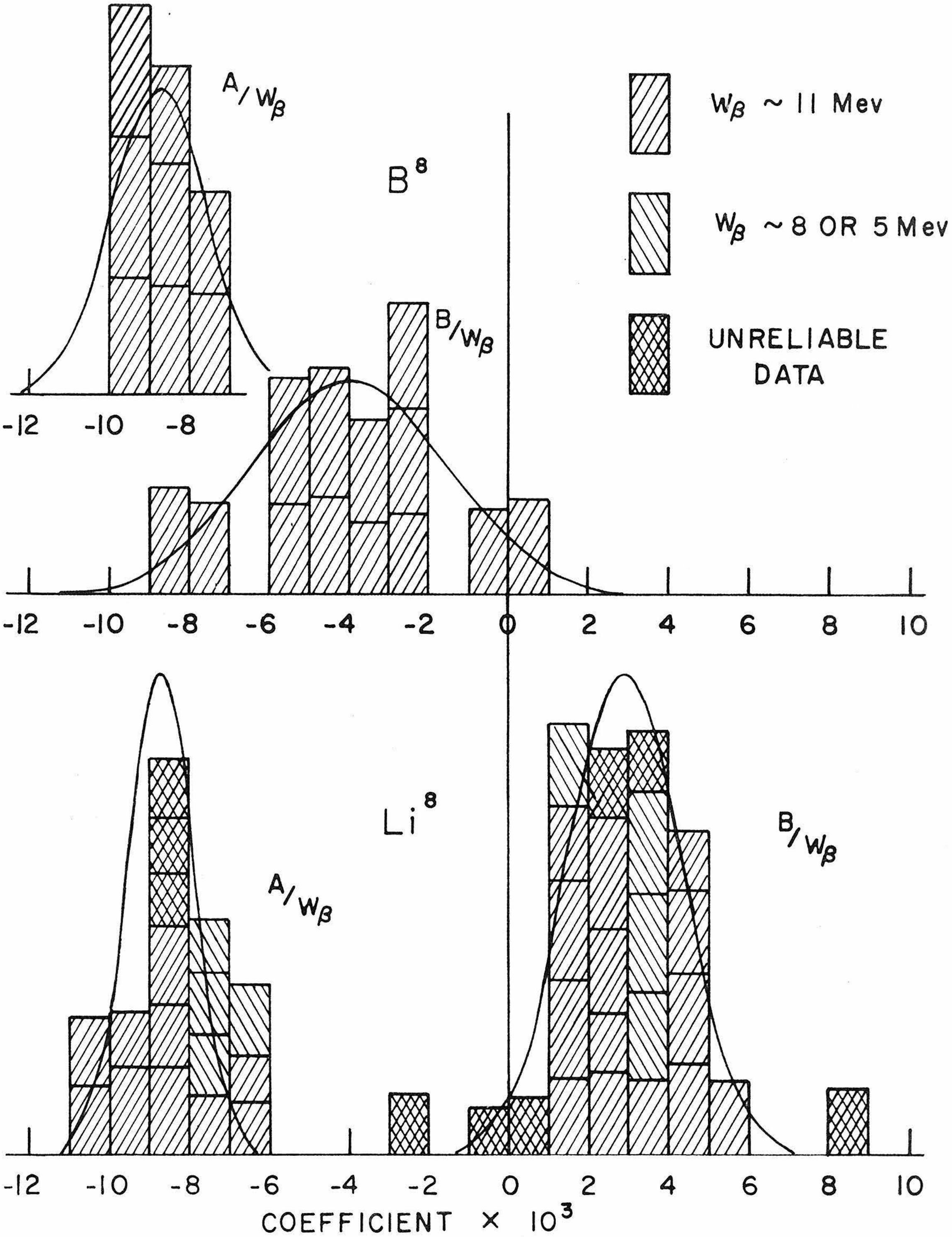

HISTOGRAM OF RESULTS

Figure 14

Figure 15 shows the response of a 2" x 3" plastic scintillator to 7.1 mev monoenergetic electrons. It is assumed that the scintillator used in this experiment has a similar response and that it can be adequately approximated by the triangular areas shown in the figure. Estimates of the distortion of the Li^8 β-spectrum and of the number of small pulses arising from high energy electrons are made from this and similar response curves at different energies. (See figure 16 and Section III, page 37.)

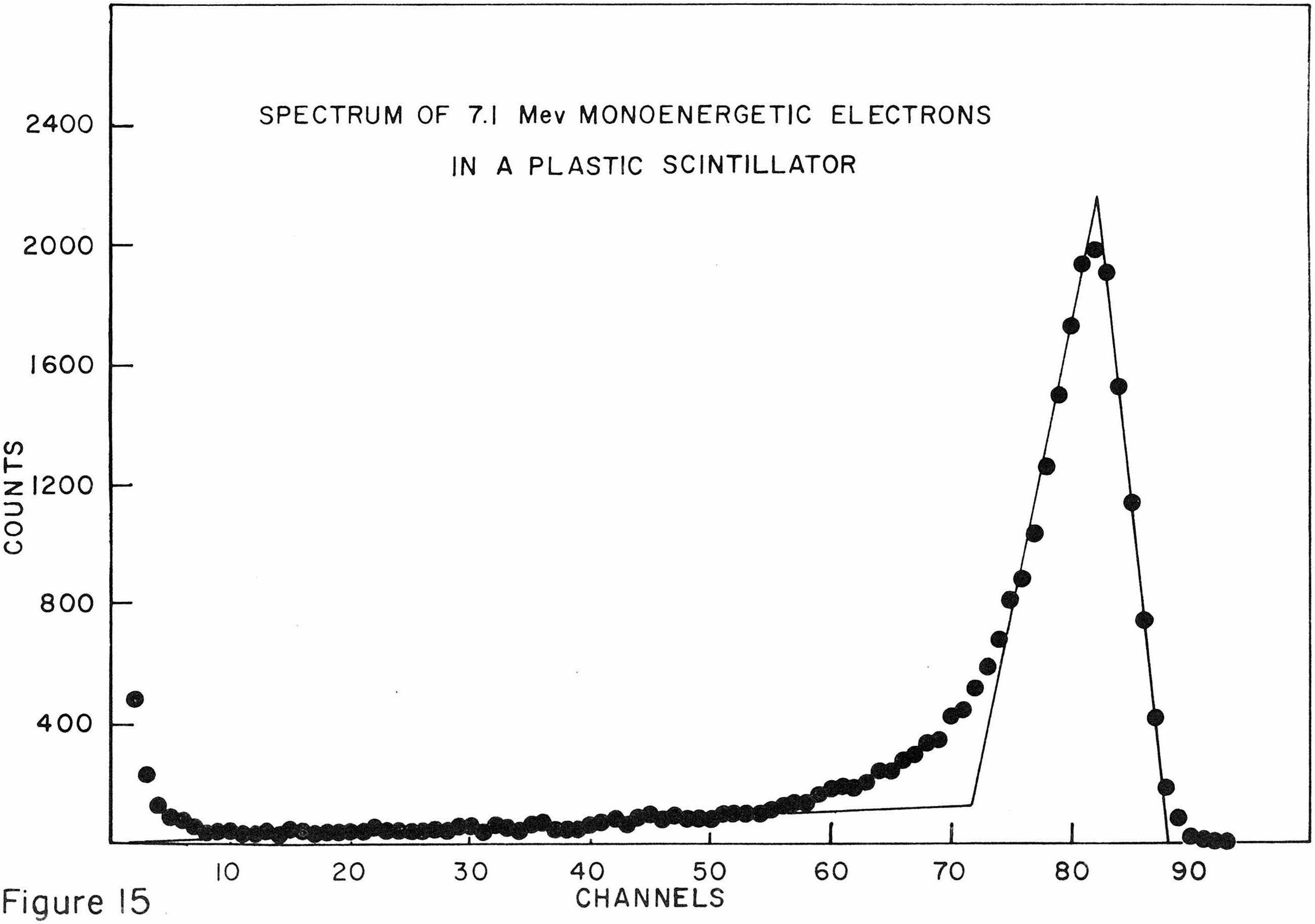
SPECTRUM OF 7.1 Mev MONOENERGETIC ELECTRONS
IN A PLASTIC SCINTILLATOR
COUNTS
2400
2000
1600
1200
800
400
10
20
30
40
50
60
70
80
90
CHANNELS

Figure 15

Figure 16 consists of three graphs of the Li^8 β-spectrum. The solid curve represents the response of the plastic scintillation counter to the β-spectrum and is identical to figure 6. The dashed curve is a magnetic spectrometer spectrum of equal area and equal abscissa for the points of half maximum. The third curve has been graphically derived from the second curve assuming a resolution function of the scintillator as in figure 15. The third curve is plotted with the same peak height as the magnetic spectrometer spectrum. It closely approximates the experimental spectrum for the higher pulse heights. Reference is made to figure 16 in Section IV, page 37.

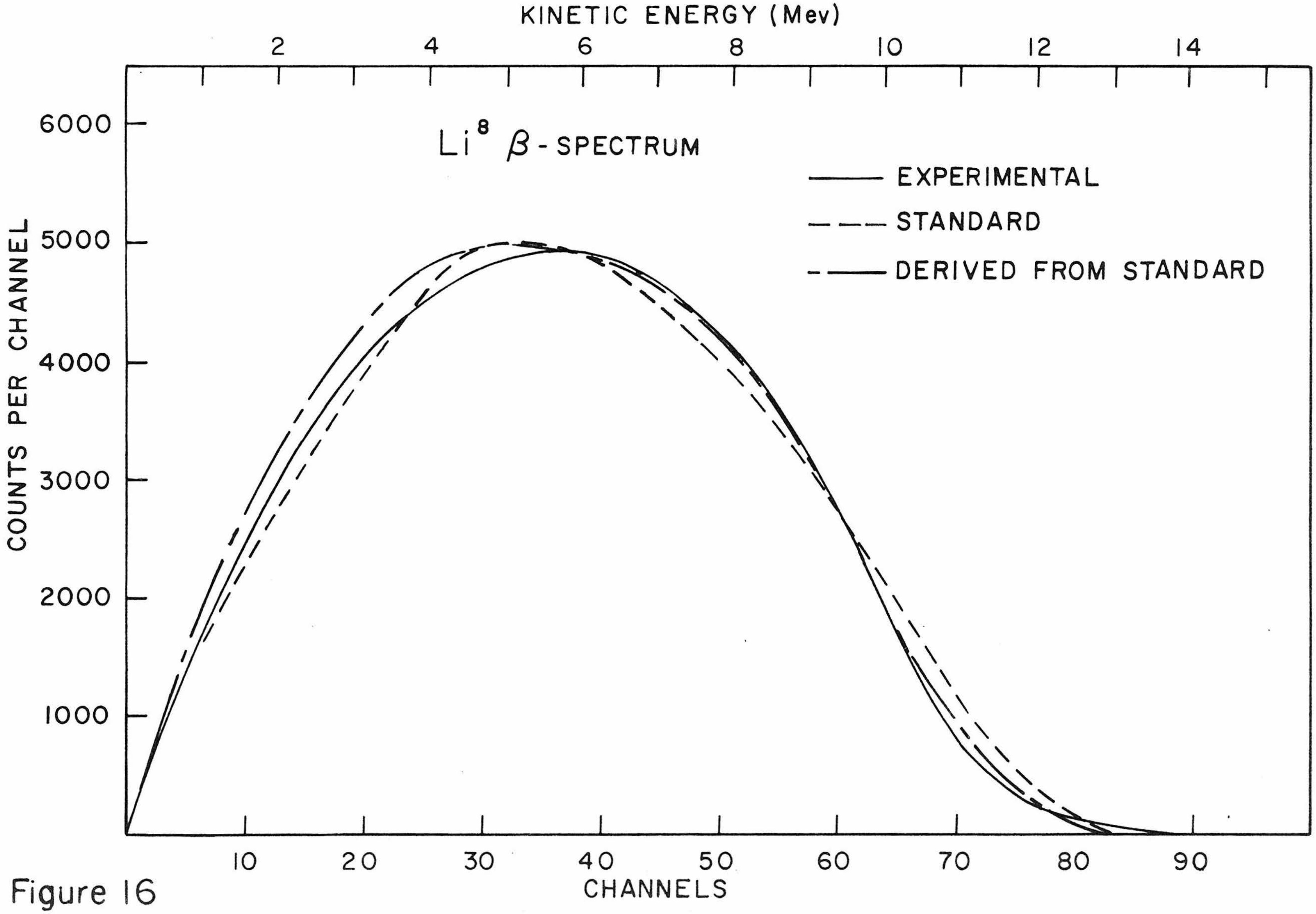
KINETIC ENERGY (Mev)
2
4
6
8
10
12
14
Li^8 β - SPECTRUM
EXPERIMENTAL
STANDARD
DERIVED FROM STANDARD
COUNTS PER CHANNEL
6000
5000
4000
3000
2000
1000
10
20
30
40
50
60
70
80
90
CHANNELS

Figure 16

Figure 17 illustrates the improvement in the coincident α-spectra following the B^8 decay in the new counting arrangement relative to the old. The primary changes are (1) that the target was changed from 30° to 15° to the beam, thereby reducing the effect of the recoil of the B^8 into the target, and (2) that the gold-silicon α-detectors are protected from sputtered material during the beam alignment procedure in the new arrangement. (See Section I, pages 7 and 8; and Section IV, page 38.)

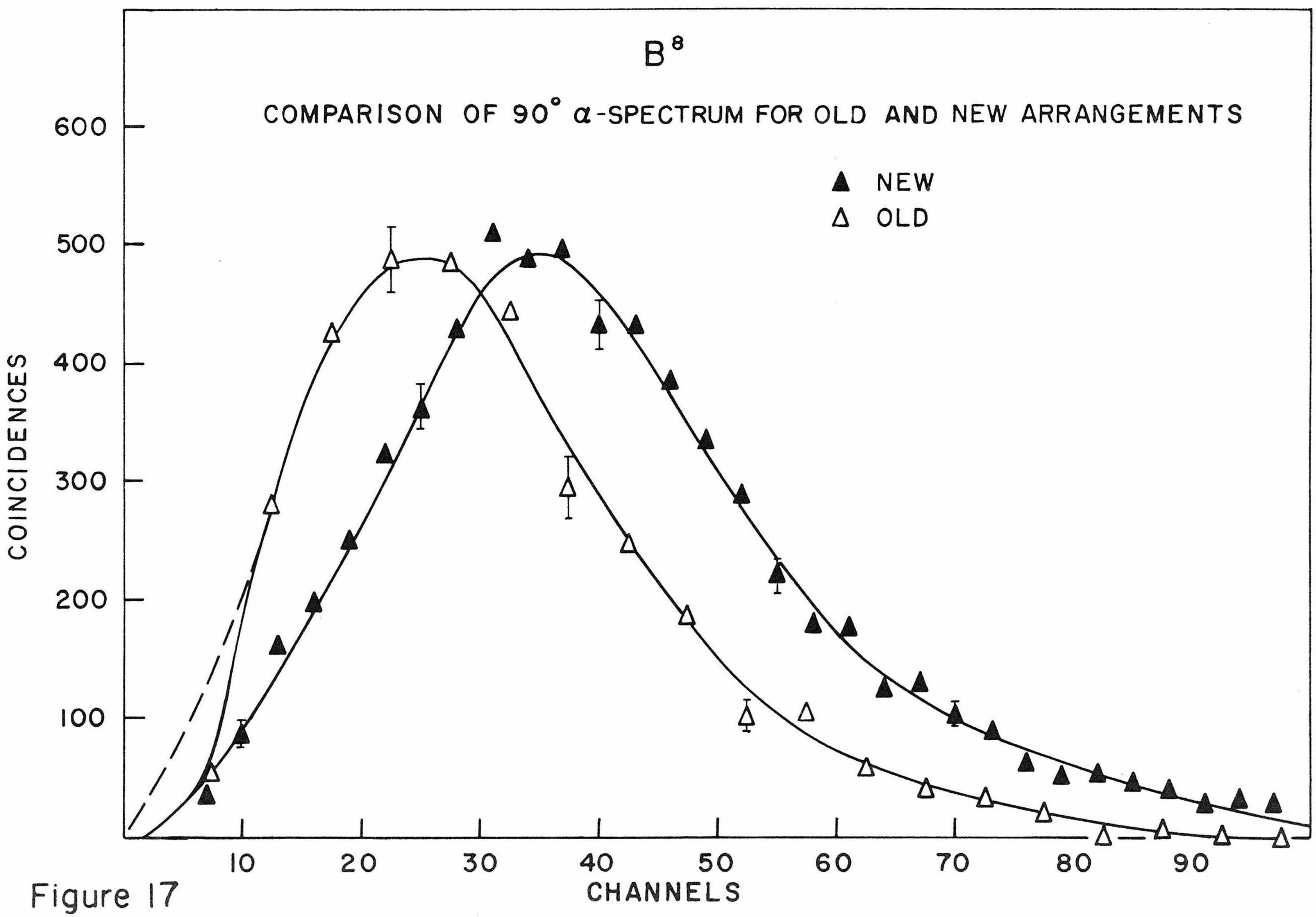
B^8
COMPARISON OF 90° α-SPECTRUM FOR OLD AND NEW ARRANGEMENTS
▲ NEW
△ OLD
COINCIDENCES
600
500
400
300
200
100
10
20
30
40
50
60
70
80
90
CHANNELS

Figure 17

Figure 18 displays the effect on the coincident α-spectra caused by the energy of the electrons. The three curves are the coincident spectra from the Li^8 beta decay at $\theta_{\beta\alpha} = 90^o$ for average total electron energies of 11, 8 and 5 Mev. The curves are all normalized to equal numbers of non-coincident electrons and have very nearly equal areas. The suppression of high energy α-particles in coincidence with high energy electrons is due to the restriction imposed by the conservation of energy. The figure is discussed in Section IV, page 42.

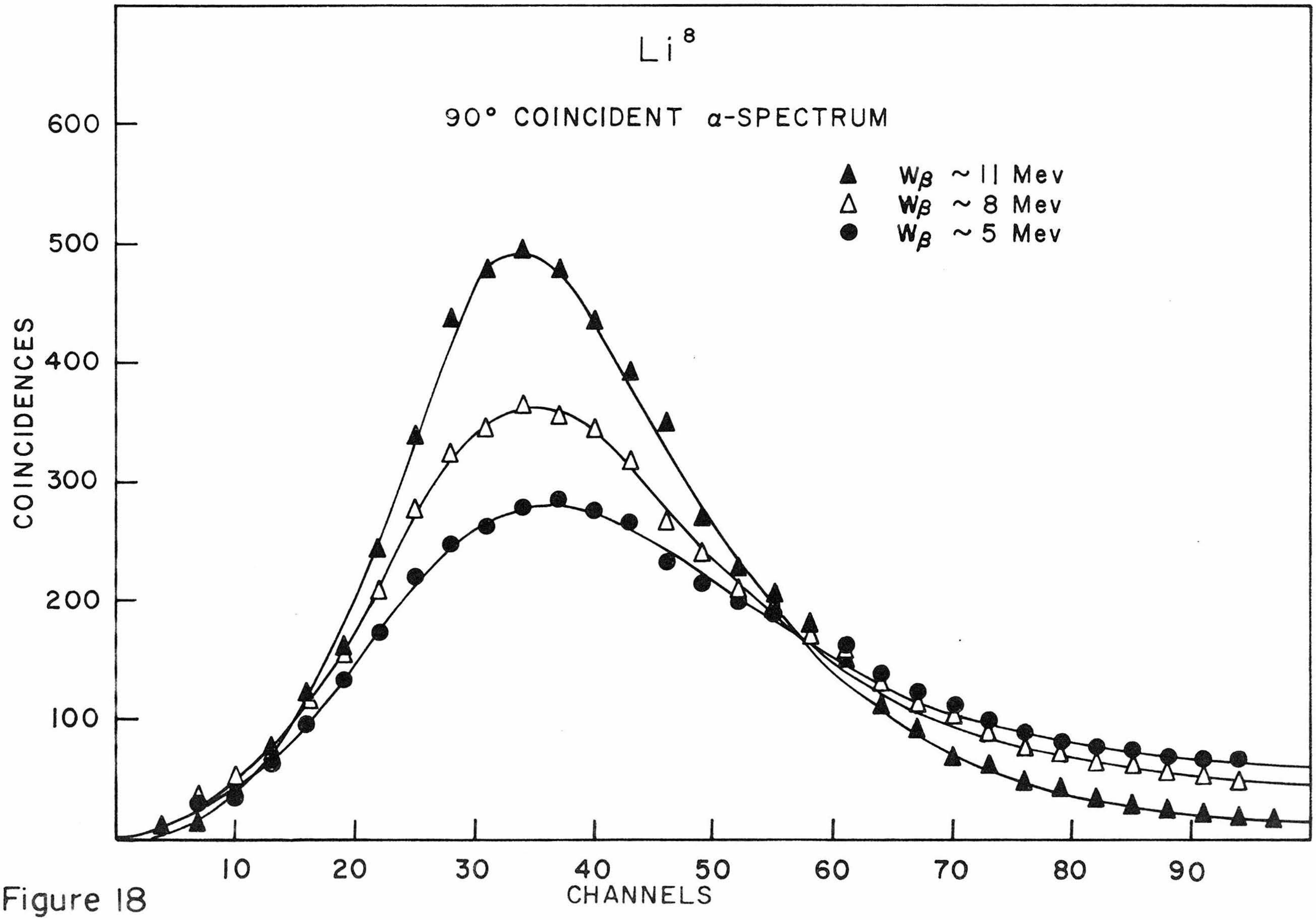
Li^8
90° COINCIDENT α-SPECTRUM
▲ W_β ~ 11 Mev
△ W_β ~ 8 Mev
● W_β ~ 5 Mev
COINCIDENCES
600
500
400
300
200
100
10
20
30
40
50
60
70
80
90
CHANNELS

Figure 18

Figure 19 represents the random coincidences of several groups of data from the Li^8 beta decay with average total electron energies about 11 Mev. As expected, the random coincidences fit the non-coincident α-spectrum of figure 6 rather than the coincident α-spectrum of figure 10. (See the discussion of figure 19 in Section IV, page 42.)

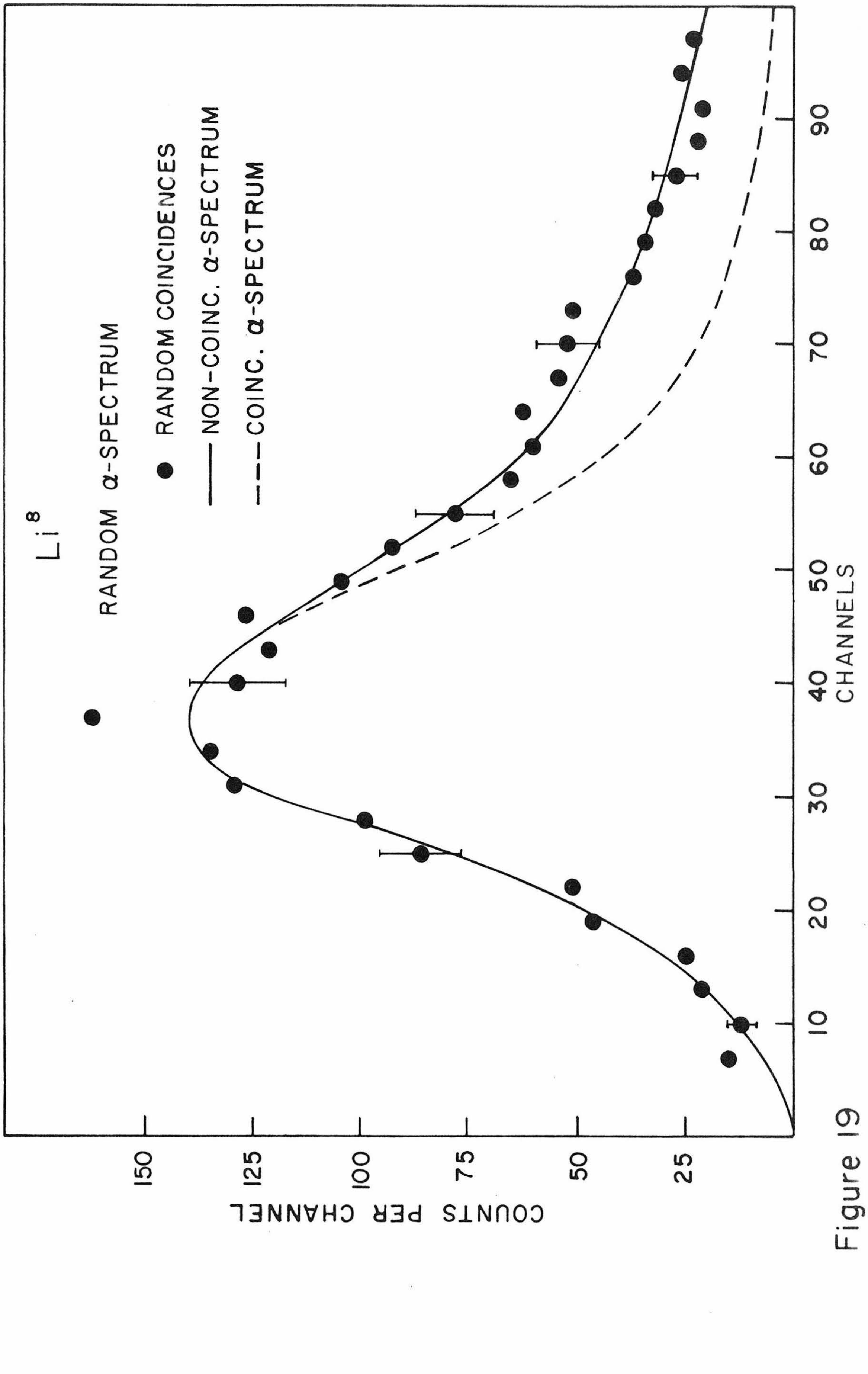
Li^8
RANDOM α-SPECTRUM
● RANDOM COINCIDENCES
— NON-COINC. α-SPECTRUM
- - - COINC. α-SPECTRUM
COUNTS PER CHANNEL
150
125
100
75
50
25
CHANNELS
10
20
30
40
50
60
70
80
90

Figure 19

Figure 20 demonstrates measurements of the effective energy required to produce an ion pair in gold-germanium detectors at 77°K and gold-silicon detectors at room temperature by 5.3 Mev α-particles. With the high bias voltages that are necessary for efficient collection of all generated ion pairs, the value of ϵ approaches 3.0 ev for germanium and 3.8 ev for silicon. The experimental points are determined from measurements of (1) the detector and preamplifier capacitance, (2) the output of the amplifier with 5.3 Mev α-particles hitting the detector, and (3) the response of the amplifier to a known charge input. The discussion of figure 20 appears in Appendix A, page 57.

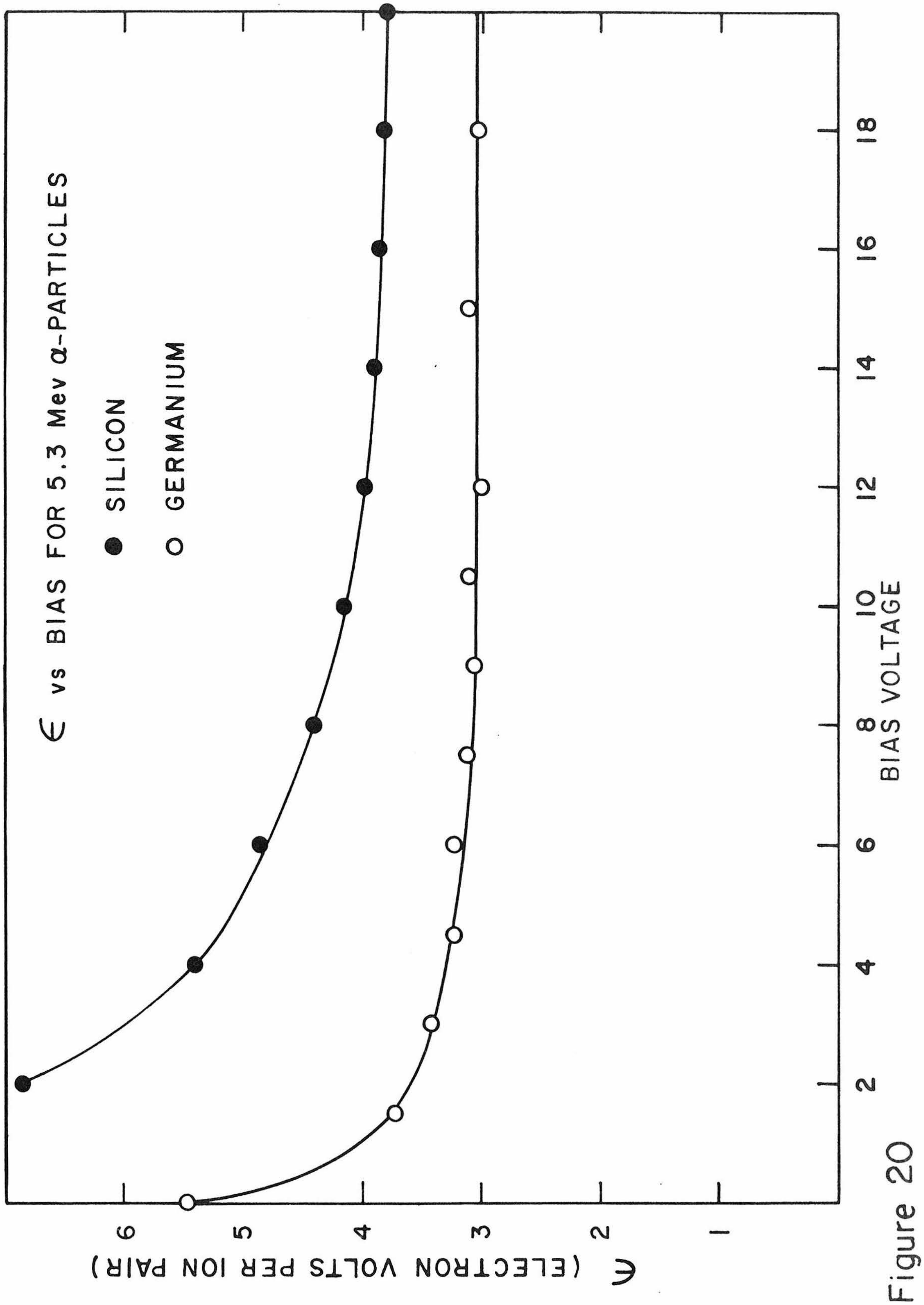
ϵ vs BIAS FOR 5.3 Mev α-PARTICLES
● SILICON
○ GERMANIUM
ϵ (ELECTRON VOLTS PER ION PAIR)
1
2
3
4
5
6
BIAS VOLTAGE
2
4
6
8
10
12
14
16
18

Figure 20

Figure 21 illustrated the general behavior of gold-silicon detectors to protons and α-particles. As a result of the mean energy required to release an electron-hole pair being independent of incident energy and particle type, the output pulse height bears a linear relation to the input energy up to the point where the incident particle penetrates

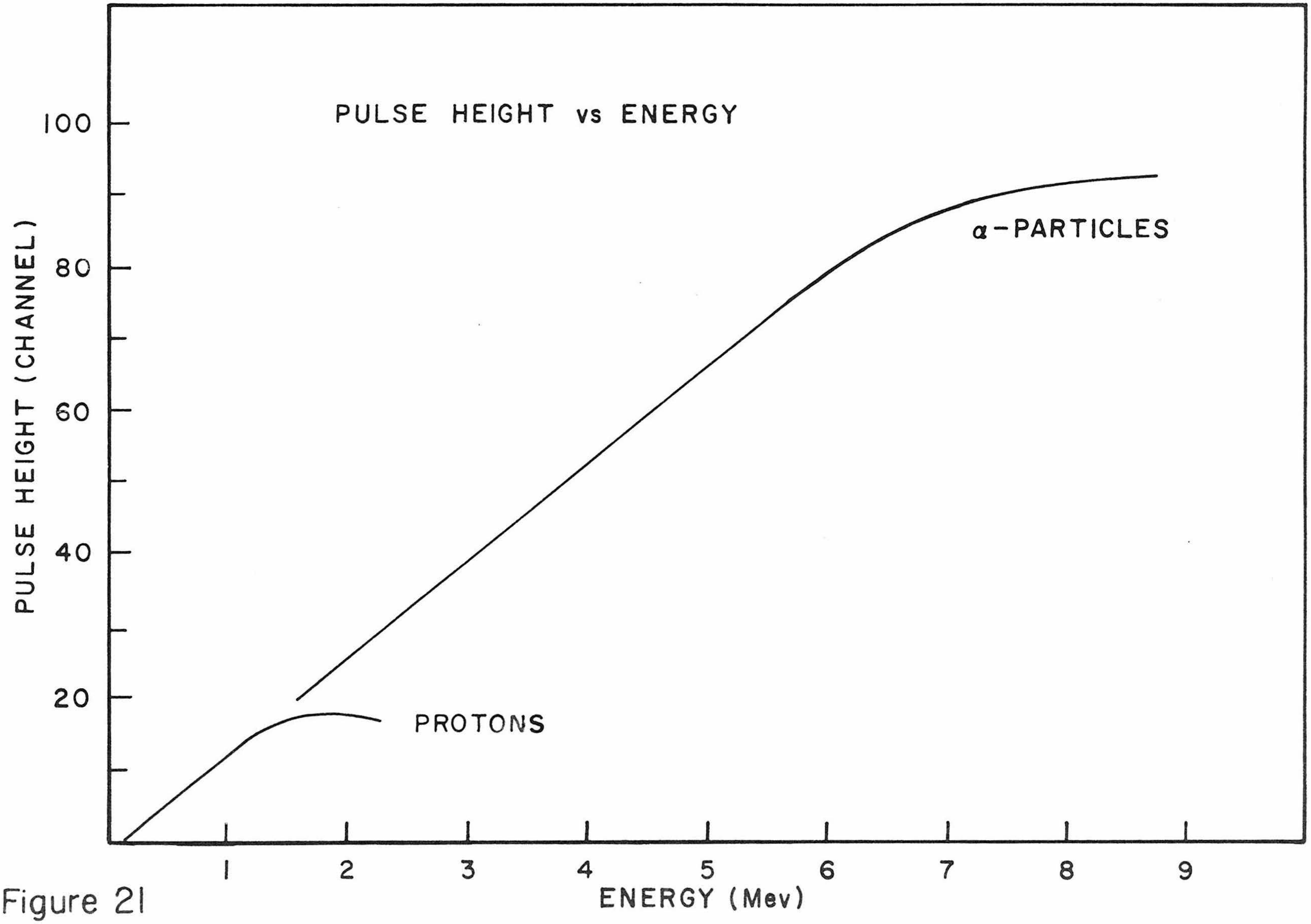
PULSE HEIGHT vs ENERGY
α-PARTICLES
PROTONS
PULSE HEIGHT (CHANNEL)
100
80
60
40
20
1
2
3
4
5
6
7
8
9
ENERGY (Mev)

Figure 21

Figure 22 shows that the inverse square of the capacitance varies approximately linearly with the bias applied to a gold-silicon detector. This relation is expected from the theoretical prediction that the depth of the depletion layer increases as the square root of the applied bias plus a surface potential. The slope of the line represents a sample of 170 Ωcm silicon. (Also see Appendix A, page 69.)

$1/C^2$ vs BIAS VOLTAGE

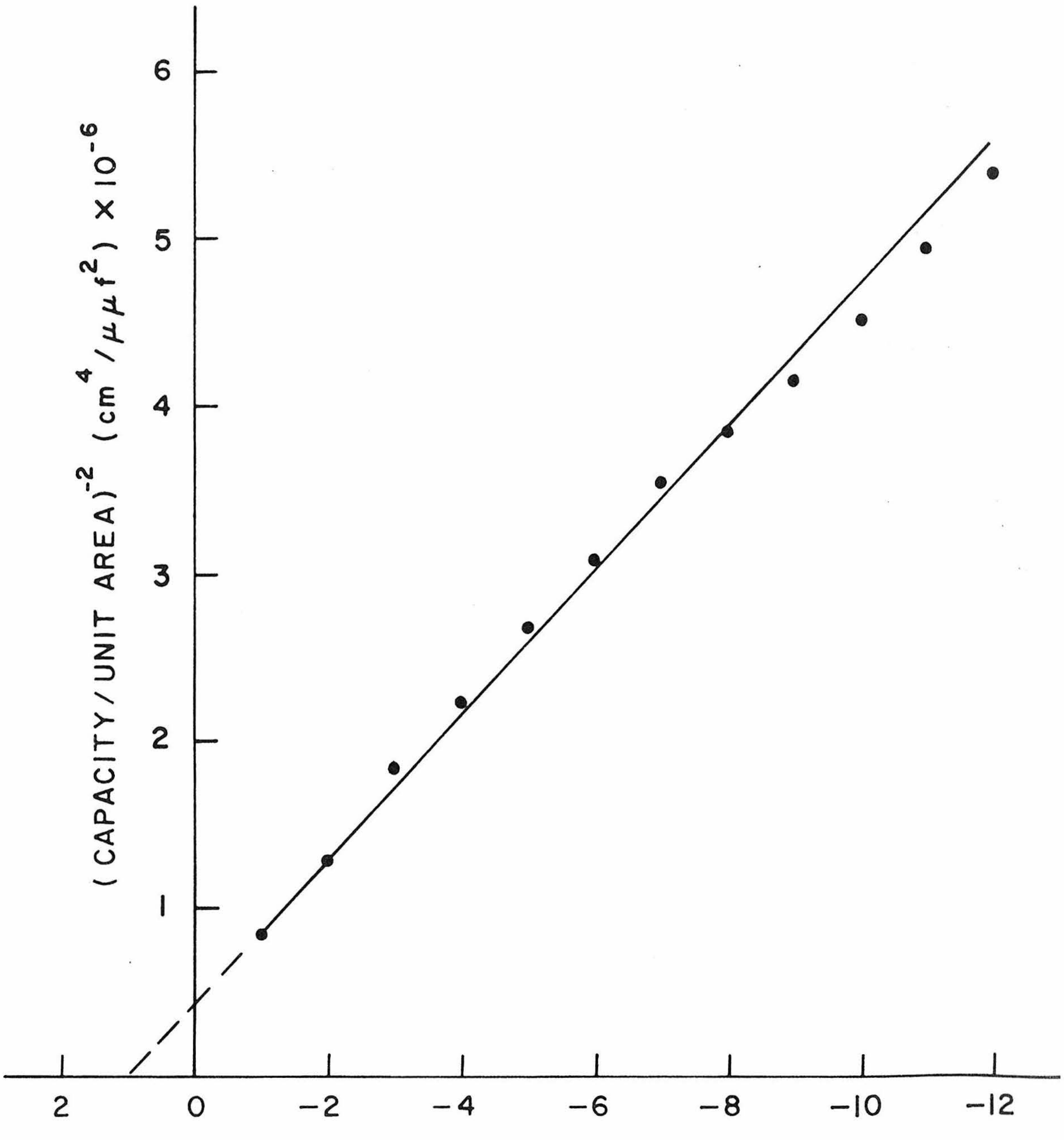

Figure 22

Figure 23 represents the direct current characteristics of various gold-germanium detectors at 77°K and gold-silicon detectors at room temperatures operated in near darkness. Empirically it is found that detectors with larger reverse currents exhibit poorer resolution. None of the characteristics illustrated represent detectors of outstanding resolution. Typical bias voltages for this experiment are about -8 volts. The reverse current of the detectors is slightly light sensitive and thus for best results the detectors are operated in near darkness. Further discussion of figure 23 is contained in Appendix A, page 61.

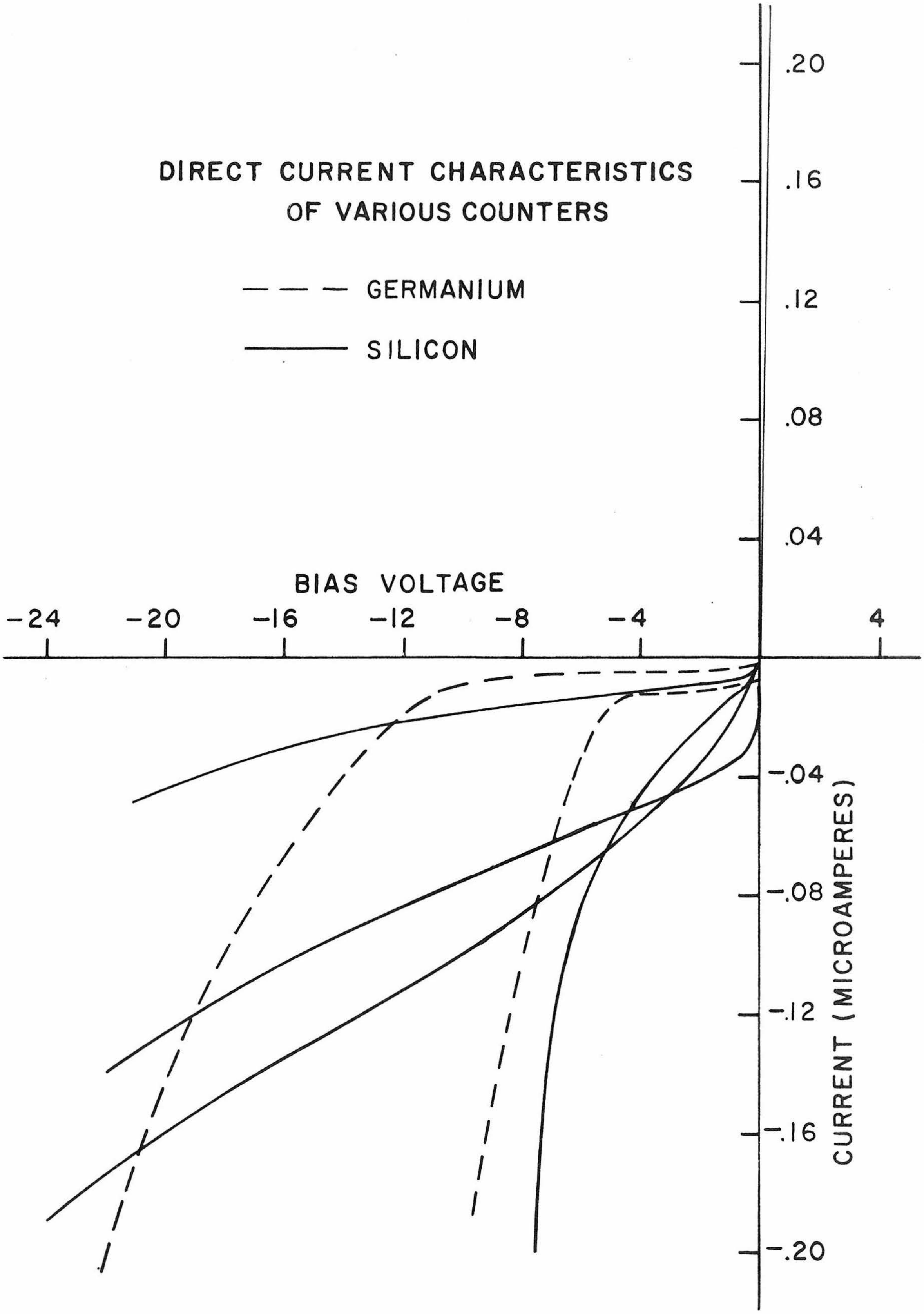
DIRECT CURRENT CHARACTERISTICS
OF VARIOUS COUNTERS
GERMANIUM
SILICON
BIAS VOLTAGE
-24
-20
-16
-12
-8
-4
4
.20
.16
.12
.08
.04
-.04
-.08
-.12
-.16
-.20
CURRENT (MICROAMPERES)

Figure 23

Figure 24 represents the solid angles accepted by the β-detector and the α-detector in the 0°, 90°, and 180° configurations. The figure is not to scale. In figure 24a the 0° configuration is merely the inversion of the α-detector in the 180° configuration through the origin at the target spot. Both detectors have solid angles defined by circular apertures, of half angle $19^{\circ}40'$ in the case of the β-detector and 9° in the case of the α-detector. The figure illustrates the definitions of the various angles used in Appendix B, page 64, for the purpose of integrating the functions, $\cos\theta_{\beta\alpha}$ and $\cos^2\theta_{\beta\alpha}$, over the solid angles.

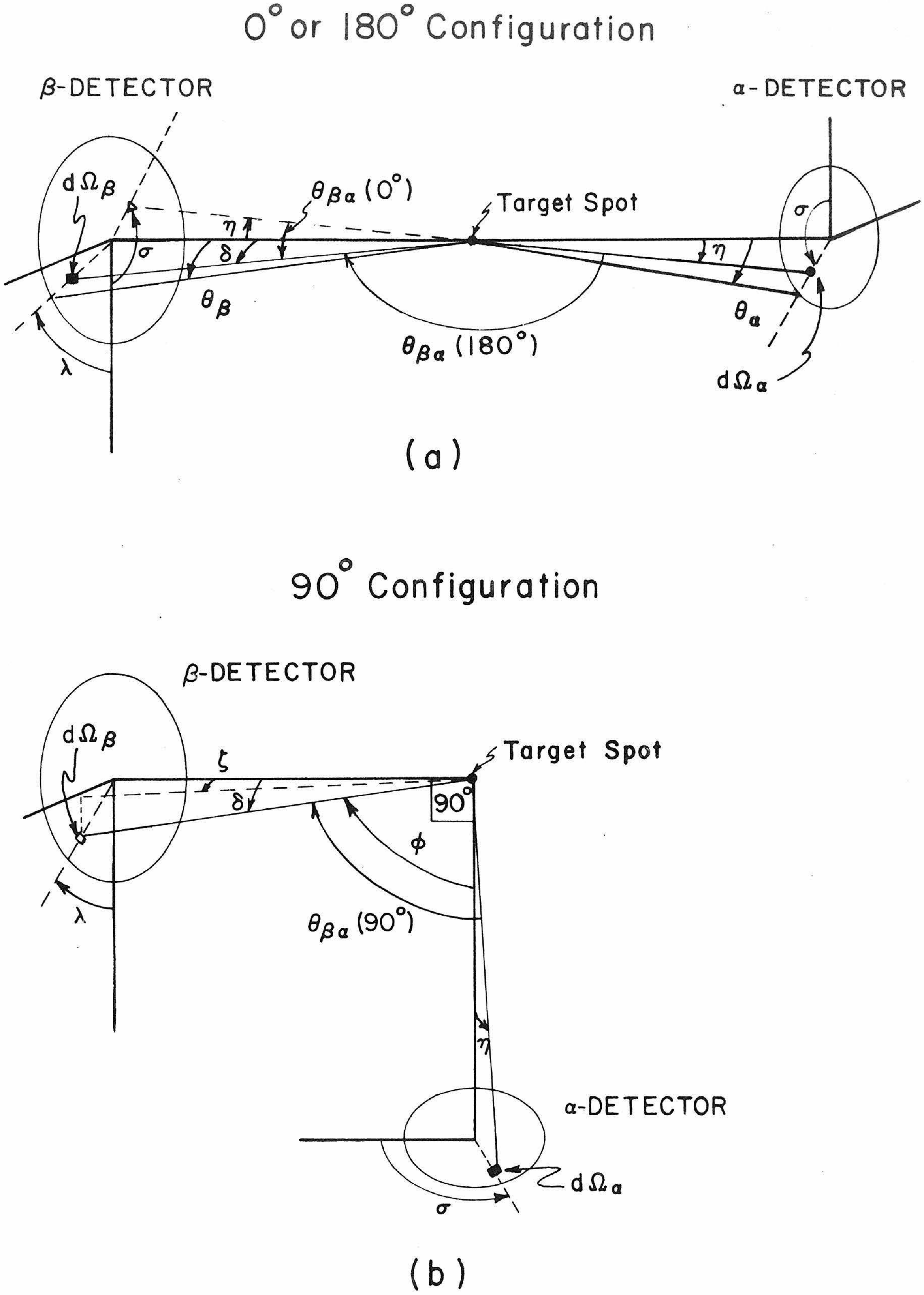

DETECTOR SOLID ANGLE CONFIGURATIONS

Figure 24

Figure 25 shows the directions of the electron, neutrino and α-particles and the angles between them in the rest system of Be^{8^*} and in the laboratory system. The particles and angles in the laboratory system are denoted by Greek letters. The drawing is not to scale. The Be^{8^*} nucleus, which is not shown, recoils from the momentum of the electron and neutrino. This recoil imparts an additional momentum in the laboratory system to the α-particles which are emitted in opposite directions in the rest system. The corresponding directional changes of the electron and neutrino are neglected. The result of the transformation is that several terms are added to the theoretical angular distribution function. The transformation is discussed in Appendix D, page 73.

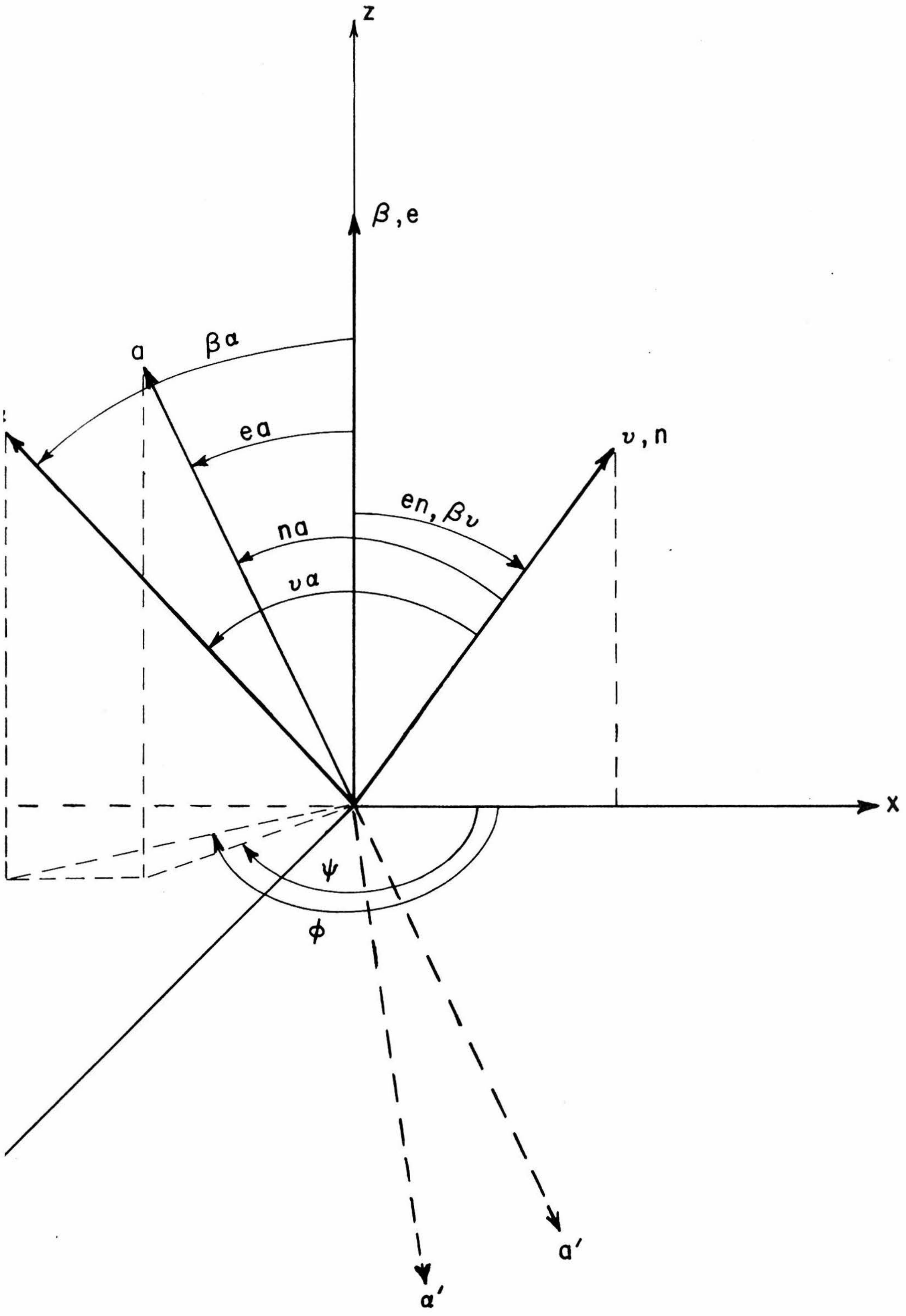

TRANSFORMATION TO LABORATORY ANGLES

Figure 25